

**FERROELECTRIC AND PYROELECTRIC  
PROPERTIES OF  
FORM IV POLY(VINYLIDENE FLUORIDE)  
AND ITS COMPOSITES**

**GAN WEE CHEN**

**THESIS SUBMITTED IN FULFILMENT OF  
THE REQUIREMENTS FOR THE DEGREE OF  
DOCTOR OF PHILOSOPHY**

**DEPARTMENT OF PHYSICS  
FACULTY OF SCIENCE  
UNIVERSITY OF MALAYA  
KUALA LUMPUR**

**2015**

## UNIVERSITI MALAYA

### ORIGINAL LITERARY WORK DECLARATION

Name of Candidate: GAN WEE CHEN

(I.C/Passport No: 810817-04-5225 )

Registration/Matric No: SHC 070085

Name of Degree: DOCTOR OF PHILOSOPHY

Title of Project Paper/Research Report/Dissertation/Thesis ("this Work"):

FERROELECTRIC AND PYROELECTRIC PROPERTIES OF  
FORM IV POLY(VINYLDENE FLUORIDE) AND ITS COMPOSITES.

Field of Study: ADVANCED MATERIALS


I do solemnly and sincerely declare that:

- (1) I am the sole author/writer of this Work;
- (2) This Work is original;
- (3) Any use of any work in which copyright exists was done by way of fair dealing and for permitted purposes and any excerpt or extract from, or reference to or reproduction of any copyright work has been disclosed expressly and sufficiently and the title of the Work and its authorship have been acknowledged in this Work;
- (4) I do not have any actual knowledge nor do I ought reasonably to know that the making of this work constitutes an infringement of any copyright work;
- (5) I hereby assign all and every rights in the copyright to this Work to the University of Malaya ("UM"), who henceforth shall be owner of the copyright in this Work and that any reproduction or use in any form or by any means whatsoever is prohibited without the written consent of UM having been first had and obtained;
- (6) I am fully aware that if in the course of making this Work I have infringed any copyright whether intentionally or otherwise, I may be subject to legal action or any other action as may be determined by UM.

  
Candidate's Signature

Date 7 July 2015

Subscribed and solemnly declared before,

  
Witness's Signature

Date 7th July 2015

Name:

Designation:

Profesor Dr. Wan Haliza Abdul Majid  
Iabatan Fizik  
Universiti Malaya  
50603 Kuala Lumpur

## ABSTRACT

The studies on ferroelectric and pyroelectric properties of the poly(vinylidene fluoride), PVDF and its composites in this work are mainly divided into three parts. In the first part, ferroelectric and pyroelectric properties of PVDF, were investigated with special interest on its Form IV thin films prepared by spin-coating cast from acetone and methyl ethyl ketone onto glass substrate. These solvents have low boiling points and low permittivities yielded mostly Form II thin films. Annealing at 140 °C induced a marked increase in crystallinity and reduce the surface roughness of the thin films. The Form II PVDF thin film was completely transformed to Form IV after the application of high electric field greater than 200 MV/m. The  $D$ - $E$  hysteresis loops that were associated with the ferroelectric polarization reversal in Form IV crystalline regions were observed by using alternating electric field,  $E$ . The remanent polarization  $P_r$  reached a maximum of 70 mC/m<sup>2</sup> with a coercive field  $E_c$  of 200 MV/m. The pyroelectric coefficient  $p_y$  determined after hysteresis loop measurement was shown to be proportional to  $P_r$ , and reached  $p_y$  of 28  $\mu$ C/m<sup>2</sup>K.

In the second part, thin films of a ferroelectric polymer matrix made of PVDF incorporated with a non-ferroelectric inclusion, TiO<sub>2</sub>, were prepared with different weight fractions (0-30 wt%). The dielectric and pyroelectric properties of the PVDF/TiO<sub>2</sub> composite thin films are measured as a function of several annealing temperatures (60 °C to 140 °C). Theoretical models, including Maxwell, Clausius-Mossotti, Furukawa and EMT were employed to describe the effective dielectric permittivity of the composites. This part of the work also studies the effect of a non-ferroelectric inclusion, which contributed to the enhancement of pyroelectric activity after the poling process, in a ferroelectric polymer matrix based composite. An increase in the dc conductivity of the polymer matrix led to an

easier poling process and reduced the required poling electric field from 260 MV/m to 120 MV/m. The pyroelectric coefficient of the polymer composite has been enhanced by 26 % at a much lower poling electric field.

In the third part, PVDF/La<sub>2</sub>O<sub>3</sub> composite thin films were prepared by spin-coating method. It is found that the pyroelectric coefficient and remanent polarization of the composites were significantly improved to 42  $\mu\text{C}/\text{m}^2\text{K}$  and 84  $\text{mC}/\text{m}^2$ , respectively. The enhancement of the measured coefficients in the composites can be achieved by introducing a very small amount (3 wt%) of La<sub>2</sub>O<sub>3</sub>. Local field in the inclusion site has shown to facilitate the poling procedure. A simple Maxwell-Wagner model, which takes into consideration of the effect of the dc conductivity of the inclusion in the thin film composite, shows a good agreement with the obtained pyroelectric and ferroelectric properties.



## ABSTRAK

Kajian sifat-sifat feroelektrik dan piroelektrik bagi poly(vinylidene fluoride), PVDF dan kompositya dalam penyelidikan ini terbahagi kepada tiga bahagian yang utama. Dalam bahagian yang pertama, sifat-sifat feroelektrik dan piroelektrik bagi PVDF khususnya filem nipis Fasa IV telah dijalankan. Filem nipis ini dihasilkan daripada acetone dan methyl ethyl ketone di atas substrat kaca dengan menggunakan teknik salutan putaran. Pelarut yang mempunyai titik didih dan berketelusan rendah ini menghasilkan kebanyakan filem nipis Fasa II. Proses penyepuh lindapan pada suhu 140 °C mengaruhkan peningkatan yang ketara pada sifat kehabluran dan mengurangkan kadar kekasaran permukaan filem tersebut. Filem nipis Fasa II ini telah bertukar sepenuhnya kepada filem nipis Fasa IV setelah medan elektrik yang tinggi ( $>200$  MV/m) digunakan. Dengan menggunakan medan elektrik ulang-alik, gelung histeresis  $D-E$  yang berkaitan dengan pengkutuban berbalik feroelektrik pada rantau kehabluran Fasa IV telah dibuat kajian. Pengkutuban remanen,  $P_r$  mencapai nilai maksima iaitu  $70 \text{ mC/m}^2$  dengan mengenakan medan daya elektrik,  $E_c$  sebanyak 200 MV/m. Pemalar piroelektrik,  $p_y$  kemudiannya ditentukan setelah pengukuran gelung histeris didapati berkadaran dengan nilai  $P_r$  dan mencapai nilai optimum,  $28 \text{ } \mu\text{C/m}^2\text{K}$ .

Dalam bahagian yang kedua, filem nipis matriks polimer feroelektrik telah dihasilkan daripada gabungan PVDF dan rangkuman bukan feroelektrik,  $\text{TiO}_2$  dengan nisbah berat yang berbeza iaitu 0-30 wt%. Disamping itu, sifat-sifat dielektrik dan piroelektrik bagi filem nipis komposit PVDF/ $\text{TiO}_2$  pada suhu sepuh lindap yang berbeza ( $60^\circ\text{C}$  to  $140^\circ\text{C}$ ) telah dipelajari. Model-model teori seperti Maxwell, Clausius-Mossotti, Furukawa and EMT telah diguna pakai untuk menjelaskan keberkesanan ketelusan dielektrik komposit tersebut. Laporan ini juga mengkaji kesan rangkuman bukan feroelektrik keatas peningkatan aktiviti piroelektrik selepas proses pengkutuban terhadap

filem nipis komposit matriks polimer feroelektrik. Peningkatan kekonduksian AT dalam matriks polimer boleh memudahkan proses pengkutuban dan menghasilkan penurunan pengkutuban medan elektrik daripada 260 MV/m kepada 120 MV/m. Oleh yang demikian, nilai pemalar piroelektrik bagi komposit polimer dapat ditingkatkan kepada 26 % dengan menggunakan medan elektrik pengkutuban yang lebih rendah.

Dalam bahagian ketiga, filem-filem nipis komposit PVDF/  $\text{La}_2\text{O}_3$  telah disediakan dengan menggunakan teknik salutan putaran. Nilai pemalar piroelektrik dan pengkutuban remanen telah ditingkatkan masing-masing kepada  $42 \mu\text{C}/\text{m}^2\text{K}$  dan  $84 \text{ mC}/\text{m}^2$ . Peningkatan nilai pemalar-pemalar ini boleh diperolehi dengan hanya mencampurkan  $\text{La}_2\text{O}_3$  (3 wt%) dalam kuantiti yang sedikit. Medan tempatan di bahagian rangkuman telah dibuktikan dapat memudahkan proses pengutuban. Model Maxwell-Wagner yang ringkas telah diperkenalkan di mana kekonduksian AT telah dipertimbangkan untuk menerangkan sifat-sifat piroelektrik dan feroelektrik yang diperolehi dan didapati persetujuan yang munasabah telah dicapai setelah factor kekonduksian AT diambil kira.

## ACKNOWLEDGEMENTS

First and foremost, I would like to express my sincere gratitude to my supervisor, Professor Dr. Wan Haliza Abd. Majid for her guidance and motivation. My special gratitude also goes to my mentor in life, Professor Dr. Takeo Furukawa from Tokyo University of Science. Their extensive scientific discussions from very beginning to the final level have been very helpful throughout my PhD life. I am also thankful to the staff at Low Dimensional Materials Research Centre for providing freedom to explore my works and characterization facilities.

My heart-felt gratitude and love is due to all my family members, especially my grandparents (the Late Mr. Gan Cheng Seng and Mdm. Tee Hoo Eng) and parents (Mr. Gan Boon Huat and Mdm. Lee Lock Mooi), for all the love, support and prayers. Last but not the least, I am indebted to my wife, Yang Pei Chin and lovely daughter, Gan Jing En, for waiting in anticipation to pursue my PhD. Without their continued support and interest, I would not able to begin the new chapter of my research life. I would like to dedicate this thesis to all of them.

I offer my warmest regards and blessing to all of friends who supported me in any respect during my PhD life.

## LIST OF PUBLICATIONS

1. Gan, W. C.; Majid, W. H. A., Effect of TiO<sub>2</sub> on enhanced pyroelectric activity of PVDF composite. *Smart Mater. Struct.* **2014**, 23 (4), 045026.
2. Tan, K. S.; Gan, W. C.; Velayutham, T. S.; Majid, W. H. A., Pyroelectricity enhancement of PVDF nanocomposite thin films doped with ZnO nanoparticles. *Smart Mater. Struct.* **2014**, 23 (12), 125006.
3. Mahdi, R.; Gan, W.; Majid, W., Hot Plate Annealing at a Low Temperature of a Thin Ferroelectric P(VDF-TrFE) Film with an Improved Crystalline Structure for Sensors and Actuators. *Sensors-Basel* **2014**, 14 (10), 19115-19127.
4. Velayutham, T. S.; Ng, B. K.; Gan, W. C.; Majid, W. H. A.; Hashim, R.; Zahid, N. I.; Chaiprapa, J., Phase sensitive molecular dynamics of self-assembly glycolipid thin films: A dielectric spectroscopy investigation. *The Journal of Chemical Physics* **2014**, 141 (8), 085101.
5. Ng, B. K.; Velayutham, T. S.; Gan, W. C.; Abd Majid, W. H.; Periasamy, V.; Hashim, R.; Zahid, N. I. M., Pyroelectricity in Synthetic Amphitropic Glycolipid for Potential Application of IR Sensor Device. *Ferroelectrics* **2013**, 445 (1), 67-73.
6. Zahariman, S.R.; Velayutham, T.S.; Abd. Majid, W. H.; Said, M.; Gan, W.C., Structural and dielectric studies on Sr<sub>0.5-3y/2</sub>La<sub>y</sub>Ba<sub>0.5</sub>Nb<sub>2</sub>O<sub>6</sub> ceramic systems with varied sintering Ttime and La concentration. *Ceramic-Silikaty* **2013**, 57 (4), 7.
7. M. H. Mohd Wahid; R. Mohd Dahan; S. Z. Sa'ad; A. N. Arshad; M. N. Sarip; H. Zulkefle; M. R. Mahmood; W. C. Gan; Majid, W. H. A., Different Surface Morphology of Annealed PVDF-TrFE Thin Films and the Effect on its Ferroelectric Properties *Advanced Materials Research* **2014**, 832, 4.
8. Velayutham, T. S.; Abd Majid, W. H.; Gan, W. C.; Khorsand Zak, A.; Gan, S. N., Theoretical and experimental approach on dielectric properties of ZnO nanoparticles and polyurethane/ZnO nanocomposites. *J. Appl. Phys.* **2012**, 112 (5), 054106.
9. Zak, A. K.; Gan, W. C.; Abd Majid, W. H.; Darroudi, M.; Velayutham, T. S., Experimental and theoretical dielectric studies of PVDF/PZT nanocomposite thin films. *Ceram. Int.* **2011**, 37 (5), 1653-1660.
10. Gan, W.C.; Wan Haliza, A. M., Dependence of pyroelectric properties of La<sub>0.03</sub>Sr<sub>0.255</sub>Ba<sub>0.7</sub>Nb<sub>2-y</sub>Ti<sub>y</sub>O<sub>(6-y/2)</sub> ceramic on electric field, grain refinement and Ti/Nb crystallite sizes. *Sains Malays* **2010**, 39 (6), 7.
11. Kwong, W. L.; Gan, W. C.; Majid, W. H. A.; Hashim, R.; Heidelberg, T., Pyroelectric detection in glycolipid thin film. *Thin Solid Films* **2010**, 518 (15), 4412-4416.

12. Gan, W. C.; W.H., A. M., The effect of gases on pyroelectric properties of PVDF/TiO<sub>2</sub> treated by plasma etcher. *Transactions of the Materials Research Society of Japan* **2009**, 34, 67-71.

**Papers to be submitted:**

1. Gan, W.C.; Abd. Majid, W.H.; Furukawa, T., Ferroelectric and pyroelectric properties of Form IV poly(vinylidene fluoride).
2. Gan, W.C.; Abd. Majid, Enhancing pyroelectric and ferroelectric properties of PVDF composite thin films by dispersing a non-ferroelectric inclusion La<sub>2</sub>O<sub>3</sub>.



# TABLE OF CONTENTS

Declaration	ii
Abstract	iii
Abstrak	v
Acknowledgements	vii
List of Publications	viii
Table of Contents	x
List of Figures	xiv
List of Tables	xviii
List of Symbols	xix

<b>Chapter 1: Introduction</b>	<b>1</b>
1.1 Introduction	1
References	7
 <b>Chapter 2: Literature Review</b>	 <b>10</b>
2.1 Introduction	10
2.2 Dielectric Properties	10
2.3 Ferroelectric Properties	18
2.3.1 Structural Symmetry	18
2.3.2 Spontaneous Polarization	22
2.3.3 Ferroelectric Domains and Hysteresis Loop	22
2.3.4 Ferroelectric Curie Point and Phase Transitions	25
2.4 Pyroelectric Properties	26

2.5	Piezoelectric Effects	29
2.6	Poly(vinylidene fluoride) Polymer	32
2.7	Role of Inclusion in Polymer Matrix	38
2.8	Summary	39
	References	40
<b>Chapter 3:</b>	<b>Experimental Methodology</b>	44
3.1	Introduction	44
3.2	Sample Preparation	44
3.2.1	PVDF Thin Films	44
3.2.2	PVDF/TiO <sub>2</sub> Composite Thin Films	45
3.2.3	PVDF/La <sub>2</sub> O <sub>3</sub> Composite Thin Films	46
3.2.4	Device Configuration	46
3.2.5	Poling	50
3.3	Structural Analysis	54
3.3.1	Fourier Transform Infrared Spectroscopy	54
3.3.2	X-ray Diffraction	54
3.3.3	Surface Morphology	55
3.4	Electrical Measurement	55
3.4.1	Dielectric Measurement	55
3.4.2	Pyroelectric Measurement	56
3.4.2.1	Experimental Considerations	58
3.4.3	Ferroelectric Measurement	60
3.4.3.1	Experimental Considerations	60
	References	61

<b>Chapter 4: Structural, Ferroelectric and Pyroelectric Properties of Form IV Poly(vinylidene fluoride)</b>	<b>62</b>
4.1 Introduction	62
4.2 The Effect of Annealing on Crystalline Structure and Morphology of Spin-cast Form II PVDF	63
4.3 Effect of Poling on Phase Transformation from Form II to Form IV PVDF	68
4.4 Ferroelectric Activity in Form IV PVDF	71
4.5 Pyroelectric Activity in Form IV PVDF	73
4.6 Dielectric Relaxation in Form II and Form IV PVDF	76
4.7 Discussion	80
4.7.1 Spontaneous Polarization of Crystallites, $P_s$ and the Local Field Effects	84
4.7.2 Degree of Crystallinity	90
4.7.3 Crystallite Orientation	91
4.7.4 Dielectric Molecular Dynamics	92
4.7.5 Linear Relationship of Pyroelectric and Ferroelectric Properties	95
4.8 Conclusion	97
References	98
 <b>Chapter 5: Pyroelectric Activity Enhancement in PVDF/TiO<sub>2</sub> Composite Thin Films</b>	 <b>102</b>
5.1 Introduction	102
5.2 Structural Analysis	103
5.2.1 Fourier Transform Infrared Spectroscopy	103
5.2.2 X-ray Diffraction	105
5.2.2.1 Effect of Poling Process	106
5.2.3 Scanning Electron Microscopy	108
5.3 Pyroelectric Activity and Poling Effect	110

5.4	Dielectric Properties and the Effect of Poling	113
5.5	Conclusion	122
	References	123
<b>Chapter 6:</b>	<b>Pyroelectric and Ferroelectric Activities Enhancement in PVDF/La<sub>2</sub>O<sub>3</sub> Composite Thin Films</b>	126
6.1	Introduction	126
6.2	Dielectric Properties	126
6.3	Pyroelectric Properties	130
6.4	Ferroelectric Properties	135
6.5	Phase Transformation from Form II to IV PVDF	137
6.6	Comparison in Between the TiO <sub>2</sub> and La <sub>2</sub> O <sub>3</sub> as a Non-ferroelectric Inclusion	140
6.7	Conclusion	142
	References	143
<b>Chapter 7:</b>	<b>Conclusion</b>	146
7.1	Conclusion	146
7.2	Future Works	149
<b>Appendix :</b>	<b>Spontaneous Polarization Calculation</b>	150

## LIST OF FIGURES

		Page
Figure 2.1	Frequency dependence of various polarization mechanisms.	12
Figure 2.2	Mechanism of polarization.	12
Figure 2.3	Scheme of the real $\epsilon'$ (black line) and the imaginary $\epsilon''$ (red line) part of the complex dielectric function for a relaxation process.	16
Figure 2.4	Schematic circuit of Sawyer-Tower bridge for ferroelectric characterization.	23
Figure 2.5	A typical $D$ - $E$ hysteresis loop in ferroelectric materials.	25
Figure 2.6	The relationship between the thermal, electrical and mechanical properties of a crystal. The solid line illustrates the primary pyroelectric effect (with strain remain constant); the red dash line illustrates the secondary pyroelectric effect when the crystal is free to deform.	27
Figure 2.7	Piezoelectricity- An intermingling of electric and elastic phenomena.	30
Figure 2.8	Piezoelectric phenomena with a simple molecular model: (a) an unperturbed molecule with no piezoelectric polarization; (b) the molecule subjected to an external force, $F$ , resulting in to polarization, $P_s$ .	30
Figure 2.9	The three chain conformations of PVDF in different polymorphs: (a) TTT planar zigzag, (b) $T_3GT_3\bar{G}$ and (c) $TGT\bar{G}$ .	34
Figure 2.10	Crystal structures of PVDF. Black rectangle in each crystal denotes the crystallographic unit cell. The $c$ -axis is parallel to the chain direction for all polymorphs. The $b$ -axis is vertical direction for Form I and horizontal direction for other polymorphs. (a) Form I is parallel all trans. (b) Form II is antiparallel and up-down $TGT\bar{G}$ . (c) Form III is parallel and up-up $T_3GT_3\bar{G}$ . (d) Form IV is parallel and up-down $TGT\bar{G}$ .	35
Figure 2.11	Schematic diagram of crystalline transformations among polymorphs of PVDF due to electrical, mechanical and thermal treatments.	37
Figure 3.1	A schematic diagram of ferroelectric device: (a) bottom electrode, (b) top electrode, (c) desired MIM structure and (d) a MIM ferroelectric device deposited on silicon wafer.	48



Figure 3.2	A schematic diagram of shadow mask: (a) top and (b) bottom electrode.	49
Figure 3.3	(a) A schematic diagram of a dielectric device (top view); (b) Picture of a dielectric device placed on the top of Peltier heater.	50
Figure 3.4	A schematic drawing of a polycrystalline ferroelectric with random orientation of grains before and after poling.	51
Figure 3.5	Schematic drawing of d.c. poling system.	52
Figure 3.6	Schematic drawing of corona poling system.	53
Figure 3.7	Schematic drawing of the experiment set-up for quasi-static pyroelectric measurement.	57
Figure 3.8	Typical triangular temperature waveform and the rectangular short-circuited pyroelectric current during the quasi-static pyroelectric measurement.	58
Figure 3.9	Pyroelectric current is decayed with time at the heating rate of 0.03 °C.	59
Figure 4.1	The dependence of FTIR spectra of PVDF thin films on annealing temperature.	64
Figure 4.2	Fraction of the Form II, $F(\alpha)$ of PVDF thin films as a function of annealing temperatures.	65
Figure 4.3	X-ray diffractograms of PVDF thin films: effect of annealing temperature.	66
Figure 4.4	SEM microstructure of PVDF thin films annealed at (a) 60 °C, (b) 80 °C, (c) 100 °C, (d) 120 °C, (e) 140 °C and (f) microstructure of PVDF in smaller scale of magnification at 140 °C.	67
Figure 4.5	Typical AFM height images of PVDF thin films annealed at (a) 60 °C, (b) 80 °C, (c) 100 °C, (d) 120 °C and (e) 140 °C.	68
Figure 4.6	X-ray diffractograms of acetone cast PVDF thin films before and after poling.	69
Figure 4.7	Deconvolution of XRD spectra of acetone cast PVDF (a) before and (b) after poling.	70
Figure 4.8	<i>D-E</i> hysteresis loops of acetone cast PVDF annealed at 140 °C in steps of 40 MV/m.	72

Figure 4.9	<i>D-E</i> hysteresis loops of acetone cast PVDF annealed at difference temperature.	73
Figure 4.10	Plots of (a) triangular temperature waveform, $T$ , (b) square pyroelectricity response, $I$ and (c) change of polarization, $\Delta P$ as a function of time for pyroelectric measurement.	74
Figure 4.11	Dependence of change of polarization, $\Delta P$ with respect to the change of temperature, $\Delta T$ .	75
Figure 4.12	Dependence of the pyroelectric coefficient, $p$ on annealing temperatures.	75
Figure 4.13	Frequency dependence of $\epsilon'$ and $\epsilon''$ for (a) unpoled and (b) poled PVDF thin films at a temperature step size of 10 °C.	77
Figure 4.14	Temperature dependence of $\epsilon'$ and $\epsilon''$ at 1 kHz for unpoled (filled circles) and poled (open circles) PVDF.	78
Figure 4.15	Observed and fitted dielectric spectra of PVDF at 140 °C.	79
Figure 4.16	Degree of crystallinity and rms roughness plotted as a function of annealing temperature.	80
Figure 4.17	Plots of the degree of crystallinity, $X_c$ , remanent polarization, $P_r$ and pyroelectric coefficient, $p_y$ as a function of annealing temperature.	81
Figure 4.18	Comparison of Form IV and Form I PVDF <i>D-E</i> hysteresis loops.	82
Figure 4.19	Switching process based on 60° rotation model in Form I.	83
Figure 4.20	Proposed switching process based on 60° rotation model in Form IV.	84
Figure 4.21	Unit cells of (a) the Form II and (b) the Form IV of PVDF shown in projection of <i>ab</i> -plane. Arrows indicate the dipole direction normal to the molecular axes. Schematic picture at the bottom represent the orientation of the (100), (020) and (110) plane in the spin-coated PVDF thin films.	85
Figure 4.22	Dipole reversal due to molecular motion in the Form II PVDF: (a) vacuum moment is aligned parallel along the molecule chain axis; and (b) vacuum moment is aligned in perpendicular with molecule chain axis.	88
Figure 4.23	Plot of $\log \tau$ vs $1/T$ for Form II and Form IV PVDF thin films.	93
Figure 4.24	Plots of the pyroelectric coefficient, $p_y$ as a function of remanent polarization, $P_r$ of PVDF.	96

Figure 5.1	FTIR spectra of (a) the PVDF films annealed at 60 °C, 100 °C and 140 °C, (b) samples P1 and PT2 annealed at 140 °C.	104
Figure 5.2	XRD spectra of PVDF annealed at 60 °C, 100 °C and 140 °C.	105
Figure 5.3	XRD spectra of PVDF and PVDF/TiO <sub>2</sub> films annealed at 140 °C.	106
Figure 5.4	XRD spectra for unpoled and poled (a) PVDF and (b) PT2 thin film; (c) deconvolution of XRD spectrum for poled PT2 thin film.	107
Figure 5.5	SEM images of (a) sample P1 annealed at 60 °C, (b) sample PT2 annealed at 140 °C and (c) an amplified picture of (b).	109
Figure 5.6	The dependence of the pyroelectric coefficient $p_y$ with respect to the weight percentage of TiO <sub>2</sub> and the annealing temperature.	111
Figure 5.7	Dielectric spectra of (a) PVDF and (b) PT2 composite after annealed at 140 °C respectively.	113
Figure 5.8	Dielectric spectra of various samples annealed at 60°C and 140°C.	115
Figure 5.9	A two phase system composed of a polymer matrix (phase 1) and spherical inclusions (phase 2).	117
Figure 5.10	Various models of the effective dielectric constant of PT2 annealed at 140 °C.	117
Figure 6.1	Dielectric and conductive spectra for PVDF and PVDF/La <sub>2</sub> O <sub>3</sub> composites at room temperature.	127
Figure 6.2	A two-phase system composed of a polymer matrix (phase 1) and spherical inclusions (phase 2).	128
Figure 6.3	Various models of the effective dielectric constant of PVDF/La <sub>2</sub> O <sub>3</sub> with 3 wt% of La <sub>2</sub> O <sub>3</sub> annealed at 140 °C.	128
Figure 6.4	Pyroelectric coefficients as a function of annealing temperature.	131
Figure 6.5	<i>D-E</i> hysteresis loops of PVDF and PVDF/La <sub>2</sub> O <sub>3</sub> annealed at 140 °C.	136
Figure 6.6	X-ray diffractograms of PVDF-La <sub>2</sub> O <sub>3</sub> (3 wt%) thin films: (a) effect of poling and (b) XRD deconvolution of Form IV PVDF after poling.	138

## LIST OF TABLES

		Page
Table 2.1	Symbols of the 32 point groups in crystallography. Remarks: * implies that piezoelectric effect may be exhibited and + implies that pyrorlectric and ferroelectric effects may be exhibited.	21
Table 4.1	Summary of x-ray diffraction results of PVDF (before and after poling).	71
Table 4.2	Spontaneous polarization of PVDF calculated with various theoretical models.	87
Table 6.1	Local field coefficient as a function of inclusion wt% (subscripts 1 and 2 denote the polymer phase and inclusion, respectively).	141
Table A1	Partial charge value.	150
Table A2	Atomic coordinates of Form I PVDF.	150
Table A3	Atomic coordinates of Form II (or Form IV).	151

## LIST OF SYMBOLS

$C$	Curie constant
$C_0$	Capacitive component
$c$	Elastic constant
$D$	Displacement
$D_0$	Average electric displacement
$d$	Piezoelectric strain coefficient
$E$	Electric field
$E_0$	Amplitude of electric field
$E_c$	Coercive electric field
$e$	Stress constant
$F$	External force
$f$	Frequency
$I$	Current
$I_C$	Capacitive component of the current
$I_R$	Resistive component of the current
$I_p$	Pyroelectric current
$L_E$	Local electric coefficient
$P$	Polarization
$P_r$	Remnant polarization
$P_s$	Spontaneous polarization
$\vec{P}$	Average polarization per unit volume
$\vec{p}$	Electric dipoles moments
$p_y$	Pyroelectric coefficient
$p _{primary\ effect}$	Primary pyroelectricity



$P _{\text{secondary effect}}$	Secondary pyroelectricity
$S$	Entropy
$T$	Temperature
$T_0$	Curie-Weiss temperature
$T_c$	Curie temperature
$\Delta T$	Small uniform change in temperature
$t$	Time
$V$	Applied voltage
$X_c$	Degree of crystallinity
$\alpha_3$	Thermal expansion coefficient
$\delta$	Phase lag
$\epsilon_0$	Permittivity of free space
$\epsilon'$	Real permittivity
$\epsilon''$	Imaginary permittivity
$\epsilon^*$	Complex relative permittivity
$\epsilon_s$	Instantaneous relative permittivity
$\epsilon_\infty$	Static dielectric permittivity
$\Delta\epsilon$	Dielectric strength
$\epsilon$	Strain
$\mu$	Dipole moment per unit volume
$\sigma^*$	Complex conductivity
$\sigma'$	Real conductivity
$\sigma''$	Imaginary conductivity
$\sigma_{dc}$	dc conductivity
$\omega$	Angular frequency

$\tau$	Relaxation time
$\theta$	Incident angle in X-ray diffraction
$\varnothing$	Weight fraction

## Chapter 1: Introduction

### 1.1 Introduction

Ferroelectric materials offer a very wide range of advantageous properties for scientist and electronic engineer to exploit. A class of dielectric materials having non-centrosymmetric crystals possess a unique axis are said to be polar. Polar crystals are piezoelectric and exhibit pyroelectricity and ferroelectricity due to its built in dielectric polarization, which is defined as spontaneous polarization,  $P_s$  within the unit cell of the crystal structure. More precisely, ferroelectric crystals exist for which the application of a sufficient magnitude of electric field to cause the  $P_s$  to switch to a different, stable direction. Upon removal of the electric field, its polarization will not return to its original direction and magnitude. Ferroelectric materials are extensively applied in a myriad of critical technologies such as nonvolatile random access memories, field-effect transistors, sensors, actuators and solar cells (Ahn et al., 1997; Garcia et al., 2009; Lu et al., 2012; J. F. Scott, 2007; James F. Scott & Paz de Araujo, 1989; Yuan et al., 2011). On the other hand, pyroelectric crystals induce a change of  $P_s$  upon changing of temperature. Such materials have a wide range of potential applications, including most notable sensors based on small changes in heat (e.g., for fire detector and child-sensing systems) and a variety of thermal imaging system (e.g., for night vision systems, medical thermography) (Uhlmann, Dawley, Poisl, Zelinski, & Teowee, 2000).

Ferroelectrics are commercially widely used in a various forms, covering from single crystals through polycrystalline ceramics and thin films to polymers. Typical examples include Rochelle salt, potassium dihydrogen phosphate ( $\text{KH}_2\text{PO}_4$ ), barium titanate ( $\text{BaTiO}_3$ ) and lead zirconate titanate (PZT). Most of them are in the form of stiff crystalline solid. There are various types of materials display ferroelectric properties. New ferroelectric materials which are different from the traditional ones in various aspects are

highly desired. One of them is a series of non-solid ferroelectric liquid crystals with a rod-like structure. Such a liquid crystal is DOBAMBC which has been synthesized by Meyer *et al.* in 1975 (Meyer, Liebert, Strzelecki, & Keller, 1975). It demonstrated ferroelectric polarization reversal in its chiral smectic C ( $S_c^*$ ) phase. The others materials include ferroelectric polymers represented by poly(vinylidene fluoride) (PVDF) and its copolymers. Both of the polymers were widely investigated these years because of their application in soft transducers and fast display as well as the unique mechanism of ferroelectricity (T. Furukawa, 1989).

In 1963, the first ever piezoelectricity were found in poly(methy methacrylate) and poly(vinyl chloride) organic polymers by Kocharyan (Kocharyan & Pachadzhyan, 1968). In 1969, Kawai has first discovered exceptionally large piezoelectric properties in poly(vinylidene fluoride), PVDF in the form of electret after poling (Kawai, 1969). PVDF was poled with an effective macroscopic separation of positive and negative charges by applying an electric field either by orienting permanent dipoles or creating space charge by injecting free charges. In 1971, the pyroelectric and non-linear optical properties of PVDF were also reported by Bergmann (Bergman, 1971). These observations led to the speculation to the possibility of classifying PVDF as ferroelectric materials (Nalwa, 1995).

Since, the term “electret” has been repeatedly used in the early discoveries of PVDF, it is worth to give a brief definition. Polymers are readily exhibited three distinct mechanisms of electric polarization (Eberle, Schmidt, & Eisenmenger, 1996; Fukada, 1989), namely ferroelectricity, electret and non-uniform space-charge. Ferroelectrics are defined as crystalline materials in which the unit cell is polar and the direction of polarization can be changed by the application of an electric field (Lines & Glass, 1977). The bistability of the polarization can be exhibited by polarization hysteresis using a cycled electric field with an amplitude larger than a characteristic coercive field. The polarization is thermal

equilibrium state. On the other hand, an electret is a material which a polarization can be induced by the application of a high electric field. It is metastable and does not represent an equilibrium ground state (Chang, Pei, & Chan, 2008; Lee, Salomon, & Labes, 1979; Mopsik & Broadhurst, 1975; Sessler, 1987). The alignment of the dipoles in the electret is primarily a consequence of the external electric field, associated with very little or no cooperative interaction among the dipoles. Because of this, the induced polarization is metastable and in the absence of an electric field, it will relax to a non-polar equilibrium state. The relaxation time of an electret can be very long, from seconds to years, resulting in an apparent polarization hysteresis as the dipolar alignment lags behind the applied electric field. Space charge is the other kind of mechanism which will produce an apparent polarization hysteresis due to time lag between field and charge transport or to the nonlinear injection from the electrodes, or both (Lee et al., 1979; Poulsen & Ducharme, 2010). Its electric displacement remains non-zero after the removal of external field. Its life span could be long enough if the traps are deep enough.

The discoveries of ferroelectricity in PVDF have eventually led to the new field of ferroelectric polymer science, and thereafter it has emerged as ferroelectric polymer par excellence. Subsequently, tremendous amount of efforts were focused on exploring the material science, physics and organic electronic of PVDF and other fluorocarbon polymers. As a result, the developments of PVDF and its copolymers with TrFE and TeFE have been extremely fast. Although, the incorporation of the copolymers with PVDF have reduced the spontaneous polarization, but the replacement of hydrogen atoms with the fluorine atoms has led to significant increase in crystallinity by annealing, whereas in PVDF, the crystallinity is typically limited to 50 %. In addition, the enormous growth in other ferroelectric polymers such as odd nylons, cyanopolymers, polyureas and ferroelectric liquid crystal polymers has also attracted attention for their electric properties. However,



these substances have not yet been developed extensively compared to PVDF. Nevertheless, PVDF appeared as the best example of a special organic ferroelectric polymer due to its compact linear molecular structure.

PVDF are well established with four polymorphs, referred as Form I, II, III and IV (alternatively  $\beta$ ,  $\alpha$ ,  $\gamma$  and  $\delta$  -phase, respectively). However, most research focus for functional ferroelectricity has been focused on Form I crystalline due to its exceptional large spontaneous polarization. Among the four polymorphs, only Form II is a non-polar. The other two: Form III and IV are polar because of their parallel packing. Yet, these polymorphs are not well understood because they are always available in mixture of various polymorphs as well as non-crystalline regions (Itoh, Takahashi, Furukawa, & Yajima, 2014). Therefore, detail analysis is needed to characterize the structural and functional electrical properties of these specific polymorphous.

In order to improve the functional properties of the ferroelectric polymer, ferroelectric ceramic inclusions such as BaTiO<sub>3</sub> (Fang, Yang, Zhang, & Wang, 2009), PbTiO<sub>3</sub> (B. Ploss, Ploss, Shin, Chan, & Choy, 1998; B. Ploss, B. Ploss, F. G. Shin, H. L. W. Chan, & C. L. Choy, 2000; Beatrix Ploss, Bernd Ploss, F. G. Shin, H. L. W. Chan, & C. L. Choy, 2000) and PbZrTiO<sub>3</sub> (Takeo Furukawa & Fukada, 1977; T. Furukawa, Ishida, & Fukada, 1979; Bernd Ploss, Ng, Chan, Ploss, & Choy, 2001) are embedded in a polymer matrix as a filler to form 0-3 type composites to enhance the desired functional properties. These ceramic inclusions are conventional ferroelectric materials which exhibit high dielectric permittivity as well as large spontaneous polarization. Furthermore, the remarkable piezoelectric, pyroelectric and ferroelectric properties of these ceramic fillers, together with the high degree of flexibility of the polymers component have offered a promising potential for functional electronic application. In the present work, an alternative method has been demonstrated to improve the pyroelectric and ferroelectric properties of

PVDF compare to the current conventional studies mentioned above. The prospect of using non-ferroelectric inclusions:  $\text{TiO}_2$  and  $\text{La}_2\text{O}_3$ , to further improve the poling mechanism on the PVDF in the field of functional electrical properties have been reconsidered. An interfacial relaxation phenomenon (Maxwell-Wagner effect) which is attributed to the heterogeneity structure of the constituents in the polymer matrix is taken into consideration to explain the enhanced efficiency of poling process. As a result, the electrical properties of the polymer composite can be enhanced at a much lower poling electric field than the values which required by the pure PVDF.

In this thesis, efforts were made to gain insight into fundamental understanding of the structural and functional electrical properties of Form IV PVDF. The main purpose of this study is to investigate the dielectric, pyroelectric and ferroelectric properties of Form IV PVDF. The specific objectives of this research are:

- To study the effect of annealing on the crystalline structural and morphology of spin-cast PVDF.
- To evaluate the pyroelectric constant and remanent polarization of Form IV PVDF.
- To study the molecular dynamic motions by using dielectric spectroscopy and its correlation with electric field.
- To investigate the effect of non-ferroelectric inclusion in PVDF thin film for its poling mechanism in order to enhance its pyroelectric and ferroelectric properties.

The principle aim of this thesis is to investigate the underlying pyroelectric and ferroelectric properties of Form IV PVDF. Chapter 2 of this thesis reviews the fundamental

aspects of mechanism involved in the polarization of dielectric, ferroelectric, pyroelectric and piezoelectric materials. The background of the material used in this study, PVDF, the unresolved issues and the motivation of the research were presented. Chapter 3 introduces the details on experimental work and theoretical aspects of the experiments. The preparation of the samples for electrical measurements is discussed in depth. The principles and equipment setup for the electrical measurement used in this study has also been presented in details.

Chapter 4 reveals the ferroelectric switching characteristics and pyroelectric properties of Form IV PVDF prepared by spin-coating technique. The samples were subjected to annealing and resulted in changes in crystallinity. It will be shown that the ferroelectric and pyroelectric properties are strongly governed by degree of crystallinity. To date, no details dielectric analysis on Form IV PVDF is presented. In particular, a wide range dielectric spectroscopy has also been extended to determine the molecular dynamic of Form IV PVDF. By combining the results from the above finding with the detail analysis on the crystalline and structure morphology, fundamental understanding on the extraordinary electrical responses of Form IV PVDF induced by electric field has been revealed.

Chapter 5 introduces an alternative approach in the use of a non-ferroelectric inclusion involving a two phase system which can enhance the pyroelectric activity after poling process. An interfacial relaxation phenomenon (Maxwell-Wagner effect) which is attributed to the heterogeneity structure of the constituents in the polymer matrix is taken into consideration to explain the enhanced efficiency of the poling process in this composite thin film.

Chapter 6 further explores the possibility of incorporating of another non-ferroelectric inclusion in PVDF matrix to further enhance its functional electrical properties. In this chapter,  $\text{La}_2\text{O}_3$  was introduced into the polymer matrix to form a two-phase composite system. The obtained results suggest that contribution of the electrical conductivity of the inclusion could enhance the pyroelectric and ferroelectric properties of the polymer matrix. A simple Maxwell-Wagner model which is attributed to the heterogeneity structure of the constituents in the polymer matrix is taken into consideration to explain the enhanced efficiency of poling process. This work provides a fundamental insight to enhance pyroelectric and ferroelectric properties of the polymer by introducing the low conductivity impurity in a composite system. Finally, Chapter 7 summarizes all the results and explores the possible future research works.

### References:

- Ahn, C. H., Tybell, T., Antognazza, L., Char, K., Hammond, R. H., Beasley, M. R., Fischer, Ø., Triscone, J.-M. (1997). Local, Nonvolatile Electronic Writing of Epitaxial  $\text{Pb}(\text{Zr}_{0.52}\text{Ti}_{0.48})\text{O}_3/\text{SrRuO}_3$  Heterostructures. *Science*, 276(5315), 1100-1103.
- Bergman, J. G. (1971). Pyroelectricity and Optical Second Harmonic Generation in Polyvinylidene Fluoride Films. *Applied Physics Letters*, 18(5), 203-205.
- Chang, C.-C., Pei, Z., & Chan, Y.-J. (2008). Artificial electrical dipole in polymer multilayers for nonvolatile thin film transistor memory. *Applied Physics Letters*, 93(14), 143302.
- Eberle, G., Schmidt, H., & Eisenmenger, W. (1996). Piezoelectric polymer electrets. *IEEE Transactions on Dielectrics and Electrical Insulation*, 3(5), 624-646.
- Fang, F., Yang, W., Zhang, M. Z., & Wang, Z. (2009). Mechanical response of barium-titanate/polymer 0–3 ferroelectric nano-composite film under uniaxial tension. *Composites Science and Technology*, 69(5), 602-605.

- Fukada, E. (1989). Introduction: Early studies in piezoelectricity, pyroelectricity, and ferroelectricity in polymers. *Phase Transitions*, 18(3-4), 135-141.
- Furukawa, T. (1989). Ferroelectric properties of vinylidene fluoride copolymers. *Phase Transitions*, 18(3-4), 143-211.
- Furukawa, T., & Fukada, E. (1977). Piezoelectric Relaxation in Composite Epoxy-PZT System due to Tonic Conduction. *Japanese Journal of Applied Physics*, 16(3), 453-458.
- Furukawa, T., Ishida, K., & Fukada, E. (1979). Piezoelectric properties in the composite systems of polymers and PZT ceramics. *Journal of Applied Physics*, 50(7), 4904-4912.
- Garcia, V., Fusil, S., Bouzehouane, K., Enouz-Vedrenne, S., Mathur, N. D., Barthelemy, A., & Bibes, M. (2009). Giant tunnel electroresistance for non-destructive readout of ferroelectric states. *Nature*, 460(7251), 81-84.
- Itoh, A., Takahashi, Y., Furukawa, T., & Yajima, H. (2014). Solid-state calculations of poly(vinylidene fluoride) using the hybrid DFT method: spontaneous polarization of polymorphs. *Polymer Journal*.
- Kawai, H. (1969). The Piezoelectricity of Poly (vinylidene Fluoride). *Japanese Journal of Applied Physics*, 8, 975-976.
- Kocharyan, N. M., & Pachadzhyan, K. B. (1968). The piezoelectric effect in polymers. *Polymer Mechanics*, 4(1), 117-119.
- Lee, H., Salomon, R. E., & Labes, M. M. (1979). Pyroelectricity due to a space-charge mechanism in a copolymer of acrylonitrile and vinylidene chloride. *Journal of Applied Physics*, 50(5), 3773-3774.
- Lines, M., & Glass, A. (1977). Principles and applications of ferroelectrics and related materials. *Oxford University Press*.
- Lu, H., Bark, C.-W., Esque de los Ojos, D., Alcala, J., Eom, C. B., Catalan, G., & Gruverman, A. (2012). Mechanical Writing of Ferroelectric Polarization. *Science*, 336(6077), 59-61.
- Meyer, R. B., Liebert, L., Strzelecki, L., & Keller, P. (1975). Ferroelectric liquid crystals. *Journal de Physique Lettres*, 36, 3.

- Mopsik, F. I., & Broadhurst, M. G. (1975). Molecular dipole electrets. *Journal of Applied Physics*, 46(10), 4204-4208.
- Nalwa, H. S. (1995). *Ferroelectric Polymers: Chemistry, Physics and Applications*. Marcel Dekker, New York, 28.
- Ploss, B., Ng, W.-Y., Chan, H. L.-W., Ploss, B., & Choy, C.-L. (2001). Poling study of PZT/P(VDF-TrFE) composites. *Composites Science and Technology*, 61(7), 957-962.
- Ploss, B., Ploss, B., Shin, F. G., Chan, H. L. W., & Choy, C. L. (1998). *Separate poling of inclusions and matrix in PT/P(VDF-TrFE) 0-3 composites*. Paper presented at the Applications of Ferroelectrics, 1998. ISAF 98. Proceedings of the Eleventh IEEE International Symposium on Applications of Ferroelectrics.
- Ploss, B., Ploss, B., Shin, F. G., Chan, H. L. W., & Choy, C. L. (2000). Pyroelectric activity of ferroelectric PT/PVDF-TRFE. *IEEE Transactions on Dielectrics and Electrical Insulation*, 7(4), 517-522.
- Ploss, B., Ploss, B., Shin, F. G., Chan, H. L. W., & Choy, C. L. (2000). Pyroelectric or piezoelectric compensated ferroelectric composites. *Applied Physics Letters*, 76(19), 2776-2778.
- Poulsen, M., & Ducharme, S. (2010). Why ferroelectric polyvinylidene fluoride is special. *IEEE Transactions on Dielectrics and Electrical Insulation*, 17(4), 1028-1035.
- Scott, J. F. (2007). Applications of Modern Ferroelectrics. *Science*, 315(5814), 954-959.
- Scott, J. F., & Paz de Araujo, C. A. (1989). Ferroelectric Memories. *Science*, 246(4936), 1400-1405.
- Sessler, G. M. (1987). *Electrets*. Springer Verlag, 33.
- Uhlmann, D. R., Dawley, J. T., Poisl, W. H., Zelinski, B. J. J., & Teowee, G. (2000). Ferroelectric Films. *Journal of Sol-Gel Science and Technology*, 19(1-3), 53-64.
- Yuan, Y., Reece, T. J., Sharma, P., Poddar, S., Ducharme, S., Gruverman, A., Yang, Y., Huang, J. (2011). Efficiency enhancement in organic solar cells with ferroelectric polymers. *Nat Mater*, 10(4), 296-302.

## **Chapter 2: Literature Review**

### **2.1 Introduction**

This chapter presents a simplified explanation of the ferroelectric phenomenon. It begins with a brief overview of mechanisms involved in the polarization of dielectric, ferroelectric, pyroelectric and piezoelectric materials. The functional electrical properties are explained with the basic mathematical formulations which have been long established. It also discusses the essential concept of ferroelectric phenomena which is important in order to explain the application in ferroelectricity. This chapter also introduces the background of the materials, the unresolved issues and the motivation of the research.

### **2.2 Dielectric properties**

The electrical properties of a ferroelectric substance can always be described by examining thoroughly the material's responses to the application of an electric field. When an external electric field is applied on a solid material, the medium adapts to the perturbation by dynamically changing the positions of the nuclei and electrons. As a result, a phenomenon called polarization is created as the dipoles are aligned under the influence of an applied electric field. In general, there are two types of dielectrics. The first type is known as polar dielectrics which have permanent electric dipole moments, whereas the second type is the non-polar dielectrics in which do not possess permanent electric dipole moment.

There are three main types of polarization: electronic, ionic (atomic) and dipolar (orientation) (Kremer & Schönhal, 2003). Figure 2.1 shows the dependence of each polarization mechanism which contributes to the overall polarization of materials on the frequency of the applied field. An electronic polarization (see Figure 2.2(a)) may be induced from a slight displacement of the electron cloud of any atom in the dielectric

relative to its positive nucleus. Typically, it occurs within frequency range of  $10^{15}$  Hz and produces a value of dielectric constant of  $\sim 2$ . An electric field which distorts the arrangement of atomic nuclei ( $\sim 10^{13}$  Hz) result in the exhibition of atomic polarization as shown in Figure 2.2(b). The orientation polarization (see Figure 2.2(c)) is found only in the substances that possess permanent dipole moments. It is induced from a rotation of the permanent moments into direction of the applied field. In addition, another source of polarization known as interfacial polarization does exist due to the space charges that are trapped at electrodes and at heterogeneous structure such as grain boundaries. Each of the polarization is strongly dependence on the applied field frequency. The total electric polarization of a dielectric substance is resulted from the sum of electronic, atomic and orientation (and sometimes present of interfacial polarization due to impurities) polarizations. The average polarization per unit volume,  $\vec{P}$  is produced by  $N$  amounts of electric dipoles moments,  $\vec{p}$  which are all aligned, is given by (Dahiya & Valle, 2013; Kremer & Schönhal, 2003):

$$\vec{P} = \frac{1}{Volume} \sum_{i=0}^N \vec{p}_i \quad (2.1)$$



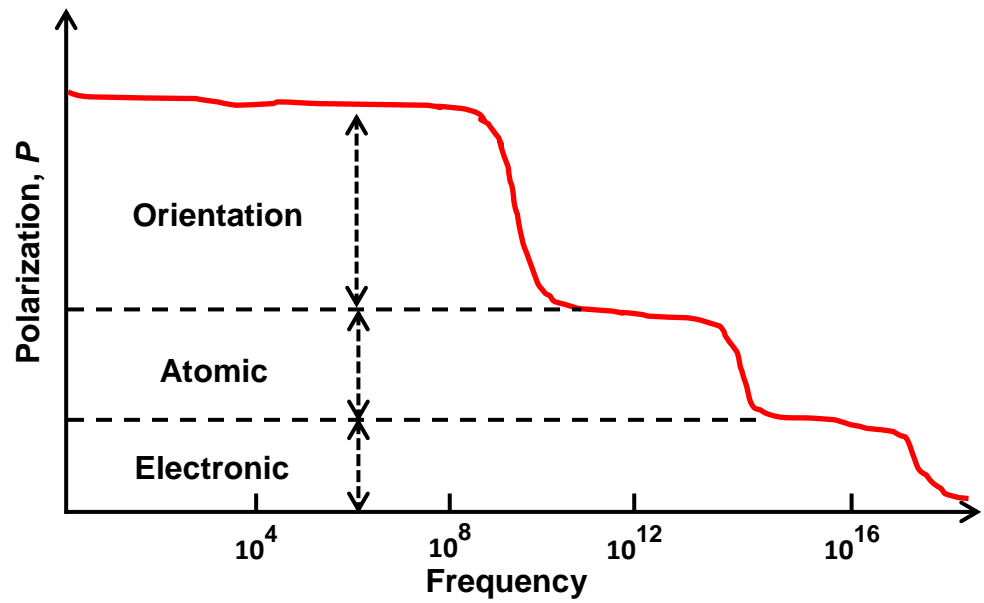


Figure 2.1: Frequency dependence of various polarization mechanisms (Dahiya & Valle, 2013; Kremer & Schönhal, 2003).

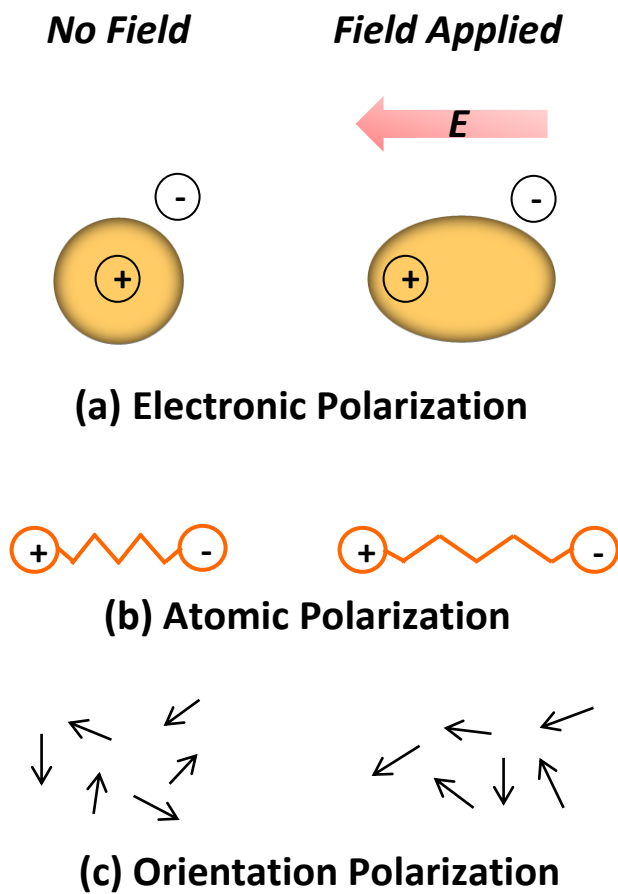


Figure 2.2: Mechanism of polarization (Dahiya & Valle, 2013).

In general, dielectric properties are characterized by the dielectric constant (representing polarization) and by the dielectric loss (representing relaxation phenomena). The dielectric constant of substances varies with frequency. Each spectrum that indicates specific relaxation processes and resonance is evaluated at different frequencies. When an external applied field is alternating on the substance, it causes a lag in attaining of equilibrium which is normally referred as relaxation. The dielectric relaxation phenomenon is the exponential decay of the polarization with time in a dielectric when the external applied field is removed. This phenomenon is due to the anomalous dispersion in which the dielectric constant decreases with increasing frequency. The relaxation time is defined as the time in which this polarization is reduced to  $1/e$  times to its original value, where  $e$  is the base of natural logarithm.

Orientation polarization of molecular dipoles is a relatively slower process if compared to that of electronic and atomic polarization which is observed in a much higher frequency range. To attain equilibrium maximum orientation polarization, a sufficient time is required to allow the application of an electric field to be realized in the material. Only if ample time is provided, the relative permittivity called *static dielectric permittivity*,  $\epsilon_{\infty}$  can be observed. In contrast, if the polarization is measured immediately after the field is applied, then a low magnitude of *instantaneous relative permittivity*,  $\epsilon_s$  will be obtained. It is expected that there will be dispersion from high to low relative permittivity in between these two extremes of time scale. A resonant effect is usually associated with electronic or atomic polarization; whereas, a relaxation effect is usually associated with orientation polarization (Kremer & Schönhal, 2003).

This phenomenon can be examined by considering an application of an alternating electric field,  $E$ , with an amplitude,  $E_0$ , and angular frequency,  $\omega$ , across a dielectric material as below:

$$E = E_0 \cos \omega t \quad (2.2)$$

If the frequency is high enough, this will produce a polarization. The orientation of any dipoles which are present will inevitable lag behind the applied field. The phase lag is denoted as  $\delta$  and this phase lag in the electric displacement,  $D$  will be defined as:

$$D = D_0 \cos(\omega t - \delta) \quad (2.3)$$

which can be rewritten as :

$$D = D_1 \cos \omega t - D_2 \sin \omega t \quad (2.4)$$

where  $D_1 = D_0 \cos \delta$  and  $D_2 = D_0 \sin \delta$

As a result, the real and imaginary permittivities can be defined as:

$$\epsilon' = \frac{D_1}{\epsilon_0 E_0} \quad \text{and} \quad \epsilon'' = \frac{D_2}{\epsilon_0 E_0} \quad (2.5)$$

thus, the tangent loss can also relate as:

$$\frac{\epsilon''}{\epsilon'} = \tan \delta \quad (2.6)$$

these quantities are presented as *complex relative permittivity*:

$$\epsilon^* = \epsilon' - i\epsilon'' \quad (2.7)$$

The meaning of the real and imaginary parts can be appreciated when considering a material in a capacitor. The current,  $I$  flows in the external circuit after application of an alternating voltage given by the real part of  $V(V = V_0 e^{i\omega t})$  can be evaluated from the complex relative permittivity as follows:

$$I = \epsilon^* C_0 \frac{dV}{dt} = i\omega \epsilon^* C_0 V = \omega C_0 (\epsilon'' + i\epsilon') V \quad (2.8)$$

this implies that a capacitive component of the current leads the voltage by  $90^\circ$ ,

$$I_C = i\omega C_0 \epsilon' V \quad (2.9)$$

where a resistive component is in phase with the voltage,

$$I_R = \omega C_0 \epsilon'' V \quad (2.10)$$

the physical meaning of the quantity  $\tan \delta$  previously defined by Eq. (2.6) becomes:

$$\tan \delta = \frac{\varepsilon''}{\varepsilon'} \sim \frac{\text{energy dissipated per cycle}}{\text{energy per cycle}} \quad (2.11)$$

The ratio of the loss tangent,  $\varepsilon''/\varepsilon'$  is usually employed for direct measurement in a dielectric loss. Relaxation time,  $\tau$  is defined as:

$$f(\tau) = \frac{1}{e} \quad (2.12)$$

that is, the time during the polarization decayed to  $1/e$  of its original value. For the maximum loss factor, the angular frequency (*critical frequency*), should be as:

$$\omega_m = \frac{1}{\tau} \quad (2.13)$$

Relaxation time,  $\tau$  is a measure of the mobility of the molecules (dipoles) that exist in a material. It is the time required for dipoles aligned in an electric field to return to  $1/e$  of its random equilibrium value (or the time required for dipoles to become oriented in an electric field). Liquid and solid materials have molecules that are in a condensed state with limited freedom to move when an electric field is applied. Constant collisions cause internal friction so that the molecules turn slowly and exponentially approach the final state of orientation polarization with relaxation time constant,  $\tau$ . When the field is removed, the sequence is reversed and random distribution is restored with the same time constant. However, it is more convenient to use the critical frequency  $f_m$  instead of  $\omega_m$ :

$$f_m = \frac{\omega_m}{2\pi} = \frac{1}{2\pi\tau} \quad (2.14)$$

One of the most important applications of dielectric spectroscopy is the investigation of relaxation processes which are due to rotational fluctuations of molecular dipoles. Relaxation processes are usually characterized by a peak in the imaginary part  $\varepsilon''$  and a step-like decrease of the real part  $\varepsilon'$  of the complex dielectric permittivity,  $\varepsilon^* = \varepsilon' -$

$i\epsilon''$  with increasing frequency as shown in Fig 2.3. In contrast, an increase of the imaginary part of the dielectric function with decreasing frequency will be observed in a conduction phenomenon. It is important to note that the real part of a complex dielectric function for pure ohmic conduction is independent of the frequency; while, the imaginary part increases with decreasing frequency. At low frequency regime, the alternating electric field is slow enough so that the dipoles are able to keep the pace with the field variations. Since the polarization is able to develop fully, the loss,  $\epsilon''$  is directly proportional to the frequency. When the frequency increases,  $\epsilon''$  continues to increase but the storage of real part  $\epsilon'$  begins to decrease due to the phase lag between the dipole alignment and the electric field. Above the relaxation frequency, both  $\epsilon'$  and  $\epsilon''$  drop off as the electric field is too fast to influence the dipole rotation and the orientation polarization disappears.

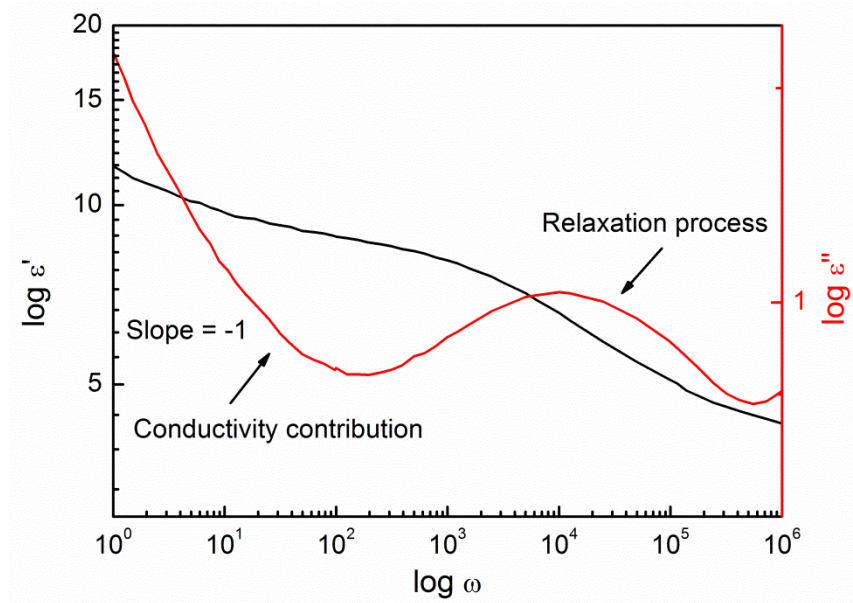


Figure 2.3: Scheme of the real  $\epsilon'$  (black line) and the imaginary  $\epsilon''$  (red line) part of the complex dielectric function for a relaxation process.

Dielectric relaxation processes are normally analyzed by using several models. Debye function serves an essential function approach which is given by (Kremer & Schönhal, 2003):

$$\varepsilon^* = \varepsilon_\infty + \frac{\Delta\varepsilon}{1 + i\omega\tau_D} \quad (2.15)$$

where  $\Delta\varepsilon$  is the dielectric relaxation strength,  $\varepsilon_\infty$  is the infinite relative dielectric permittivity and Debye relaxation time,  $\tau_D$  which is related to the relaxation peak's position. In reality, the relaxation peaks are asymmetric with a high frequency tail where its half width of measured loss peaks is much broader as predicted by Debye function. This is literally called as non-Debye (non-ideal) relaxation behavior. As a result, we have a broadening of the dielectric function as described by Cole-Cole (Kremer & Schönhal, 2003):

$$\varepsilon^* = \varepsilon_\infty + \frac{\Delta\varepsilon}{1 + (i\omega\tau_{CC})^\alpha} \quad (2.16)$$

where  $0 < \alpha \leq 1$  leads to a symmetrical broadening of the relaxation peaks which is comparable to Eq. (2.15). When  $\alpha = 1$ , the Debye function is obtained. The relaxation time,  $\tau_{CC}$  denotes the position of a maximal loss where  $\omega = 1/\tau_{CC}$ .

Cole-Davidson function shows that the complex dielectric function can have also an asymmetric broadening peak as stated by (Kremer & Schönhal, 2003):

$$\varepsilon^* = \varepsilon_\infty + \frac{\Delta\varepsilon}{(1 + i\omega\tau_{CD})^\alpha} \quad (2.17)$$

Here,  $\alpha$  parameter describes an asymmetric broadening of the relaxation function. It should be noted that the relaxation time of this asymmetric model does not coincide with the relaxation time which is related to the position of a maximal loss. The relationship of both quantities depends on the shape parameters. A more general solution was then introduced

by Havriliak and Negami (HN-function) which is in fact a combination of the Cole-Cole and the Cole-Davidson function (Kremer & Schönhal, 2003):

$$\varepsilon^* = \varepsilon_\infty + \frac{\Delta\varepsilon}{((1 + i\omega\tau_{CD})^\alpha)^\beta} \quad (2.18)$$

For the fractional share parameters  $\alpha$  and  $\beta$  which describes the symmetric and asymmetric broadening of the complex dielectric function  $0 < \alpha, \alpha\beta \leq 1$  holds. The  $\alpha$  and  $\beta$  are related to the limiting behavior of the complex dielectric function at low and high frequencies. HN-function offers a better fitting scheme for a complete description of an isolated region with at least a set of four parameters involved which will be applied in this study.

## 2.3 Ferroelectric Properties

### 2.3.1 Structural Symmetry

Structural symmetry of a crystal is depending on its lattice structure. The lattice structure is described by Bravais unit cell of the crystal. There are more than thousands of crystals in nature. However, only thirty-two macroscopic symmetry types of crystals (32 point groups) (Xu, 1991). The thirty-two point groups with their symbols are shown in Table 2.1. A point group consists of eight symmetry elements (excluding translation symmetry). These eight symmetry elements are listed as the following: rotation axes: 1 (without rotation), 2 (rotation diad), 3 (rotation triad), 4 (rotation tetrad), 6 (rotation hexad),  $\bar{4}$  (rotation-inversion tetrad axis), inversion center  $i$  and reflection mirror  $m$ . If translation symmetry element is counted in, these symmetry elements comprise 230 microscopic symmetry types (space groups) (Xu, 1991).

Both structural and physical properties of a crystal are mainly governed by structural symmetry of the crystal. Neumann's principle stated that symmetry elements of

all physical properties in a crystal should include all symmetry element of the point group of this crystal. Thus, if a physical parameter is subjected to a symmetry operation of this crystal, the value of this physical parameter should remain invariant. Piezo- and pyroelectricity arise from changes in the internal polarization of a dielectric material for small changes in stress and temperature respectively. A material which exhibits piezo- and pyroelectric if its crystalline is inherently asymmetric, i.e., the material lacks an inversion center.

Among the thirty-two point groups, there are eleven point groups that are centrosymmetry type with a symmetry center (Xu, 1991). A crystal having a symmetric center does not possess any polarity. These eleven point groups are  $\bar{1}$ ,  $2/m$ ,  $mmm$ ,  $4/m$ ,  $(4/m)mm$ ,  $\bar{3}$ ,  $\bar{3}m$ ,  $6/m$ ,  $(6/m)mm$ ,  $m\bar{3}$  and  $m\bar{3}m$ . The rest of twenty-one point groups among the thirty-two point group do not have a centrosymmetry. The crystal that has these point-group symmetry possess one or more crystallographically unique direction axes. The two opposite ends of a crystallographically unique direction axis cannot be made coincide with each other by any symmetry operation of this crystal. All the noncentrosymmetric point groups, except point group 432, exhibit piezoelectric effect along a unique direction axis. Even though the 432 does not have any centrosymmetry, it has other symmetry elements whose combination can exclude the piezoelectric activity.

The other twenty point groups may exhibit piezoelectric effect (Xu, 1991). Ten points group out of the mentioned twenty point groups have only one unique direction axis. They are 1, 2,  $m$ ,  $mm2$ , 4,  $4mm$ , 3,  $3m$ , 6, and  $6mm$ . A crystal having this point-group symmetry has a unique rotation axis, but does not have any mirror perpendicular to this axis. Along a unique rotation axis, the atomic arrangement at one end is different from that at the other (opposite end). Such kinds of crystals are called polar crystals which exhibit



spontaneous polarization. A restricted group of pyroelectrics have the property of being ferroelectric although there is as yet no general basis for deciding whether a material will be ferroelectric. However, a crystal is regarded to be ferroelectric when it has two or more orientation stages (in the absence of an electric field) which can be switched from one state to the other by an electric field. These two orientation states have identical crystal structure but differ only in electric polarization vector at zero electric field. Thus, there are no ferroelectrics which are not pyroelectric just as there are no pyroelectrics which are not piezoelectric. Nevertheless, the converse relationship in above statement is not true, i.e., not all piezoelectrics are pyroelectric; not all pyroelectrics are ferroelectric.

Crystal system	International notation	Schönflies' notation	Remarks
Triclinic	1	$C_1$	* +
	$\bar{1}$	$C_1(S_2)$	-
Monoclinic	2	$C_2$	* +
	$m(\bar{2})$	$C_s(C_{1h})$	* +
	$2/m$	$C_{2h}$	-
Orthorhombic	$2mm$	$C_{2v}$	* +
	222	$D_2(V)$	*
	$mmm$	$D_{2h}(V_h)$	-
Tetragonal	4	$C_4$	* +
	$\bar{4}$	$S_4$	*
	$\bar{4}2m$	$D_{2d}(V_d)$	*
	422	$D_4$	*
	$4mm$	$C_{4v}$	* +
	$4/m$	$C_{4h}$	-
	$4/mmm$	$D_{4h}$	-
Trigonal	3	$C_3$	* +
	$\bar{3}$	$C_{3l}(S_6)$	-
	$3m$	$C_{3v}$	* +
	32	$D_3$	*
	$\bar{3}m$	$D_{3d}$	-
Hexagonal	6	$C_6$	* +
	$\bar{6}$	$C_{3h}$	*
	$6mm$	$C_{6v}$	* +
	$6/m$	$C_{6h}$	-
	622	$D_6$	*
	$\bar{6}m2$	$D_{6h}$	*
	$6/mmm$	$D_{6h}$	-
Cubic	23	$T$	*
	$\bar{4}3m$	$T_d$	*
	$m\bar{3}$	$T_h$	-
	432	$O$	-
	$m\bar{3}m$	$O_h$	-

Table 2.1: Symbols of the 32 point groups in crystallography. Remarks: \* implies that piezoelectric effect may be exhibited and + implies that pyroelectric and ferroelectric effects may be exhibited (Xu, 1991).

### 2.3.2 Spontaneous Polarization

Spontaneous polarization is defined by the value of the dipole moment per unit volume, or by the value of the charge per unit area on the surface perpendicular to the axis of spontaneous polarization. A spontaneous polarization can be written as below:

$$P_s = \left( \iiint \mu \, dv \right) / \text{volume} \quad (2.19)$$

where  $\mu$  is the dipole moment per unit volume. It is important to note that the electrical properties are strongly correlated with the crystal structure, thus, the axis of spontaneous polarization is always a crystal axis.

Although a crystal with polar axes might exhibits piezoelectric effect, it does not necessary to have a spontaneous polarization vector. This is because the net result of electric moments along all polar axes may be equal to zero. Thus, only a crystal with a unique polar axis exhibits a spontaneous polarization vector,  $P_s$  along this axis. This spontaneous polarization cannot directly be measured from the charges on the surface of the crystal, because these charges are compensated by external or internal carrier carrying an electric current, or the charges on the boundaries of two opposite ends.

### 2.3.3 Ferroelectric Domains and Hysteresis Loop

Ferroelectricity was first discovered by Valasek in Rochelle salt in 1921. Ferroelectric crystals exhibit a spontaneous polarization,  $P_s$  in a certain temperature range and the direction of  $P_s$  can be reoriented by an external electric field. One of the important characteristic of ferroelectrics is the ferroelectric hysteresis loop where the polarization,  $\mathbf{P}$  is a double-valued function of the applied electric field,  $\mathbf{E}$ . The ferroelectric hysteresis loop can be observed by a Sawyer-Tower circuit as shown in Figure 2.4. An alternating voltage,  $V$  is imposed across the electrodes in parallel on the surfaces of the ferroelectric sample,  $C_x$

which is placed on the horizontal plates of an oscilloscope. Thus, the values plotted on the horizontal axis are proportional to the electric field across the sample. A linear capacitor,  $C_o$  is connected in series with the sample,  $C_x$ . The voltage across the  $C_o$  is therefore proportional to the polarization of the sample  $C_x$ . This voltage is monitored by the vertical plates of the oscilloscope.

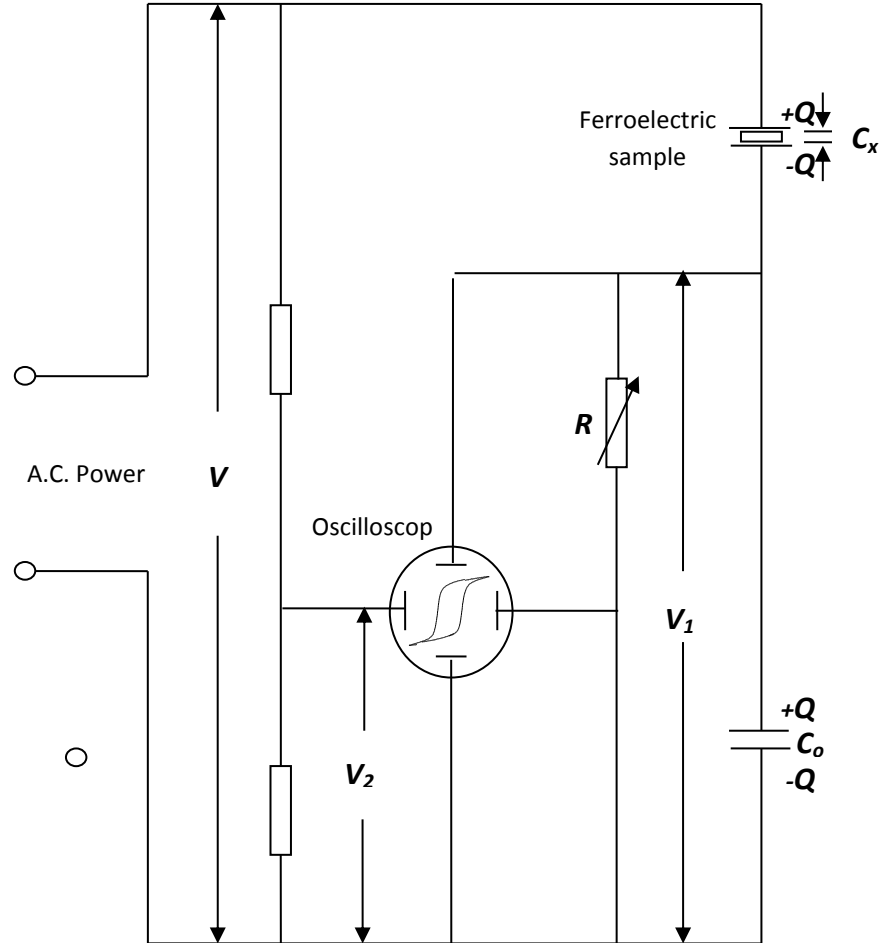


Figure 2.4: Schematic circuit of Sawyer-Tower bridge for ferroelectric characterization.

If a small amount of electric field is first applied on the ferroelectric sample, only a linear relationship of  $D$  and  $E$  will be observed. The applied electric field is rather too small to switch any domain or dipoles, and the ferroelectric crystal will behave as a normal dielectric material (paraelectric). This corresponds to the segment 0-1 of the

curves in Figure 2.5. As the electric field strength increases, the negative domains (which have a polarization opposite to the applied electric field) will be switched over in positive direction (along the field direction). If the electric field is kept increasing, the polarization will increase rapidly (segment 1-2) until all the domains are aligned in the positive direction. Here, we simply call this as a state of saturation in which the crystal is composed of a single domain. When the electric field decreases and reduced to zero, the polarization will generally decrease, but does not return back to zero. This is because some of the domains will remain aligned in the positive direction and the crystal will exhibit a remanent polarization  $P_r$ . The extrapolation of the linear line from point 2 back to the polarization axis (zero electric field) represents the value of the spontaneous polarization  $P_s$ .

The remanent polarization  $P_r$  in a crystal remained unchanged until the applied electric field in the opposite (negative sign) direction reaches a certain value (point 4). The electric field which is required to reduce the polarization to zero is called the ‘coercive field’,  $E_c$ . Further increase of the electric field in the negative direction will cause a complete alignment of the dipoles in this direction and the cycle of a hysteresis loop can be completed by reversing the electric field direction again as shown in Figure 2.5.

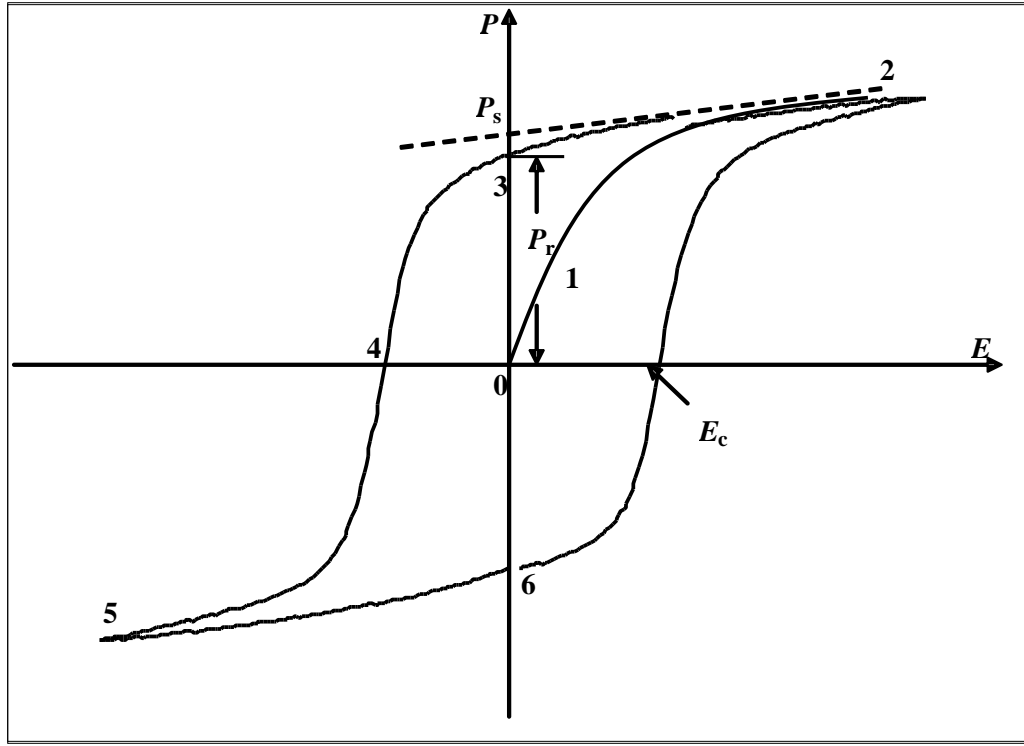


Figure 2.5: A typical  $P$ - $E$  hysteresis loop in ferroelectric materials.

### 2.3.4 Ferroelectric Curie Point and Phase Transitions

One of the most important ferroelectric characteristic when a phase transition temperature takes place is defined as Curie point,  $T_c$ . When the temperature increases through Curie point, a ferroelectric crystal undergoes a structural change from a ferroelectric phase to a paraelectric phase. At a paraelectric stage, the crystal does not exhibit ferroelectricity. The symmetry of the ferroelectric phase is always lower than the symmetry of the paraelectric phase. Above the Curie point, the dielectric permittivity falls off with temperature according to the Curie-Weiss law (Xu, 1991):

$$\varepsilon = \varepsilon_0 + \frac{C}{T - T_0} \approx \frac{C}{T - T_0} \quad (2.20)$$

where  $C$  is the Curie constant,  $T_0$  is the Curie-Weiss temperature. Some ferroelectrics like barium titanate,  $\text{BaTiO}_3$ , undergo several phase transition into successive ferroelectric

phases. However, only transition into the first ferroelectric phase is defined as Curie point. In general, the transition into a ferroelectric phase leads to anomalies in the dielectric, elastic, thermal and other properties of the material and is always accompanied with changes in the dimensions of the crystal unit cell. The associated strain is called the spontaneous strain,  $x_s$ . It shows the relative difference in the dimensions of the ferroelectric and paraelectric unit cells (M. J. Haun, Furman, Jang, McKinstry, & Cross, 1987; Michael J. Haun, Zhuang, Furman, Jang, & Cross, 1989). It is also related to the spontaneous polarization via electrostrictive coefficients.

## 2.4 Pyroelectricity Properties

Pyroelectric crystals develop an electric polarization when their temperature change. Alternatively, if a spontaneous polarization is already present, a change of temperature may alter it. If there is a small uniform change in temperature,  $\Delta T$  over the crystal, the change in the polarization vector,  $\Delta P_i$  is given by:

$$\Delta P_i = p_i \Delta T \quad (2.21)$$

where  $p_i$  is the pyroelectric coefficient.

In order to observe pyroelectricity, we need to heat a crystal uniformly and observe the change in polarization. Theoretically, this experiment can be done in two different ways: either the shape and size of the crystal held to be fixed during heating, or the crystal may be released so that the thermal expansion occurs freely. In the early case, the effect observed with the clamped crystal is called *primary pyroelectricity*. In the second case, an additional effect which is much easier to achieve experimentally with free expansion is called secondary pyroelectricity. The pyroelectric coefficient for a mechanically free sample is defined as:

$$P|_{total} = P|_{primary\ effect} + P|_{secondary\ effect} \quad (2.22)$$

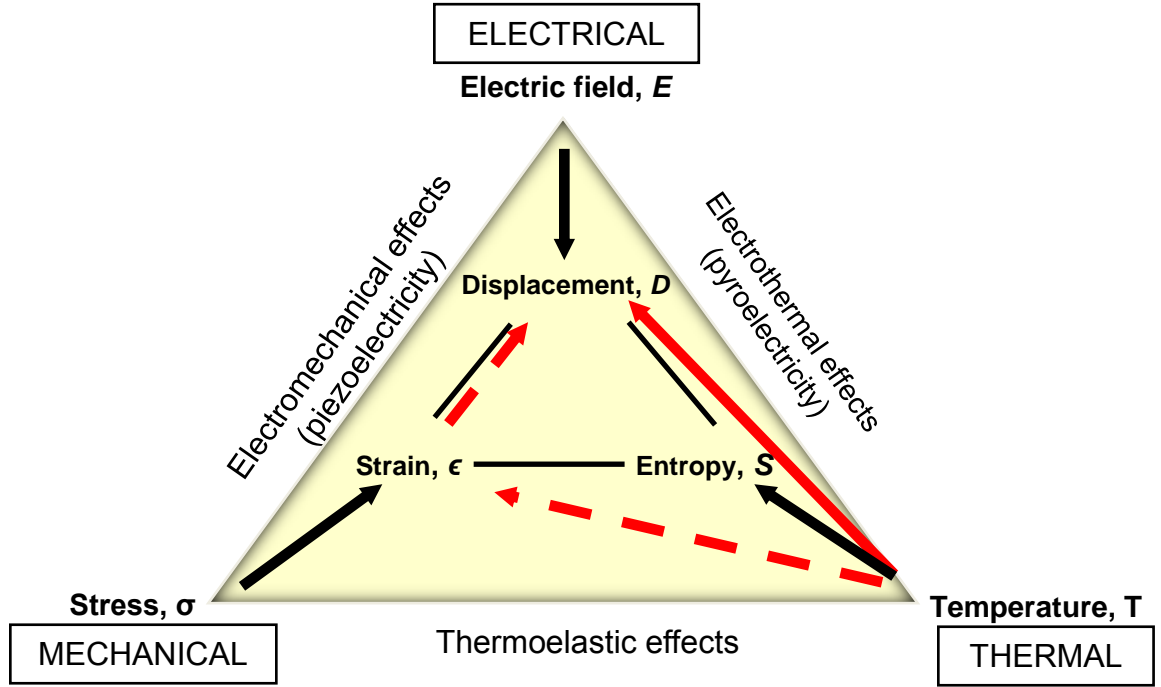


Figure 2.6: The relationship between the thermal, electrical and mechanical properties of a crystal. The solid line illustrates the primary pyroelectric effect (with strain remain constant); the red dash line illustrates the secondary pyroelectric effect when the crystal is free to deform (Dahiya & Valle, 2013).

Throughout this section, electric field,  $E$  is held constant. Since  $D = f_1(\epsilon, T)$  and  $\epsilon = f_2(\sigma, T)$ , we may write:

$$dD = \left(\frac{\partial D}{\partial \epsilon}\right)_T d\epsilon + \left(\frac{\partial D}{\partial T}\right)_\epsilon dT \quad (2.23)$$

$$d\epsilon = \left(\frac{\partial \epsilon}{\partial \sigma}\right)_T d\sigma + \left(\frac{\partial \epsilon}{\partial T}\right)_\sigma dT \quad (2.24)$$

Putting  $d\sigma = 0$  and dividing by  $dT$ , we obtain

$$\begin{array}{ccc} \text{primary} & & \text{secondary} \\ \left(\frac{\partial D}{\partial T}\right)_\sigma & = & \left(\frac{\partial D}{\partial T}\right)_\epsilon + \left(\frac{\partial D}{\partial \epsilon}\right)_T \left(\frac{\partial \epsilon}{\partial T}\right)_\sigma \end{array} \quad (2.25)$$



The term of  $(\partial D/\partial T)_\sigma$  in eq. (2.25) defined the pyroelectric effect measured at a constant stress when the crystal is free to change its shape. This equation shows that the measured effect can be divided into two parts. First, the primary (or ‘true’) pyroelectric effect is given by  $(\partial D/\partial T)_\epsilon$ , where the displacement is measured by a temperature change if the shape and volume of the crystal are under clamped condition. Microscopic origin of this phenomenon is the crystal lattice reconstruction as a result of the temperature change, but without the crystal deformation. The secondary pyroelectric effect is measured as the additional pyroelectricity when the crystal is free to deform or expand. It represents the piezoelectric effect contribution to the total pyroelectric effect. In Fig. 2.6, this additional pyroelectricity arises from the path  $T \rightarrow \epsilon \rightarrow D$ . As a result, when the crystal is free to deform or expand, thermal expansion causes a strain, which in turn, by the piezoelectric path  $\epsilon \rightarrow D$ , contributes to a displacement,  $D$ . This effect is pseudo pyroelectric effect or false pyroelectric of the first kind. Spontaneous polarization shows changes due to this effect even if no structural changes in crystal take place. Temperature changes in lattice constant are connected with the changes of elementary dipole moments and therefore result in the polarization (Tichý, Erhart, Kittinger, & Přívratská, 2010).

In fact, the secondary effect is always numerically greater than the primary (Furukawa, Wen, Suzuki, Takashina, & Date, 1984). To deduce the true pyroelectric coefficient,  $(\partial D/\partial T)_\epsilon$ , piezoelectric is an essential subject to be understood in order to determine its elastic and thermal expansion coefficients accurately. In addition, the magnitude of  $(\partial D/\partial T)_\epsilon$  is relatively small, a small error in the determination of  $(\partial D/\partial T)_\sigma$  may cause the difference between finding a finite primary effect. As a result,  $(\partial D/\partial T)_\sigma$  becomes a common pyroelectric coefficient to be measured. *Tertiary pyroelectricity*, or ‘false pyroelectricity of the second kind’, is essentially resulting of a non-homogeneous

temperature distribution in the sample (i.e. temperature gradient) due to the internal thermal stress. Uneven heating during the experiments may cause the temperature gradients by thermal expansion, cause non-uniform stresses and strains. These in turn can produce a polarization by piezoelectric effects, unless the experiments are carefully performed (Tichý et al., 2010).

## **2.5 Piezoelectric Effects**

The piezoelectric effect is defined as the generation of an electric charge as a result of force exerted on a material as shown in Fig. 2.7. Before an external stress/force is applied on the material, the center of the positive and negative charges of each molecule coincides and result in a neutral electrical charge within a molecule (see Fig. 2.8(a)) (Dahiya & Valle, 2013). However, in presence of an external mechanical stress onto the material, the internal reticular can be deformed, causing the separation of the positive and negative charge in the molecule. As a result, it generates little dipoles and the material is polarized (see Fig. 2.8(b)). This effect is called direct piezoelectric effect. The electric field generated by the polarization can be used to transform the mechanical energy into electrical energy.

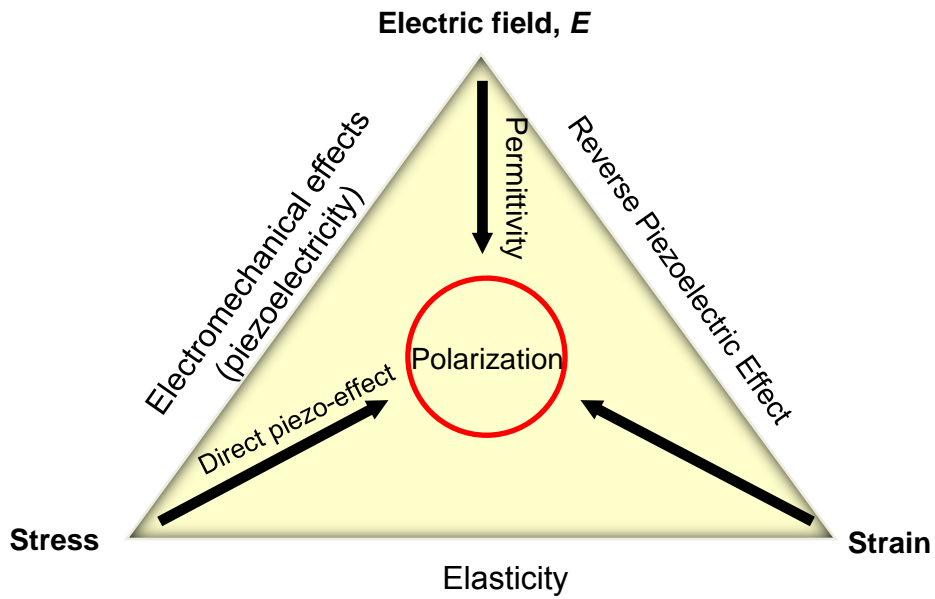


Figure 2.7: Piezoelectricity- An intermingling of electric and elastic phenomena (Dahiya & Valle, 2013).

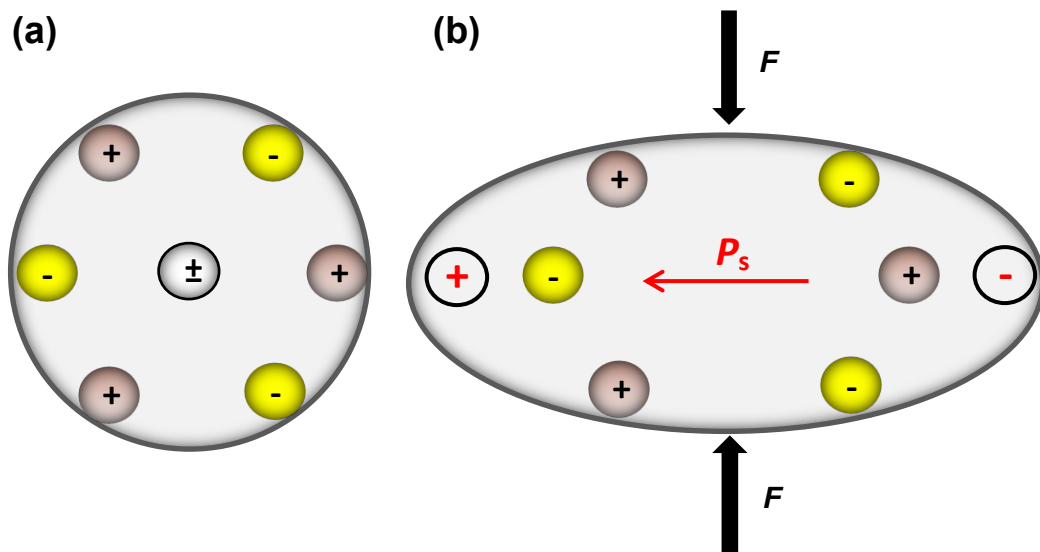


Figure 2.8: Piezoelectric phenomena with a simple molecular model: (a) an unperturbed molecule with no piezoelectric polarization; (b) the molecule subjected to an external force,  $F$ , resulting in polarization,  $P_s$

When a poled piezoelectric material is mechanically strained, it becomes electrically polarized and resulting in fixed electric charge on the surface of the material. According to the linear theory of piezoelectricity, the density of generated fixed charge in a piezoelectric material is proportional to the external stress (Dahiya & Valle, 2013). This relationship can be written as:

$$P = d \times T \quad (2.26)$$

where  $P$  is the piezoelectric polarization vector, whose magnitude is equal to the fixed charge density produced as a result of piezoelectric effect. Here, we defined piezoelectric strain coefficient as  $d$  and  $T$  is the stress applied to the material. These definitions are denoted with different characters to those described in pyroelectric activity to avoid confusions. In addition, the direct or reverse piezoelectric effect is defined as:

$$S = d \times E \quad (2.27)$$

where  $S$  is the mechanical strain produced by reverse piezoelectric effect and  $E$  is the applied electric field. If the effect of the elastic properties also being considered, the direct and reverse piezoelectric effects can be rewritten as:

$$P = d \times T = d \times c \times S = e \times S \quad (2.28)$$

$$T = c \times S = c \times d \times E = e \times E \quad (2.29)$$

where  $c$  is the elastic constant relating the generated stress and applied strain ( $T = c \times S$ ),  $s$  is the compliance coefficient which relates to the deformation by the application of a stress ( $S = s \times T$ ), and  $e$  is the stress constant (Dahiya & Valle, 2013).

## 2.6 Poly(vinylidene fluoride) Polymer

Piezoelectricity was first discovered in a biological material, wood in early 1940's. Thereafter, piezoelectric effect were successfully discovered in many other natural biological substances, such as flax, silk, bamboo, bones, tendon, muscle, skin, hair and blood vessels. In the early 1960's, piezoelectricity was first observed in synthetic organic materials, such as polypeptides. Among these synthetic polymers, poly(vinylidene fluoride) (PVDF) has turned up to be the most representative polymer because of their possible applications for soft transducers and fast display elements as well as their unique mechanisms of ferroelectricity.

PVDF has attracted much interest since its strong piezoelectricity was discovered by Kawai in 1969 (Kawai, 1969). It is revealed as one of the most representative functional polymers due to its exceptional piezo-, pyro- and ferroelectric properties. This semi-crystalline polymer exhibits at least four polymorphs, known as Form I ( $\beta$ -phase), II ( $\alpha$ ), III ( $\gamma$ ) and IV ( $\delta$ ), which possess different chain conformations as shown in Fig. 2.9 and Fig. 2.10 (Furukawa, 1989; Lovinger, 1983; Scott, 2007). The Form I crystal has an all *trans* (TTT) planar zigzag chain conformation. In this polymorph, molecular dipoles associated with  $-\text{CH}_2\text{CF}_2-$  monomer unit are aligned in one direction perpendicular to the chain axis and carries a vacuum dipole moment of  $\mu_v = 7 \times 10^{-30}$  Cm (2.1 Debyes). Such dipoles are rigidly attached to main chain carbon. Summing up  $\mu_v$  over a unit volume and yields a large spontaneous polarization,

$$P_s = \frac{2\mu_v}{abc} = 130 \text{ mC/m}^2 \quad (2.30)$$

where  $a$ ,  $b$  and  $c$  are the lattice constants;  $a = 0.858$  nm,  $b = 0.491$  nm and  $c = 0.256$  nm. Spontaneous polarization,  $P_s$  is one of the most important properties that reflect ferroelectric cooperative interactions which can be experimentally determined by  $D$ - $E$

hysteresis measurements. Conventional Form I PVDF samples prepared by melt crystallization and cold drawing exhibit a crystallinity of about 50%. The reported value of  $P_r$  is ranged in 50-80 mC/m<sup>2</sup>. Special treatments such as high pressure crystallization and ultra-drawing could cause an increase in crystallinity and induced  $P_r$  as large as 100 mC/m<sup>2</sup>. Form II is the most common polymorph which consists of TGT $\bar{G}$  molecules packed in an antiparallel fashion. For Form III, the molecules adopt an intermediate conformation T<sub>3</sub>GT<sub>3</sub> $\bar{G}$  and form a polar crystalline due to its parallel packing. Form IV polymorph comprised of a parallel packing of TGT $\bar{G}$  molecules. This polymorph is also considered as the polar version of Form II which is our primary target in this study. Regarding the molecular packing of these forms, ‘parallel’ and ‘antiparallel’ are related to the dipole orientation in the direction perpendicular to the chain axis. Among the four common polymorphs, only the Form II is nonpolar, while the remaining three are polar. From a vector sum of constituent dipoles, the spontaneous polarization of the Form III and IV is around one half that of the Form I.

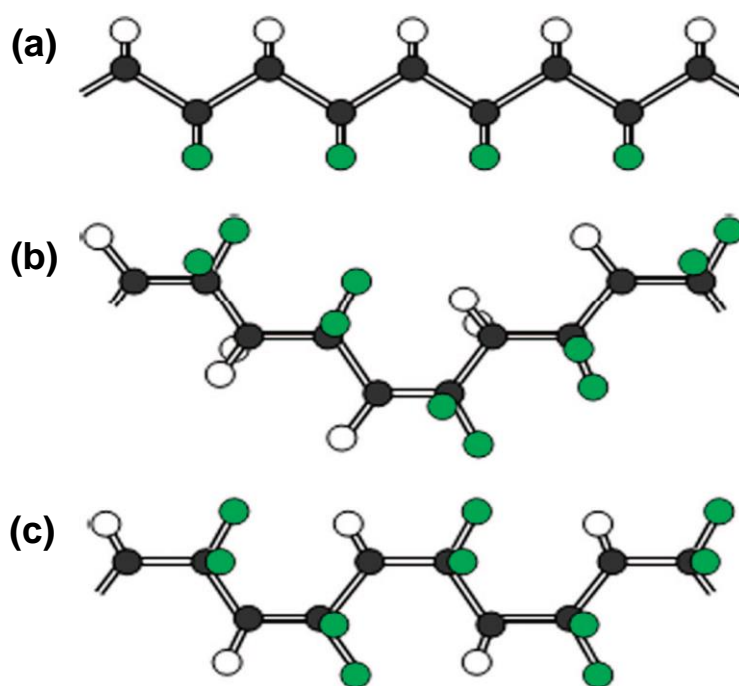


Figure 2.9: The three chain conformations of PVDF in different polymorphs: (a) TTT planar zigzag, (b)  $T_3GT_3\bar{G}$  and (c)  $TGT\bar{G}$ ; Green, white and grey colour indicates the fluorine, hydrogen and carbon atom, respectively. (after Akira Itoh et al (Itoh, Takahashi, Furukawa, & Yajima, 2014)).

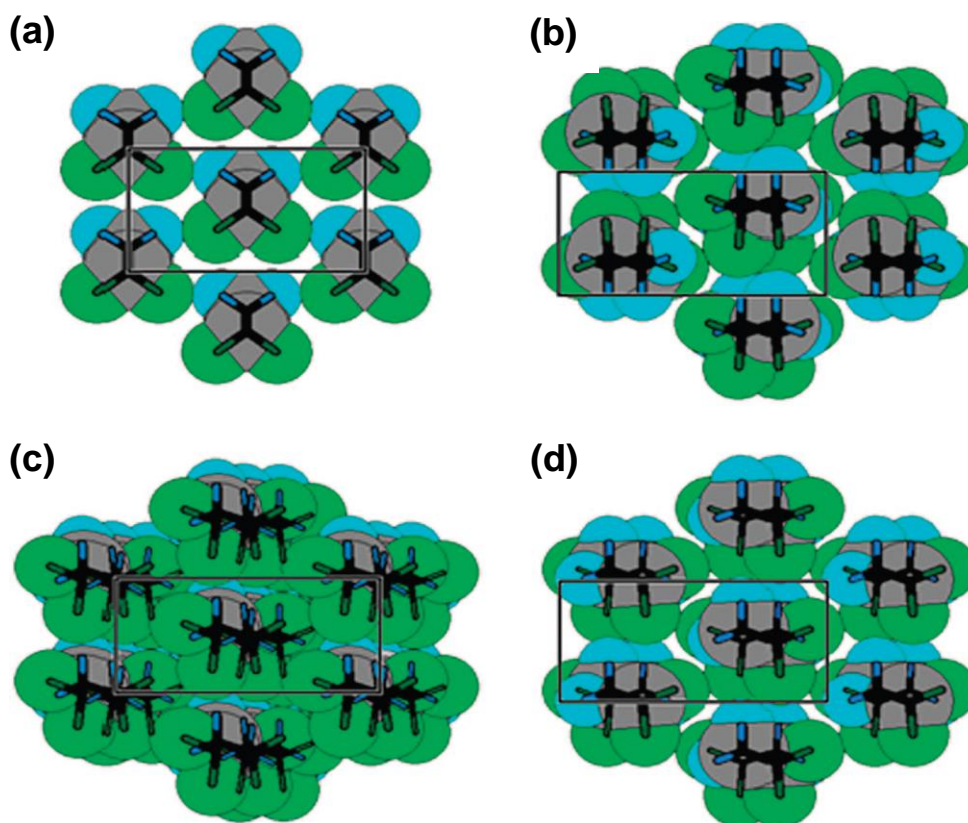


Figure 2.10: Crystal structures of PVDF. Black rectangle in each crystal denotes the crystallographic unit cell. The  $c$ -axis is parallel to the chain direction for all polymorphs. The  $b$ -axis is vertical direction for Form I and horizontal direction for other polymorphs. (a) Form I is parallel all trans. (b) Form II is antiparallel and up-down  $TGT\bar{G}$ . (c) Form III is parallel and up-up  $T_3GT_3\bar{G}$ . (d) Form IV is parallel and up-down  $TGT\bar{G}$ . (after Akira Itoh et al (Itoh et al., 2014)).

Here, the antiparallel and parallel packing in Forms II and III, respectively, refer to the dipole orientation perpendicular to the chain axis. In  $TGT\bar{G}$  and  $T_3GT_3\bar{G}$  conformations, molecular dipoles are oriented not only perpendicular to, but also along the chain axis. The latter generates chain sense and yields three types of chain packing, all up or down, regular up-down and statistical up-down. Among them, the statistical up-down was shown to be most probable based on the detailed X-ray intensity analysis (Bachmann, Gordon,



Weinhold, & Lando, 1980). The dielectric studies have shown that Form II PVDF exhibits a marked crystalline relaxation associated with cooperative dipole fluctuations along the chain axis. Miyamoto et al (Miyamoto, Miyaji, & Asai, 1980) suggested a possible microscopic feature arising from conformational changes between  $TGT\bar{G}$  and  $\bar{G}TGT$  through some defects. Thus, the statistical up-down packing incorporates intramolecular up-down motion was induced by the active crystalline motion.

A specific polymorph PVDF can be obtained by combinations of thermal, mechanical and electrical treatments (Furukawa, 1989) as shown in Fig. 2.11. Melt crystallization is known to yield a Form II film. Uniaxial drawing leads to a conversion from Form II to Form I in accord with the chain elongation from  $TGT\bar{G}$  to extended all-trans. Heat treatment of a Form II film at an appropriate temperature induces transformation into Form III. The application of a high electric field was shown to cause a transformation of Form II into its polar counterpart, Form IV. Further increase in applied electric fields will lead to additional conversion into Form I via Form III. These phase transformation schemes have been well established by a number of authors (Das-Gupta & Doughty, 1977, 1978, 1980; Das-Gupta, Doughty, & Shier, 1979; Davis, McKinney, Broadhurst, & Roth, 1978; Naegel, Yoon, & Broadhurst, 1978).

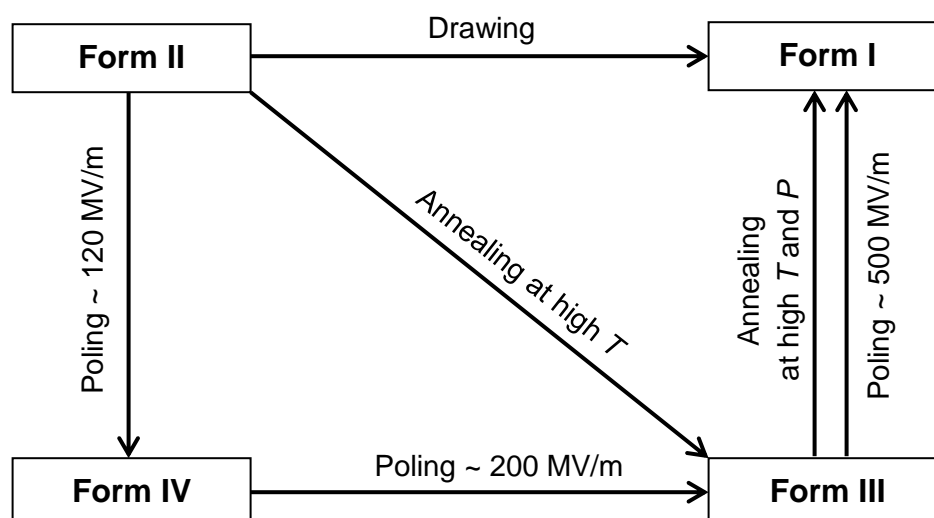


Figure 2.11: Schematic diagram of crystalline transformations among polymorphs of PVDF due to electrical, mechanical and thermal treatments (Furukawa, 1989).

In recent years, much effort has been devoted to investigate the effect of the type of solvent, humidity, concentration, temperature and substrate on the polymorph formation of solution cast PVDF (Benz, Euler, & Gregory, 2002; J. R. Gregorio & Cestari, 1994; Gregorio Jr & Borges, 2008; R. Gregorio, 2006; Li, Shimizu, Furumichi, Takahashi, & Furukawa, 2007; Tashiro, 1995). Among them, the choice of solvent and the crystallization temperature are the keys to prepare specific crystalline phase. Solvents with low evaporation rate (high boiling point): dimethylformamide (DMF) and dimethyl sulfoxide (DMSO) favour the polar Form I, whereas solvents with high evaporation rate (low boiling point): methy ethyl ketone (MEK) and acetone tend to yield nonpolar Form II.

## 2.7 The Role of Inclusion in The Polymer Matrix

An electromechanical transducer, for example, may require a combination of properties such as large piezoelectric coefficient ( $d$  or  $g$ ), low density and mechanical flexibility (Newnham, Skinner, & Cross, 1978). In general, ferroelectric ceramics are brittle and stiff lacking the flexibility; while polymers offer the desired mechanical properties but coupling with weak piezoelectric properties. As such, ferroelectric polymer based composites would be a solution to this problem by exploiting the desirable features of both components. To combine the materials with two distinct properties, it is essential to choose the component phases with the right properties, and also coupling them in the best manner. Connectivity of the individual phases is of utmost importance, because this controls the electric flux pattern as well as the mechanical properties (Newnham et al., 1978).

One of the most studied subjects in composites science is the composites in 0-3 connectivity, which contain ferroelectric ceramic inclusions such as lead titanate (PT), lead zirconate titanate (PZT),  $\text{BaTiO}_3$  (BT) in a ferroelectric polymer matrix especially of PVDF and its copolymers (Chan, Chan, Zhang, & Choy, 1998; Chan, Ng, & Choy, 1999; Dang, Wang, Peng, & Nan, 2008; Furukawa, Suzuki, & Date, 1986). Such materials offer a considerable potential in sensor and transducer applications, due to the possibility of tailoring its properties to specifications by a judicious selection of constituent components and of their volume fraction (Ploss, Ploss, Shin, Chan, & Choy, 2000). Low acoustic impedance and low permittivity are also the remarkable advantages for the composites being used as sensor elements. Non-ferroelectric polymers such as polyurethane, epoxies and polyethylene with a very low permittivity and a low conductivity as compared with ceramic inclusions have been employed as polymer matrix for composites fabrication (Furukawa, Fujino, & Fukada, 1976; Furukawa, Ishida, & Fukada, 1979; Kwok, Lau, Wong, & Shin, 2007; Sakamoto, Marin-Franch, & Das-Gupta, 2002). A few theoretical

models have been well developed which included the effect of interfacial charge and the conductivity of the polymer matrix to understand the peculiar experimental observations and the poling mechanism in the ferroelectric composites (Furukawa et al., 1976; Furukawa & Fukada, 1977; Kwok et al., 2007; Bernd Ploss, Ng, Chan, Ploss, & Choy, 2001; B. Ploss, Ploss, Shin, Chan, & Choy, 1998; Beatrix Ploss, Bernd Ploss, F. G. Shin, H. L. W. Chan, & C. L. Choy, 2000). However, effort to embed a non-ferroelectric inclusion into a ferroelectric polymer matrix as an alternative route to enhance the desired pyroelectric and ferroelectric properties has not been observed.

## 2.8 Summary

From the technology point of view, most investigations on organic ferroelectric PVDF were basically focused on Form I due to its exceptional electrical properties for application purposes. The studies on the other two polar polymorphs, Form III and IV, were almost discontinued 40 years ago since their remanent polarizations are expected to be much smaller than Form I. In the present work, we re-examined the ferroelectric switching characteristics and pyroelectric properties of Form IV PVDF prepared by spin-coating technique. The samples were subjected to annealing and resulting changes in crystallinity. It will be shown that the ferroelectric and pyroelectric properties are strongly governed by degree of crystallinity. To date, no details dielectric analysis on Form IV PVDF is presented. In particular, a wide range dielectric spectroscopy has also been extended to determine the molecular dynamic of Form IV PVDF. By combining the results from the above finding with the detail analysis on the crystalline and structure morphology, we would like to provide fundamental understanding on the extraordinary electrical responses of Form IV PVDF induced by electric field. Such data are important considerations to determine the ultimate mechanisms which produce ferroelectric effect in Form IV PVDF.

**References:**

- Bachmann, M., Gordon, W. L., Weinhold, S., & Lando, J. B. (1980). The crystal structure of phase IV of poly(vinylidene fluoride). *Journal of Applied Physics*, 51(10), 5095-5099.
- Benz, M., Euler, W. B., & Gregory, O. J. (2002). The Role of Solution Phase Water on the Deposition of Thin Films of Poly(vinylidene fluoride). *Macromolecules*, 35(7), 2682-2688.
- Chan, H. L. W., Chan, W. K., Zhang, Y., & Choy, C. L. (1998). Pyroelectric and piezoelectric parameters of lead titanate/vinylidene fluoride-trifluoroethylene copolymer 0-3 composites. *IEEE Transactions on Dielectrics and Electrical Insulation*, 5(5), 505-512.
- Chan, H. L. W., Ng, P. K. L., & Choy, C. L. (1999). Effect of poling procedure on the properties of lead zirconate titanate/vinylidene fluoride-trifluoroethylene composites. *Applied Physics Letters*, 74(20), 3029-3031.
- Dahiya, R. S., & Valle, M. (2013). *Robotic Tactile Sensing: Technologies and System*. Dordrecht: Springer Netherlands.
- Dang, Z.-M., Wang, H.-Y., Peng, B., & Nan, C.-W. (2008). Effect of BaTiO<sub>3</sub> size on dielectric property of BaTiO<sub>3</sub>/PVDF composites. *Journal of Electroceramics*, 21(1-4), 381-384.
- Das-Gupta, D. K., & Doughty, K. (1977). Changes in x-ray diffraction patterns of polyvinylidene fluoride due to corona charging *Applied Physics Letters*, 31, 585-587.
- Das-Gupta, D. K., & Doughty, K. (1978). Piezo- and pyroelectric behaviour of corona-charged polyvinylidene fluoride. *Journal of Physics D: Applied Physics*, 11(17), 2415-2423.
- Das-Gupta, D. K., & Doughty, K. (1980). Piezoelectricity in uniaxially stretched and corona poled polyvinylidene fluoride. *Journal of Physics D: Applied Physics*, 13(1), 95-105.
- Das-Gupta, D. K., Doughty, K., & Shier, D. B. (1979). A study of structural and electrical properties of stretched polyvinylidene fluoride films. *Journal of Electrostatics*, 7(0), 267-282.

- Davis, G. T., McKinney, J. E., Broadhurst, M. G., & Roth, S. C. (1978). Electric-field-induced phase changes in poly(vinylidene fluoride). *Journal of Applied Physics*, 49(10), 4998-5002.
- Furukawa, T. (1989). Ferroelectric properties of vinylidene fluoride copolymers. *Phase Transitions*, 18(3-4), 143-211.
- Furukawa, T., Fujino, K., & Fukada, E. (1976). Electromechanical Properties in the Composites of Epoxy Resin and PZT Ceramics. *Japanese Journal of Applied Physics*, 15, 2119-2129.
- Furukawa, T., & Fukada, E. (1977). Piezoelectric Relaxation in Composite Epoxy-PZT System due to Tonic Conduction. *Japanese Journal of Applied Physics*, 16(3), 453-458.
- Furukawa, T., Ishida, K., & Fukada, E. (1979). Piezoelectric properties in the composite systems of polymers and PZT ceramics. *Journal of Applied Physics*, 50(7), 4904-4912.
- Furukawa, T., Suzuki, K., & Date, M. (1986). Switching process in composite systems of PZT ceramics and polymers. *Ferroelectrics*, 68(1), 33-44.
- Furukawa, T., Wen, J. X., Suzuki, K., Takashina, Y., & Date, M. (1984). Piezoelectricity and pyroelectricity in vinylidene fluoride/trifluoroethylene copolymers. *Journal of Applied Physics*, 56(3), 829-834.
- Gregorio, J. R., & Cestari, M. (1994). Effect of crystallization temperature on the crystalline phase content and morphology of poly(vinylidene fluoride). *Journal of Polymer Science Part B: Polymer Physics*, 32(5), 859-870.
- Gregorio Jr, R., & Borges, D. S. (2008). Effect of crystallization rate on the formation of the polymorphs of solution cast poly(vinylidene fluoride). *Polymer*, 49(18), 4009-4016. doi: 10.1016/j.polymer.2008.07.010
- Gregorio, R. (2006). Determination of the  $\alpha$ ,  $\beta$ , and  $\gamma$  crystalline phases of poly(vinylidene fluoride) films prepared at different conditions. *Journal of Applied Polymer Science*, 100(4), 3272-3279.
- Haun, M. J., Furman, E., Jang, S. J., McKinstry, H. A., & Cross, L. E. (1987). Thermodynamic theory of  $\text{PbTiO}_3$ . *Journal of Applied Physics*, 62(8), 3331-3338.

- Haun, M. J., Zhuang, Z. Q., Furman, E., Jang, S.-J., & Cross, L. E. (1989). Electrostrictive Properties of the lead Zirconate Titanate Solid-Solution System. *Journal of the American Ceramic Society*, 72(7), 1140-1144.
- Itoh, A., Takahashi, Y., Furukawa, T., & Yajima, H. (2014). Solid-state calculations of poly(vinylidene fluoride) using the hybrid DFT method: spontaneous polarization of polymorphs. *Polymer Journal*, 46, 207-211.
- Kawai, H. (1969). The Piezoelectricity of Poly (vinylidene Fluoride). *Japanese Journal of Applied Physics*, 8, 975-976.
- Kremer, F., & Schönhals, A. (2003). *Broadband Dielectric Spectroscopy*. Berlin, Heidelberg: Springer-Verlag Berlin Heidelberg.
- Kwok, K. W., Lau, S. T., Wong, C. K., & Shin, F. G. (2007). Effects of electrical conductivity on poling of ferroelectric composites *Journal of Physics D: Applied Physics*, 40(21), 6.
- Li, Y., Shimizu, H., Furumichi, T., Takahashi, Y., & Furukawa, T. (2007). Crystal forms and ferroelectric properties of poly(vinylidene fluoride)/polyamide 11 blends prepared by high-shear processing. *Journal of Polymer Science Part B: Polymer Physics*, 45(19), 2707-2714.
- Lovinger, A. J. (1983). Ferroelectric polymers. *Science*, 220, 1115-1121.
- Miyamoto, Y., Miyaji, H., & Asai, K. (1980). Anisotropy of dielectric relaxation in crystal form II of poly(vinylidene fluoride). *Journal of Polymer Science: Polymer Physics Edition*, 18(3), 597-606.
- Naegele, D., Yoon, D. Y., & Broadhurst, M. G. (1978). Formation of a New Crystal Form ( $\alpha$ p) of Poly(vinylidene fluoride) under Electric Field. *Macromolecules*, 11(6), 1297-1298.
- Newnham, R. E., Skinner, D. P., & Cross, L. E. (1978). Connectivity and piezoelectric-pyroelectric composites. *Materials Research Bulletin*, 13(5), 525-536.
- Ploss, B., Ng, W.-Y., Chan, H. L.-W., Ploss, B., & Choy, C.-L. (2001). Poling study of PZT/P(VDF-TrFE) composites. *Composites Science and Technology*, 61(7), 957-962.

- Ploss, B., Ploss, B., Shin, F. G., Chan, H. L. W., & Choy, C. L. (1998). *Separate poling of inclusions and matrix in PT/P(VDF-TrFE) 0-3 composites*. Paper presented at the Applications of Ferroelectrics, 1998. ISAF 98. Proceedings of the Eleventh IEEE International Symposium on Applications of Ferroelectrics.
- Ploss, B., Ploss, B., Shin, F. G., Chan, H. L. W., & Choy, C. L. (2000). Pyroelectric activity of ferroelectric PT/PVDF-TRFE. *IEEE Transactions on Dielectrics and Electrical Insulation*, 7(4), 517-522.
- Ploss, B., Ploss, B., Shin, F. G., Chan, H. L. W., & Choy, C. L. (2000). Pyroelectric or piezoelectric compensated ferroelectric composites. *Applied Physics Letters*, 76(19), 2776-2778.
- Sakamoto, W. K., Marin-Franch, P., & Das-Gupta, D. K. (2002). Characterization and application of PZT/PU and graphite doped PZT/PU composite. *Sensors and Actuators A: Physical*, 100(2-3), 165-174.
- Scott, J. F. (2007). Applications of Modern Ferroelectrics. *Science*, 315(5814), 954-959.
- Tashiro, K. (1995). Crystal structure and phase transitions of PVDF and related copolymers. In H. S. E. Nalwa (Ed.), *Ferroelectric Polymers*. NY: Marcel Dekker, 63-180.
- Tichý, J., Erhart, J., Kittinger, E., & Přivratská, J. (2010). *Fundamentals of Piezoelectric Sensorics: Mechanical, Dielectric, and Thermodynamical Properties of Piezoelectric*. Heidelberg: Springer Science & Business Media.
- Xu, Y. (1991). *Ferroelectric Materials and Their Applications*. The Netherlands: North-Holland.



## CHAPTER 3: Experimental Methodology

### 3.1 Introduction

This chapter presents the experimental and analytical details employed in this work. The contents of this chapter are divided into three major sections. Sample preparation procedure for PVDF and PVDF composites is briefly described in Section 3.2. Section 3.3 presents the surface morphology and structural analysis of the samples. Section 3.4 provides the principles and the equipment setup for the electrical measurement used in this work.

### 3.2 Sample Preparation

#### 3.2.1 PVDF thin films

PVDF, KF850 was supplied by Kureha Corporation, Japan. Acetone and methyl ethyl ketone (MEK) were used for preparation of solution-cast thin films in an attempt to obtain Form II dominant PVDF films. These solvents are of reagent grade and used without further purification at a concentration of 5 wt%. PVDF solutions were prepared at the temperature slightly higher than the boiling point of the respective solvents for one hour. The thin films were spin coated at elevated temperature of about 60 °C with a spinning speed of 6000 rotations per minute. The PVDF thin films were then annealed at a temperature ranging from 70 °C to 155 °C for 1 hour to examine the structural change. A 30 nm thick aluminum top electrode was vacuum deposited to produce a metal-insulator-metal structure. The sample thickness was 200-300 nm as measured with a KLA Tencor P-6 mechanical profiler. The effective working area of the thin films for dielectric measurement is 2 mm × 2 mm. However, the working area of the thin films for ferroelectric measurement is 110 μm × 110 μm.

### 3.2.2 PVDF/TiO<sub>2</sub> Composite Thin Films

Rutile phase TiO<sub>2</sub> were supplied by Sigma-Aldrich. The PVDF powders were dispersed with 10 wt% to 30 wt% powdered TiO<sub>2</sub> (particles size < 50 nm), and dissolved in acetone. Acetone was chosen as the solvent because it has higher evaporation rate than a polar solvent such as DMSO or DMF. Thus, a homogeneous and thin film that is free from pin-holes can be spin-casted onto aluminized glass substrates. The PVDF composite solutions were stirred with a magnetic stirrer at 60 °C for 1 hour to ensure complete mixing of the solutions. The PVDF/TiO<sub>2</sub> composite thin films with doping concentrations of 10 wt%, 20 wt% and 30 wt% (PT1, PT2 and PT3, respectively) were prepared by spin-casting (at 3000 rpm for 30 seconds at room temperature) the composite solution onto a glass substrate coated with a 50-nm-thick aluminum electrode. The films were treated with different annealing temperatures from 60 °C to 140 °C for one hour in order to study the effect of annealing temperature on the pyroelectric activity of the thin films. Any further increase in the annealing temperature is not recommended as the molten phase of PVDF is around 150 °C. A 30-nm-thick aluminum top electrode was then thermally evaporated onto the films to produce the desired metal-insulator-metal (MIM) structure. The thickness of the thin films was measured in the range from 300 nm to 500 nm with a KLA Tencor P-6 mechanical profiler. The TiO<sub>2</sub> powders were compressed into a pellet form with a diameter of 13 mm and thickness of 1 mm. The pellet was used to measure the dielectric constant of TiO<sub>2</sub>.

### 3.2.3 PVDF/La<sub>2</sub>O<sub>3</sub> Composite Thin Films

La<sub>2</sub>O<sub>3</sub> powder was purchased from SIGMA-ALDRICH. The average grain size of La<sub>2</sub>O<sub>3</sub> is around 100 nm. The La<sub>2</sub>O<sub>3</sub> contents in the PVDF/ La<sub>2</sub>O<sub>3</sub> composites were prepared to the designated weight fraction, i.e. 1%, 3% and 5%. The powders were dissolved in acetone and stirred at 80 °C for one hour. The solutions were then immersed in ultrasonic bath for 30 minutes to ensure they were fully dissolved. Prior to spin-coating, the solutions were kept at the temperature of ~ 60 °C before being transfer onto the aluminum-coated glass substrate at room temperature. The thickness of the thin-film samples was about 300 nm. The spin-coated thin films were kept in an oven at 80 °C for two hours in order to remove the residual solvent. The thin films were then subsequently, annealed at a temperature 140 °C for one hour such that smooth surface with increased crystalline structure can be obtained. Aluminum electrodes of 2 mm × 2 mm in size were coated by thermal evaporation.

### 3.2.4 Device Configuration

Ferroelectric devices were prepared in MIM structure as mentioned in Section 3.2.1, 3.2.2 and 3.2.3. The aluminum electrode's patterns were designed using shadow masks as shown in Figure 3.1 and 3.2. The aluminum bottom electrodes were first thermally deposited onto glass or silicon substrates as shown in Figure 3.1 (a), which the line's width is confined to 0.110 mm with about 13 mm long. The chemical solutions were then spin cast onto the top of the aluminum's surface and treated with different annealing temperature. Subsequently, the top electrodes were evaporated using shadow mask as shown in Figure 3 (b). Figure 3 (c) and (d) illustrate a schematic diagram and picture of a desired device, respectively with an active area of 0.110 mm × 0.110 mm. Since the electric

field applied on the thin films was in the range from 250 MV/m to 300 MV/m, it is essential to reduce the area size to avoid dielectric breakdown.

Figure 3.3 shows the electrode geometry for the dielectric measurement. The active electrode area is  $2\text{ mm} \times 2\text{ mm}$ . The main reason that the dielectric devices were prepared with larger area is to cover fillers (with average particle's size of 100 nm) in the 0-3 composite thin films. Sometime, larger electrode area which is  $1\text{ cm} \times 1\text{ cm}$  was prepared for composite thin films in order to obtain accurate measurement. Silver paint was then applied in between the top electrode and the aluminum wires prepared from aluminum foils.

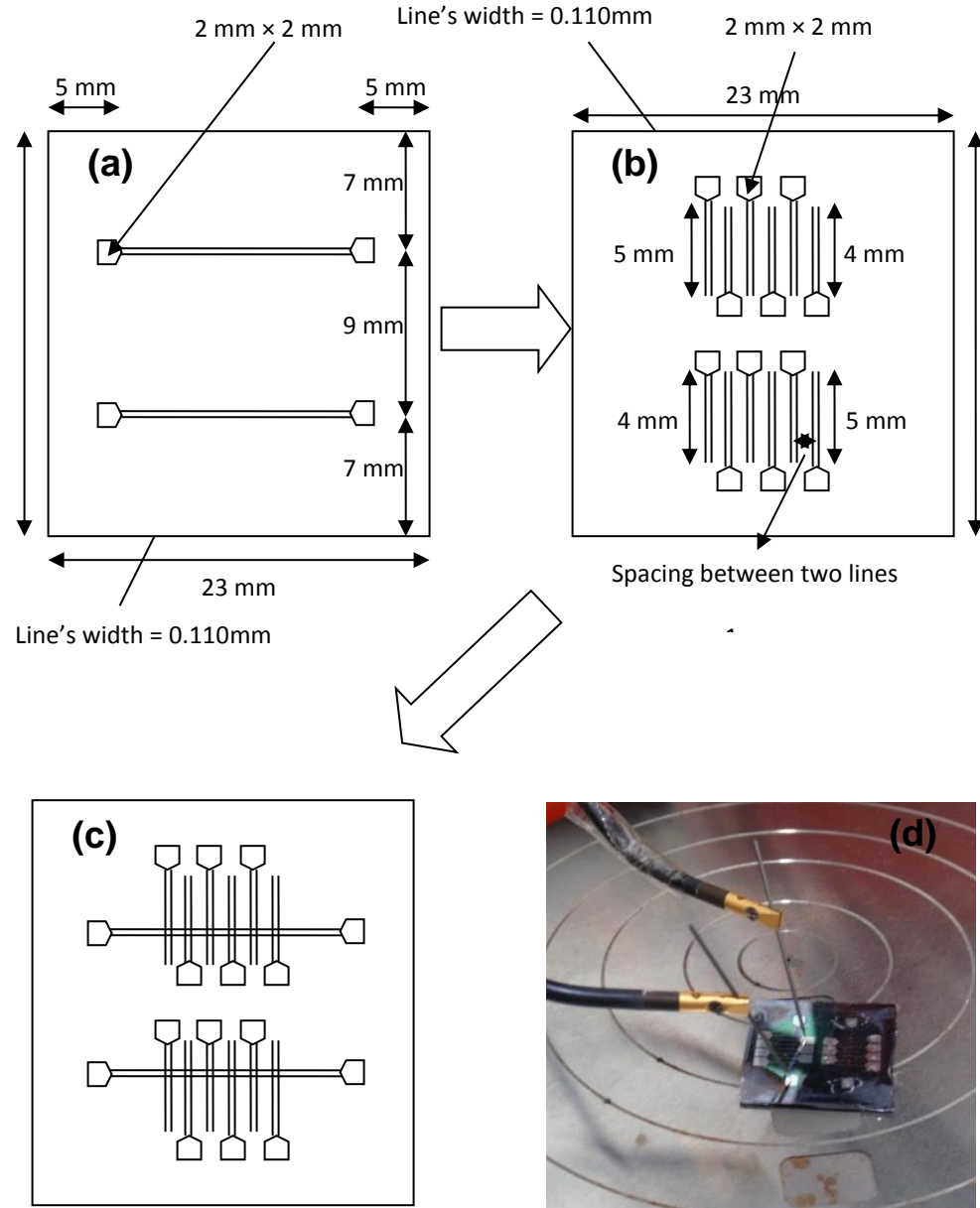


Figure 3.1: A schematic diagram of ferroelectric device: (a) bottom electrode, (b) top electrode, (c) desired MIM structure and (d) a MIM ferroelectric device deposited on silicon wafer.

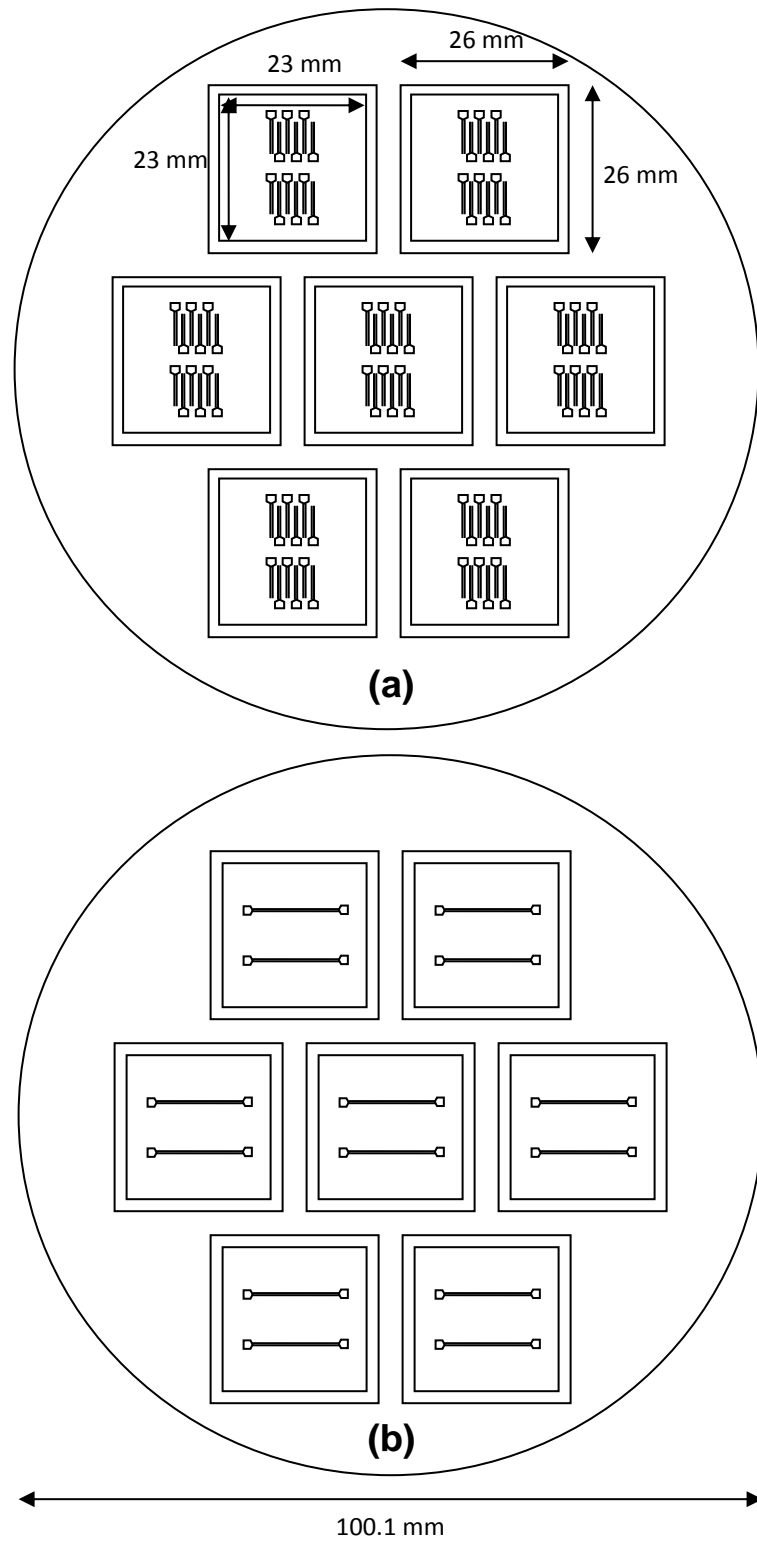


Figure 3.2: A schematic diagram of shadow mask: (a) top and (b) bottom electrode.

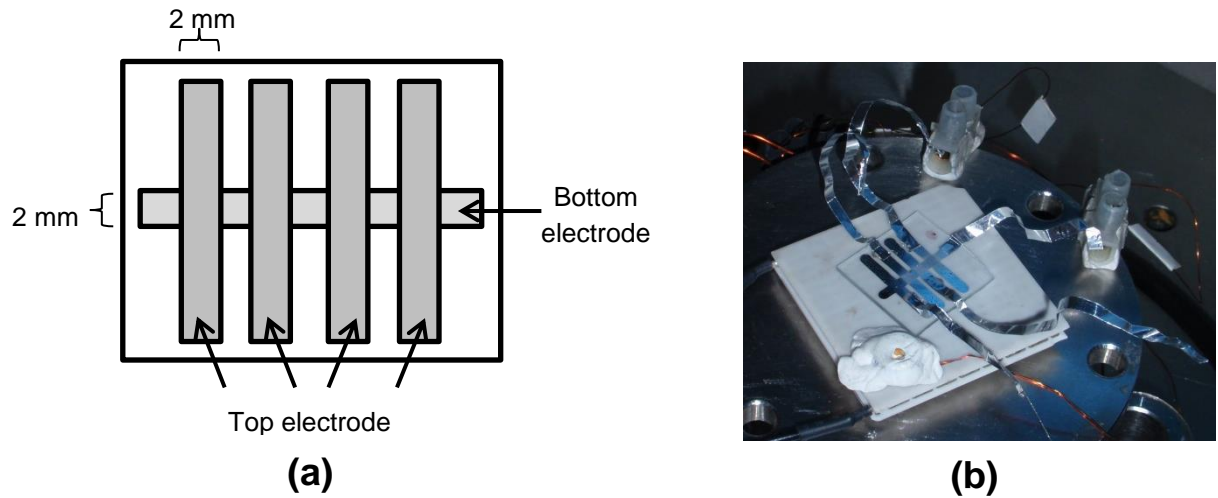


Figure 3.3: (a) A schematic diagram of a dielectric device (top view); (b) Picture of a dielectric device placed on the top of Peltier heater.

### 3.2.5 Poling

Ferroelectric grains in ceramics and polycrystalline films are normally split into many domains. Ferroelectric materials could be turned into a polar state by applying a strong electric field, usually at elevated temperatures. Before poling, the direction of the dipoles in domains is randomly distributed and cancels off each other, in such a way the net spontaneous polarization is zero as shown in Figure 3.4. Ferroelectric materials could be turned into a polar state by applying a strong electric field called poling process, usually at elevated temperatures. Poling process will realign the polar axes of the dipoles and as a result, a poled ferroelectric material exhibits pyroelectric and piezoelectric properties.

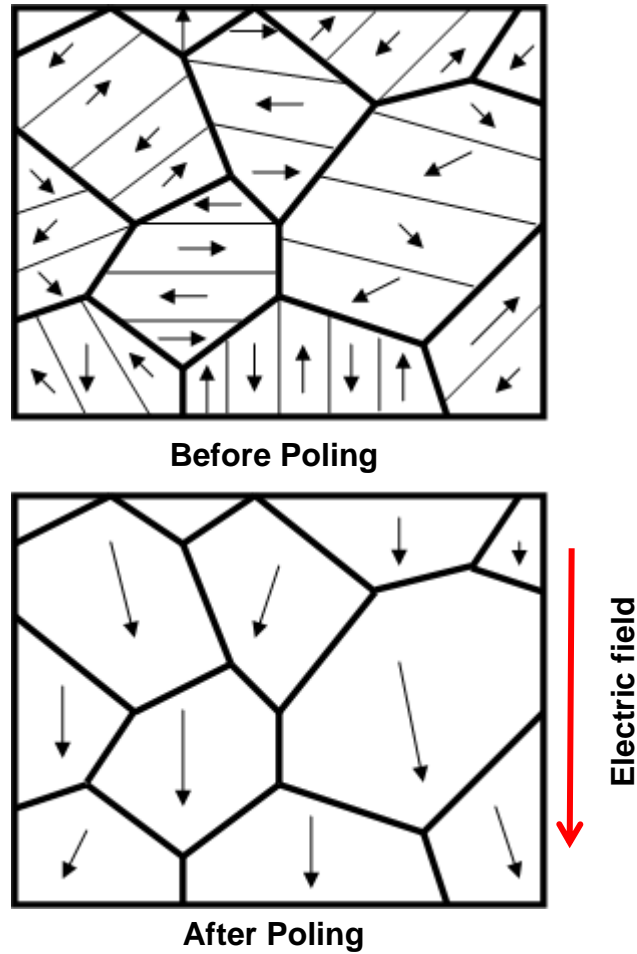


Figure 3.4: A schematic drawing of a polycrystalline ferroelectric with random orientation of grains before and after poling.

There are two types of poling process applied in this study. The first one, direct current (d.c.) poling at 250 to 300 MV/m was applied on the thin films at room temperature for 15 to 30 minutes in order to obtain its pyroelectricity. A schematic diagram of the d.c. poling method is presented in Figure 3.5. Conventionally, it is essential to apply the conducting electrodes which are thermally evaporated, sputtered, painted or pressed on the polymer surfaces with the voltage potential (T.R. Dargaville, 2005). The voltage potential applied to the electrodes produces an electric field across the samples. During this poling process, samples will be immersed in a silicon oil bath to prevent arcing or dielectric



breakdown that will permanently damage the samples. It is important to note that permanent electrodes prepared by thermal evaporated, sputtered, and painted are preferred over the pressed-on electrode (Copper or Aluminum tape) because of the superior contact between the interface of the electrodes and samples. The poor contact prepared by pressed electrode may lead to space charges trapped in the interface and caused inhomogeneity in the poling field. Application of high voltages for a prolonged period may increase the probability of dielectric breakdown. As a result, a variable field at low frequency with either sinusoidal or triangular waveforms has also been used (Li, Kagami, & Ohigashi, 1992). This process is normally called as ‘hysteretic poling’ by using hysteresis measurement apparatus (Bauer, 1983).

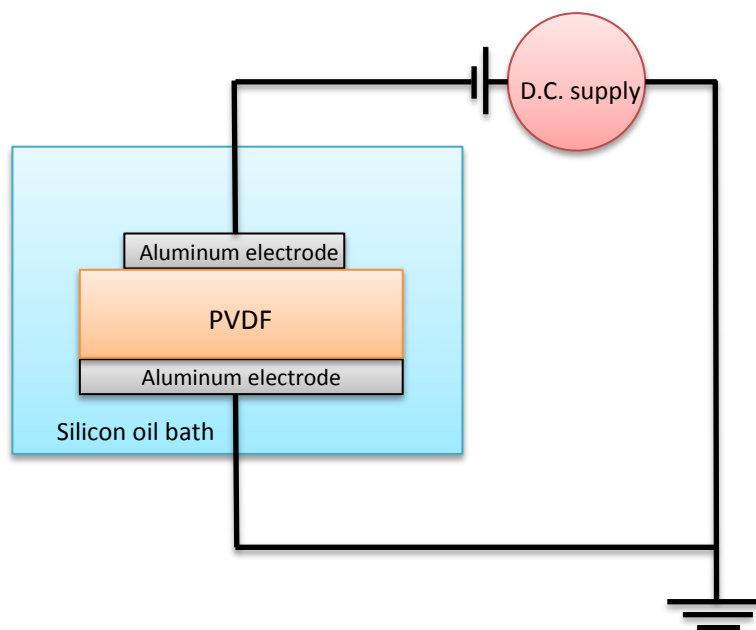


Figure 3.5: Schematic drawing of d.c. poling system.

Alternatively, a negative charge's corona poling was applied on the samples at room temperature in order to attain a phase transformation from Form II to polar Form IV. A schematic diagram of the corona poling method is shown in Figure 3.6. The surface of

the thin films from a corona needles point was connected to a negative terminal of an EHT supply and the bottom aluminum electrode was grounded to earth. The direction of the polarizing electric field is normally perpendicular to the thin films surface. The distance between the corona needle point and the thin films' surface was kept at 5 mm. The EHT supply was introduced at 3 - 4 kV potential to obtain a uniform charging. When the corona discharge occurs, the ionized particles are accelerated towards ground and deposited on the sample's surface. The surface potential was being monitored at around 100 V to 150 V by a voltmeter and the poling time should not exceed 5 minutes. The electric field applied on the thin films was in a range from 250 MV/m to 300 MV/m. The advantage of the corona poling are that it is more amenable to film imperfections, electrodes are not required and large area samples may be poled. However, the drawback is that it is considered more difficult to setup and optimize compared to that of the d.c. method (Dargaville et al., 2005).

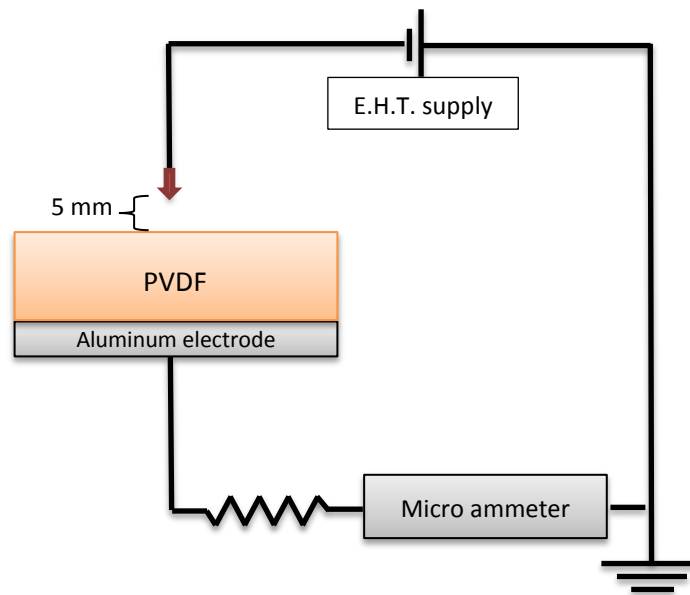


Figure 3.6: Schematic drawing of corona poling system.

### 3.3 Structural Analysis

#### 3.3.1 Fourier Transform Infrared Spectroscopy

Fourier transform infrared (FTIR) spectroscopy is one of the major characterization techniques to identify the chemical bonding of organic and inorganic materials. IR radiation constitutes a broad electromagnetic spectrum range between visible and microwave regions, covering wavenumber portions from 4000 to 400  $\text{cm}^{-1}$ . A number of vibrational modes can be detected and assigned to various bonds of the materials within this region. Each chemical bond possesses a characteristic absorption frequency and the resulting spectrum can be used as “fingerprint identification” for the chemical bonds existing in the materials (Stuart, 2000). Perkin Elmer 2000 FTIR spectroscopy system has been employed to determine the chemical bonding of PVDF thin films. The scans of FTIR were performed in the range of 400 to 1500  $\text{cm}^{-1}$ , with a resolution of 4  $\text{cm}^{-1}$  in the transmittance mode.

#### 3.3.2 X-ray Diffraction

X-ray diffraction (XRD, PANalytical -Empyrean) measurements were carried out to examine the crystalline structure and the effect of annealing in the samples. The wavelength of the X-ray source is 0.154 nm. 2 Theta-Omega ( $2\theta$ - $\omega$ ) scan with a step size of  $2\theta = 0.02^\circ$  was applied. The obtained XRD results were used to study the effect of annealing and to provide evidence of the phase transformation from Form II to IV in PVDF after subjected to poling process.

### 3.3.3 Surface Morphology

The surface morphology was obtained with a Hitachi (SU8000) field emission scanning electron microscope (SEM) and NT-MDT atomic force microscopy (AFM). SEM results suggest that annealing will eliminate the pin-hole and induce the formation of spherulite with an increase in crystallinity. The surface morphology of the samples were then re-examined by using AFM. Root-Mean-Square (RMS) roughness as a function of annealing temperature was studied to discuss the role of smooth surface in the application of the ferroelectric switching under a high electric field.

## 3.4 Electrical Measurement

### 3.4.1 Dielectric Measurement

The dielectric measurements were conducted using a combined system consisting of a laboratory-made dielectric spectrometer (10 mHz – 100 kHz) (Furukawa, Yasuda, & Takahashi, 2004) and an impedance analyzer HP 4194A (100 Hz – 40 MHz) to cover a broad frequency range. The measurement results were expressed in terms of either the complex permittivity

$$\varepsilon^* = \varepsilon' - i\varepsilon'' \quad (3.1)$$

or the complex conductivity

$$\sigma^* = \sigma' + i\sigma'' \quad (3.2)$$

From these equations, these constants can be mutually converted through

$$\sigma' = \omega\varepsilon'' \quad \sigma'' = \omega\varepsilon' \quad (3.3)$$

where  $\omega$  is the angular frequency,  $2\pi f$  (where  $f$  is the frequency).

### 3.4.2 Pyroelectric Measurement

Generally, the most common way that has been used to measure pyroelectric coefficient is a quasi-static method and a dynamic temperature method. The quasi-static method utilizes temperature variations under nearly thermal equilibrium condition whereas the dynamic temperature method use fast temperature changes which are caused by a pulsed or a periodically modulated heat flux (Kwong, Gan, Majid, Hashim, & Heidelberg, 2010). Prior to pyroelectric measurement, direct current (d.c.) poling at 250 to 300 MV/m was applied on the thin films in silicon oil at room temperature in order to obtain pyroelectricity. A quasi-static method was employed to evaluate the pyroelectric coefficient in this study.

Figure 3.7 shows the experiment set-up for the quasi-static pyroelectric activity measurement. The sample was mounted on a Peltier heater which was connected to a LakeShore 331 temperature controller. For better heat conduction purpose, heat sink compound was applied to establish good thermal contact between the thin films and heater. In particular, this unit of Peltier heater could be operated in the temperature range of 25 °C to 80 °C. It may also be operated below room temperature (minimum of 15 °C) with the assist of water cooling system using a chiller. The temperature of the thin films was measured using a highly sensitive silicon diode sensor. The temperature of the sample was set to increase at constant rates in order to generate a triangular temperature waveform while recording the short-circuited pyroelectric current (Gan & Abd Majid, 2010; Kwong et al., 2010). The heating rates which have been used in this experiment were 0.01 °C/s, 0.02 °C/s, 0.03 °C/s, 0.04 °C/s and 0.05 °C/s. The temperature of the sample (from 25 °C to 26 °C) was increased and subsequently decreased at a constant rate by a non-radiative heat source, which generates a periodic triangular temperature waveform (using a LakeShore 331 temperature controller), while the short-circuited pyroelectric current was measured by

a Keithley 617 electrometer. Figure 3.8 shows the typical result obtained from the pyroelectric measurement. The IEEE-488 GPIB interface was used to allow the computer to control and receive data from the two instruments. Pyroelectric coefficient,  $p$  is then evaluated by the change in spontaneous polarization,  $\Delta P$  of the samples with the change of temperature,  $\Delta T$  applied:

$$p = \frac{\Delta P}{\Delta T} \quad (3.4)$$

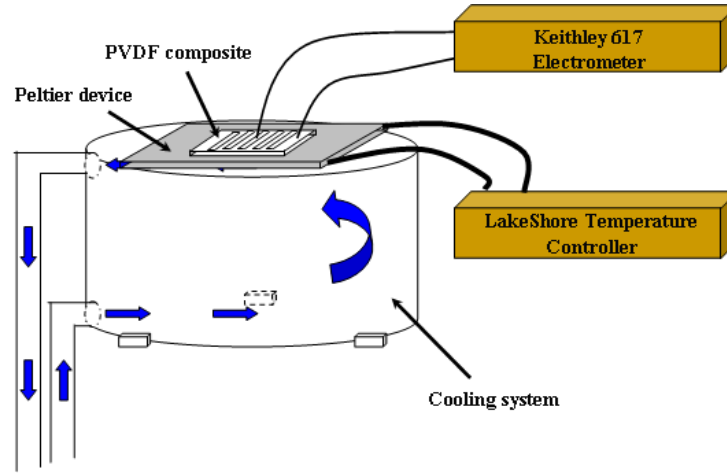


Figure 3.7: Schematic drawing of the experiment set-up for quasi-static pyroelectric measurement.

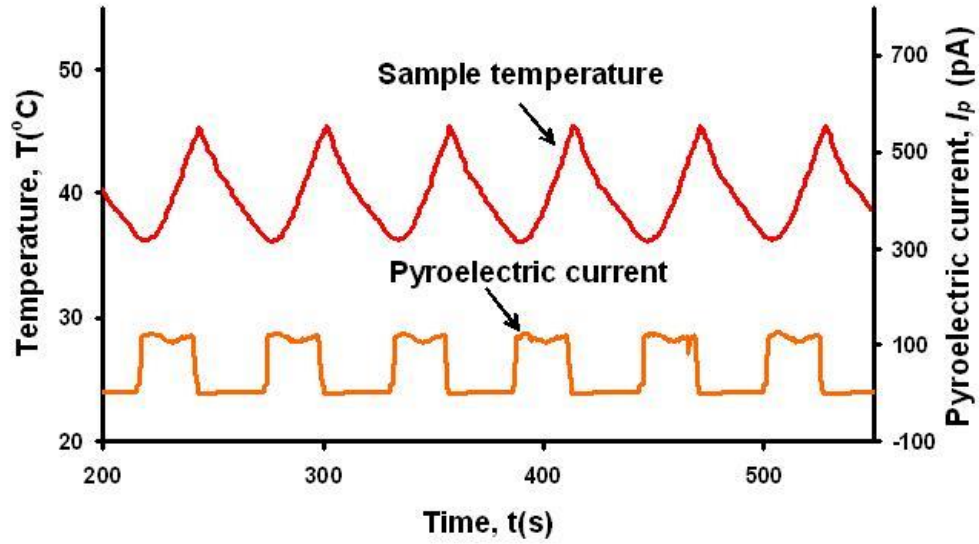


Figure 3.8: Typical triangular temperature waveform and the rectangular short-circuited pyroelectric current during the quasi-static pyroelectric measurement.

#### 3.4.2.1 Experimental Considerations

Non-uniform heating and injected space charges were two major issues which required serious attention in the quasi-static pyroelectric measurement. Non-uniform heating will invite the serious tertiary pyroelectric response from the samples. Note that the magnitude of temperature change applied in this experiment is only  $1^{\circ}\text{C}$  (that is  $25^{\circ}\text{C}$  to  $26^{\circ}\text{C}$ ), thus the applied heating rates were  $0.01^{\circ}\text{C/s}$ ,  $0.02^{\circ}\text{C/s}$ ,  $0.03^{\circ}\text{C/s}$ ,  $0.04^{\circ}\text{C/s}$  and  $0.05^{\circ}\text{C/s}$ . If the heating rate of the samples was set higher than  $0.05^{\circ}\text{C}$  in this experiment, the temperature supplied to the sample is unable to follow the set-point temperature. As a result, the sample's temperature may be significantly out of phase with the set-point temperature. Lower magnitude of pyroelectric current will be measured compared to that of expected results. In addition, non-uniform stresses applied to the samples as a result of inhomogeneous heating would contribute to tertiary pyroelectric effect. If heating rate more

than  $0.05\text{ }^{\circ}\text{C}$  is applied during the experiment, it is advisable to increase the temperature magnitude from  $1\text{ }^{\circ}\text{C}$  to about  $5\text{ }^{\circ}\text{C}$  to ensure that temperatures (sample and set-point) are in phase.

During the poling process, external charges were forced to be injected to the ferroelectric thin film in order to realign its dipoles in one direction prior to pyroelectric measurement. It is best to carry out the poling process in a silicon oil bath at an elevated temperature. The temperature applied during the poling process was about  $60\text{ }^{\circ}\text{C}$ . Higher temperature was not recommended here, even though it may help to accelerate the whole process because this may lead to the deterioration of spontaneous polarization at the same time. In addition, it is recommended to short circuit the sample after the poling process for hours depending on the condition of poling. During the poling process, considerable amount of charges will be injected to the samples. If the electrode of the sample or contact was not deposited properly, some charges might be trapped in between the surface interface (electrode and polymer). A non-reproducible short circuit pyroelectric current decaying with time would be observed as shown in Figure 3.9.

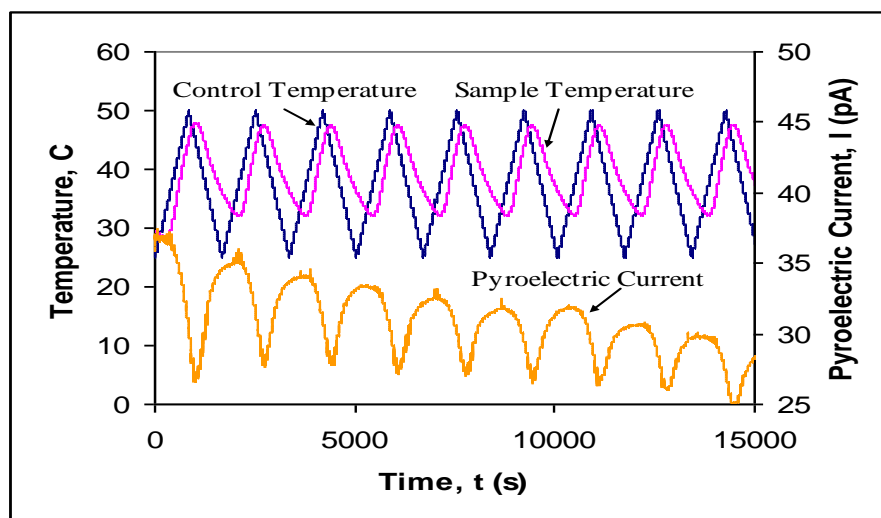


Figure 3.9: Pyroelectric current is decayed with time at the heating rate of  $0.03\text{ }^{\circ}\text{C}$ .



### 3.4.3 Ferroelectric Measurement

The  $D$ - $E$  hysteresis measurements were performed under a controlled applied field with a desired remnant polarization by using Radiant Technology Precision LC unit. A sinusoidal waveform electric field with a frequency of 100 Hz was applied to the samples at room temperature. Sample was immersed in a silicon oil bath to prevent arcing or dielectric breakdown. The voltage was increased in a step size of every 5 or 10 V.

#### 3.4.3.1 Experiment considerations

There is one major issue requires serious attention during ferroelectric measurements. The required coercive field,  $E_c$  apply to the Form I is 50-100 MV/m; in particular,  $E_c$  for Form IV is more than 200 MV/m in this study. Thin films treated under the high electric field leads to the dielectric breakdown easily. As a result, it is advisable to immerse the thin film in silicon oil during the measurement. It helps to prevent dielectric breakdown which will permanent damage the thin films. In order to optimize the ferroelectric properties of the pure PVDF thin films, electrodes of the samples were prepared in the size of  $110\ \mu\text{m} \times 110\ \mu\text{m}$ . As such, samples would be able to sustain much higher electric field and reduce arcing problem. However, larger electrode area is required for PVDF composite samples. Electrode area of  $1\ \text{mm} \times 1\text{mm}$ ,  $2\ \text{mm} \times 2\text{mm}$  and  $1\ \text{cm} \times 1\text{cm}$  were deposited to the composite sample to make sure consistent result would be obtained. The drawback of applying larger area of electrode is that, it is easier for the samples to experience dielectric breakdown when excessive higher conductivity inclusions were introduced to the composite thin films.

## References

- Bauer, F. (1983). PVF2 polymers: Ferroelectric polarization and piezoelectric properties under dynamic pressure and shock wave action. *Ferroelectrics*, 49(1), 231-240.
- Dargaville, T. R., Celina, M. C., Elliott, J. M., Chaplya, P. M., Jones, G. D., Mowery, D. M., Assink, R.A., Clough, R.L. & Martin, J. W. (2005). Characterization, Performance and Optimization of PVDF as a Piezoelectric Film for Advanced Space Mirror Concepts. *Sandia Report, SAND2005-6846*, 49.
- Furukawa, T., Yasuda, K., & Takahashi, Y. (2004). Dielectric and conductive spectra of the composite of barium titanate and LiClO<sub>4</sub>-doped polyethylene oxide. *IEEE Transactions on Dielectrics and Electrical Insulation*, 11(1), 65-71.
- Gan, W. C., & Abd Majid, W. H. (2010). Dependence of Pyroelectric Properties of La<sub>0.03</sub>Sr<sub>0.255</sub>Ba<sub>0.7</sub>Nb<sub>2-y</sub>Ti<sub>y</sub>O<sub>(6-y/2)</sub> Ceramic on Electric Field, Grain Refinement and Ti/Nb Crystallite Sizes. *Sains Malaysiana*, 39(6), 1007-1013.
- Kwong, W. L., Gan, W. C., Majid, W. H. A., Hashim, R., & Heidelberg, T. (2010). Pyroelectric detection in glycolipid thin film. *Thin Solid Films*, 518(15), 4412-4416.
- Li, G. R., Kagami, N., & Ohigashi, H. (1992). The possibility of formation of large ferroelectric domains in a copolymer of vinylidene fluoride and trifluoroethylene. *Journal of Applied Physics*, 72(3), 1056-1061.
- Stuart, B. (2000). Infrared Spectroscopy *Kirk-Othmer Encyclopedia of Chemical Technology*: John Wiley & Sons, Inc.
- T.R. Dargaville, M. C. C., J.M. Elliott, P.M. Chaplya, G.D. Jones, D.M. Mowery, R.A. Assink, R.L. Clough, J.W. Martin. (2005). Characterization, performance and optimization of PVDF as a piezoelectric film for advanced space mirror concepts. *Sandia Report, SAND2005-6846*, 49.

## **CHAPTER 4:            Structural, Ferroelectric and Pyroelectric Properties of Form IV Poly(vinylidene fluoride)**

### **4.1     Introduction**

Poly(vinylidene fluoride) (PVDF) is a high performance engineering polymer exhibits at least four crystalline polymorphs which are defined as Form I, II, III and IV (or  $\beta$ ,  $\alpha$ ,  $\gamma$  and  $\delta$  –phase, respectively). Accordingly, only Form I, III and IV are polar crystals and shows spontaneous polarization,  $P_s$  which is originated from the permanent dipoles and the long range rotation of the molecular chains via short range van der Waals interactions. From the technology point of view, most investigations on organic ferroelectric PVDF were basically focused on Form I due to its exceptional electrical properties for application purposes. The studies on the other two polar polymorphs, Form III and IV, were almost discontinued 40 years ago since their remanent polarizations are expected to be much smaller than Form I. The properties of these polymorphs are not well established, in particular for its pyroelectric and ferroelectric properties because the samples prepared are normally mixture of various polymorphs as well as amorphous regions. In the present work, we re-examined the ferroelectric switching characteristics and pyroelectric properties of Form IV PVDF prepared by spin-coating technique. The samples were subjected to annealing which results in changes in crystallinity. It will be shown that the ferroelectric and pyroelectric properties are strongly governed by degree of crystallinity. To date, no details study on dielectric properties of Form IV PVDF is presented. In particular, a wide range of dielectric spectroscopy has also been extended to determine the molecular dynamic of Form IV PVDF. By combining the results from the above finding with the detail analysis on the crystalline and structure morphology, fundamental understanding on the extraordinary electrical responses of Form IV PVDF when induced by electric field can

be established. Such data are important in order to describe the mechanisms that govern the ferroelectric and pyroelectric properties of Form IV PVDF.

#### **4.2 The Effect of Annealing on Crystalline Structure and Morphology of Spin-cast Form II PVDF**

Figure 4.1 illustrates the transmission infrared (IR) spectra of the PVDF thin films as a function of annealing temperature from 60 °C to 140 °C cast from acetone. The absorption bands observed at 531, 612, 766, 796, 855, 873 and 976  $\text{cm}^{-1}$  are characteristic of Form II whereas the absorption band at 510 and 840  $\text{cm}^{-1}$  are characteristic of the Form I (Gregorio Jr & Borges, 2008; R. Gregorio, 2006). Here, the 510 and 531  $\text{cm}^{-1}$  bands are assigned to  $\text{CF}_2$  bending mode; whereas both the 612 and 766  $\text{cm}^{-1}$  bands are assigned to  $\text{CF}_2$  bending coupled to skeletal bending; the 796 and 855  $\text{cm}^{-1}$  are assigned to  $\text{CH}_2$  rocking. The 840, 873 and 976  $\text{cm}^{-1}$  bands, assigned to  $\text{CH}_2$  rocking coupled to  $\text{CF}_2$  antisymmetric stretching, backbone stretching and bending mode, and  $\text{CH}_2$  twisting mode, respectively (Kobayashi, Tashiro, & Tadokoro, 1975; Tashiro, Itoh, Kobayashi, & Tadokoro, 1985). It is shown that the absorption peaks at 510  $\text{cm}^{-1}$  and 840  $\text{cm}^{-1}$  (Form I) are relatively small compare to Form II absorption bands, even though the films are treated with a low annealing temperature at 60 °C. It is important to note that the intensity of the absorption peak at 873  $\text{cm}^{-1}$  has reduced significantly with the increase of annealing temperature.

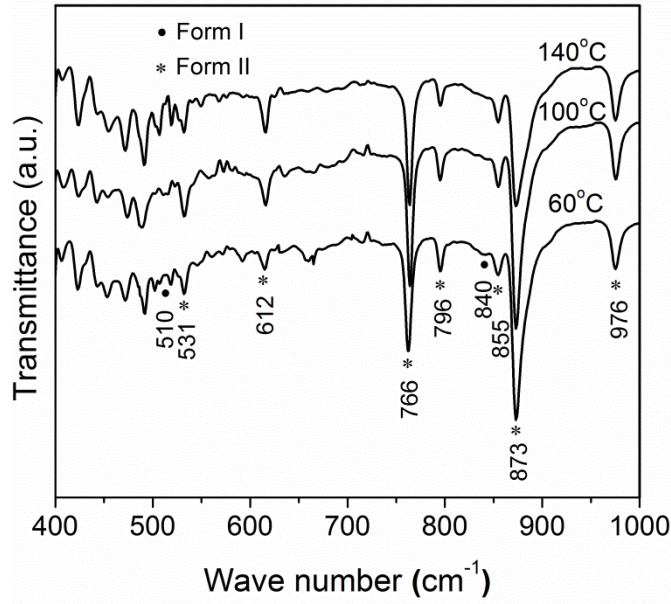


Figure 4.1: The dependence of FTIR spectra of PVDF thin films on annealing temperature.

The relative fraction of Form II,  $F(II)$ , in the samples which contain both Form I and II, was calculated by a method proposed by Osaki and Kotaka (J. R. Gregorio & Cestari, 1994; Li, Shimizu, Furumichi, Takahashi, & Furukawa, 2007; Osaki & Kotaka, 1981). On the basis of Lambert-Beer,  $F(II)$  is confirmed by:

$$F(II) = \frac{X_{II}}{X_I + X_{II}} = \frac{A_{II}}{A_{II} + (K_{II}/K_I)A_I} = \frac{A_{II}}{A_{II} + 0.769A_I} \quad (4.1)$$

where  $A_{II}$  and  $A_I$  are the intensities at  $766 \text{ cm}^{-1}$  (representing Form II) and  $840 \text{ cm}^{-1}$  (representing Form I), respectively.  $X$  is the degree of crystallinity of the Form I and II.  $K$  is referring to the absorbance at the corresponding wavenumber;  $K_{II}$  is  $6.1 \times 10^4 \text{ cm}^2 \text{ mol}^{-1}$  and  $K_I$  is  $7.7 \times 10^4 \text{ cm}^2 \text{ mol}^{-1}$ . Figure 4.2 shows the fraction of the Form II of PVDF as a function of annealing temperature. It shows the content of Form II of the PVDF thin films cast from acetone and MEK is  $> 90 \%$ , which is relatively high and independent of the annealing temperature. This indicates that the PVDF thin films prepared from the solvents with low boiling point promote the formation of Form II PVDF.

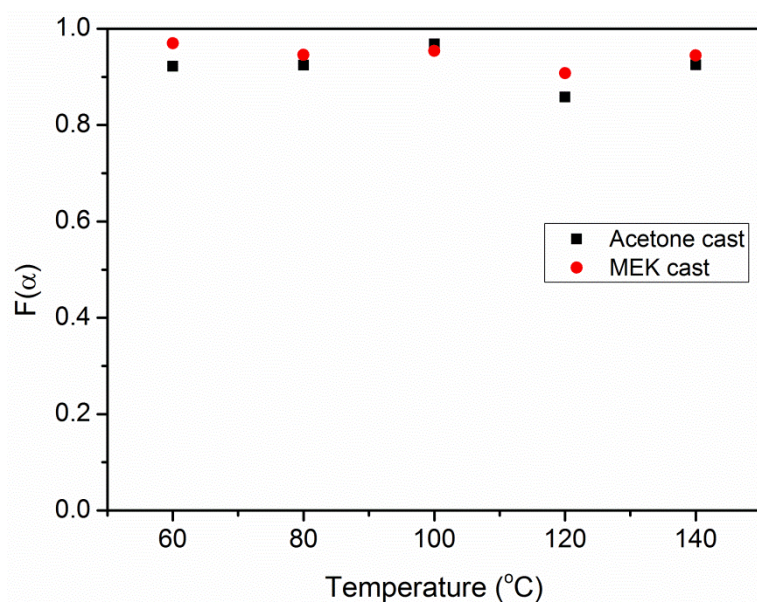


Figure 4.2: Fraction of the Form II,  $F(\alpha)$  of PVDF thin films as a function of annealing temperature.

Figure 4.3 shows the x-ray diffraction patterns of the PVDF thin films subjected to annealing at various temperatures. No prominent peak was being observed at  $2\theta$  range around  $16^\circ$  to  $21^\circ$  for the PVDF thin films annealed at temperature below  $100^\circ\text{C}$ . The broad shoulder within this region is attributed to halo from the non-crystalline region. Thin films annealed at temperatures above  $100^\circ\text{C}$  begin to show sharp crystalline peaks in the X-ray diffraction patterns. The peaks observed at  $2\theta = 17.6^\circ, 18.6^\circ, 19.9^\circ, 25.8^\circ$  and  $26.7^\circ$  are assigned to (100), (020), (110), (120) and (021) reflections respectively, characteristics of Form II PVDF (Broadhurst & Davis, 1984; Das-Gupta & Doughty, 1977, 1978, 1980; Das-Gupta, Doughty, & Shier, 1979; Davis, McKinney, Broadhurst, & Roth, 1978; Naegele, Yoon, & Broadhurst, 1978). Annealing induces growth of the peaks and diminishment of the broad shoulder. Both X-ray and IR spectra indicate that PVDF thin films spin-coated from acetone and MEK are Form II dominant. For quantitative analysis, the crystalline peaks and the non-crystalline halo were deconvoluted using Gaussian

function to determine the degree of crystallinity,  $X_c$ . The height of the crystalline peaks increased and the non-crystalline shoulder diminishes with increasing annealing temperature, while the total area remains constant. The degree of crystallinity,  $X_c$  was evaluated from the ratio of crystalline area to total area of crystalline and non-crystalline.

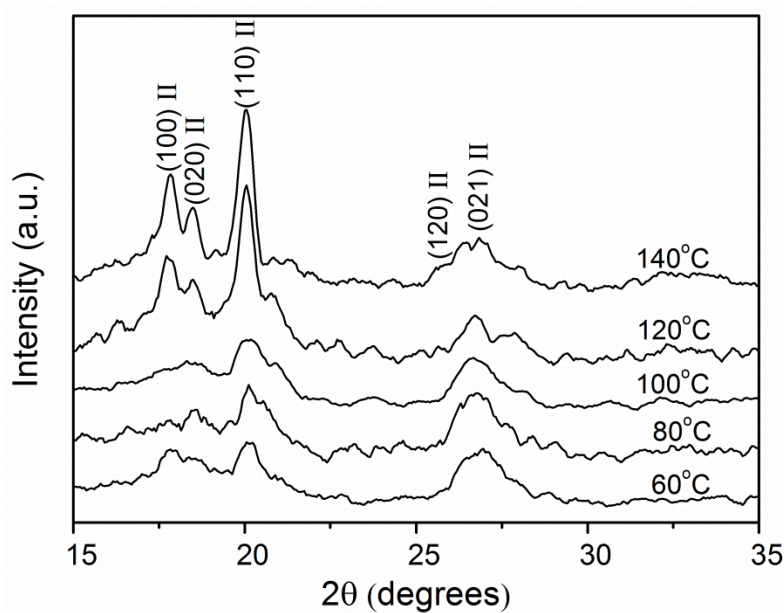


Figure 4.3: X-ray diffractograms of PVDF thin films: effect of annealing temperature.

Surface morphology of the annealed PVDF was performed by SEM and AFM. Figure 4.4 shows the SEM microstructures of the PVDF thin films. The PVDF thin films annealed at 60 °C and 80 °C exhibit sponge-like porous structure as shown in Figure 4.4 (a) and (b). The appearance of such porous structure is undesirable under a high electric field for the poling process. The pin-hole will caused electrical break down even at relatively low poling electric fields. As it is annealed at 120 °C, the sponge-like porous structure was eliminated and the growth of irregular spherulite becomes more obvious. It is suggesting that the formation of spherulite is growth in parallel with an increase in crystallinity. Annealing at 140 °C induces a growth of root-like spherulite and a formation of large

spherulite domains. The average spherulite domain size is estimated to be 50 nm in diameter (see Figure 4.4 (f)). The surface morphology of the samples were then re-examined by using AFM. Figure 4.5 shows the AFM height images of the annealed samples. It is shown that the roughness of the samples has been significant reduced as the annealing temperature increased to 140 °C. The role of smooth surface will be discussed later for the application of the ferroelectric switching under a high electric field.

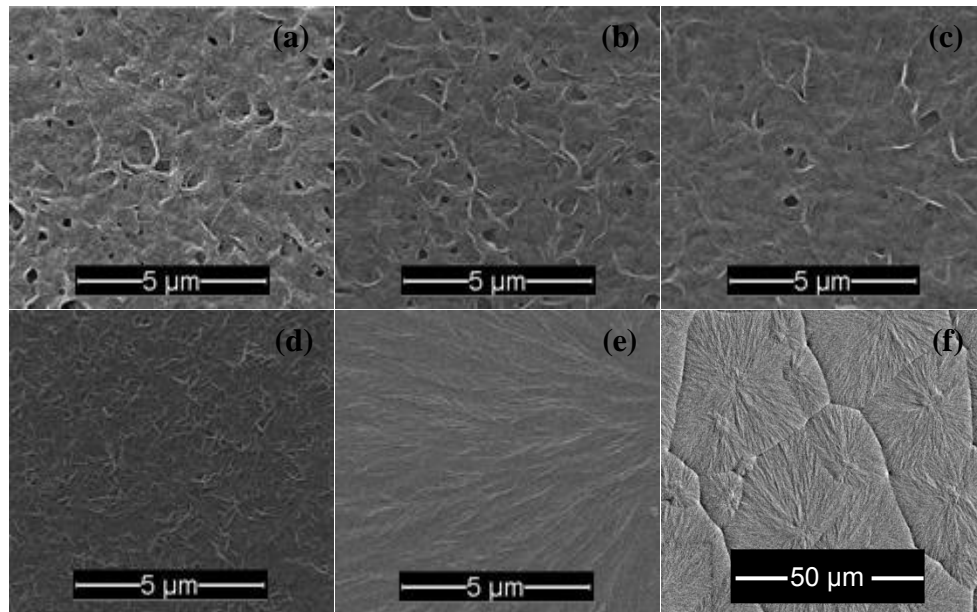


Figure 4.4: SEM microstructure of PVDF thin films annealed at (a) 60 °C, (b) 80 °C, (c) 100 °C, (d) 120 °C, (e) 140 °C and (f) microstructure of PVDF in smaller scale of magnification at 140 °C.



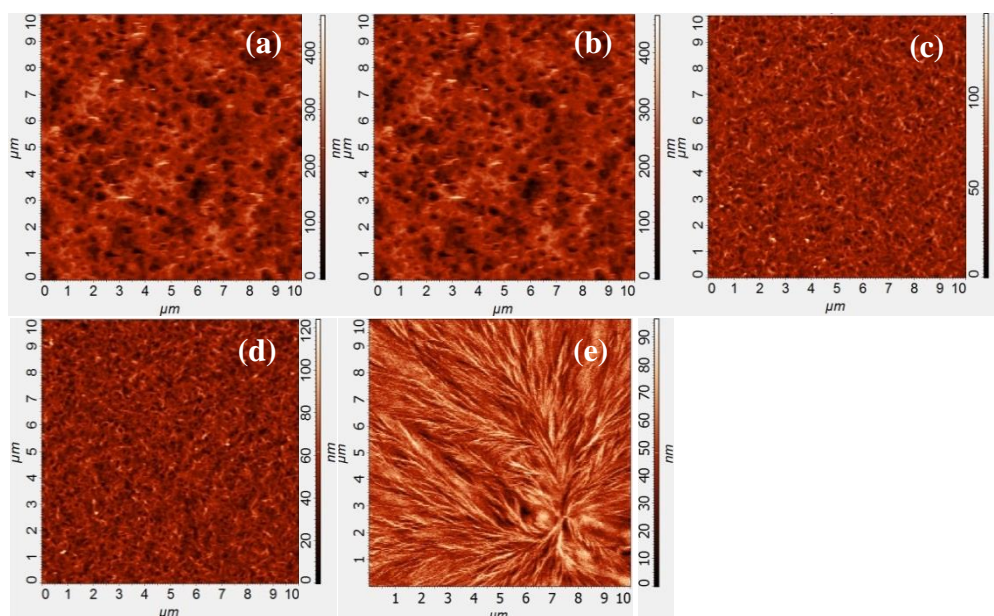


Figure 4.5: Typical AFM height images of PVDF thin films annealed at (a) 60 °C, (b) 80 °C, (c) 100 °C, (d) 120 °C and (e) 140 °C.

### 4.3 Effect of Poling on Phase Transformation from Form II to Form IV PVDF

XRD results were presented here to explain phase transformation from Form II to Form IV due to poling process on the PVDF thin films. The influence of a high electric field on Form II can be seen from the XRD results as shown in Figure 4.6. The predominant changes to be noted here is the increase in the intensity of the (110) reflection and the significant decrease in the (100) and (120) reflection planes after the poling process. In order to conduct thorough quantitative analysis, the XRD patterns were deconvoluted as shown in Figure 4.7 and the area under the peaks were calculated and tabulated in Table 4.1.

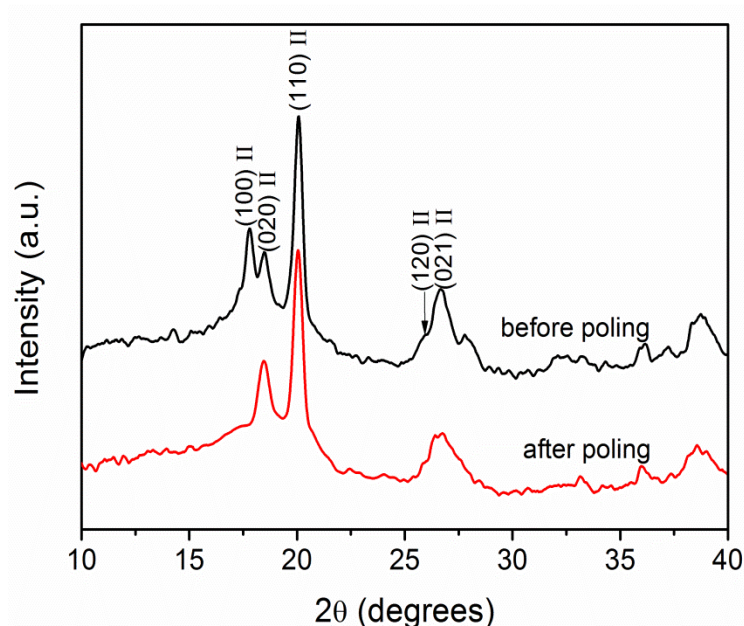


Figure 4.6: X-ray diffractograms of acetone cast PVDF thin films before and after poling.

The results show large reductions in the areas of (100) and (120) reflection planes and the peaks intensities were almost completely diminished after poling process. These are attributed to phase transition in PVDF that took place during the poling process (Broadhurst & Davis, 1984; Das-Gupta & Doughty, 1977, 1978, 1980; Das-Gupta et al., 1979; Davis et al., 1978; Naegele et al., 1978). Field induced changes in the intensity of X-ray reflections from Form II to IV is interpreted as due to rotation about the chain axis without altering the chain conformation or unit cell dimensions (Davis et al., 1978). When a very high electric field is applied to Form II crystal, it will causes the molecular stem within the crystal to rotate about its axis so that the dipoles are then parallel in a polar crystal form. The X-ray results have clearly shown that strong electric field has induced a phase transition from Form II to the highly polar Form IV. Furthermore, the results show no formation of signature Form I crystalline peak at  $2\theta = 20.9$  after the poling process. It suggests that the PVDF thin films have fully transformed from Form II to Form IV which contradict the

findings made by Das Gupta et al and Southgate (Das-Gupta & Doughty, 1977; Southgate, 1976).

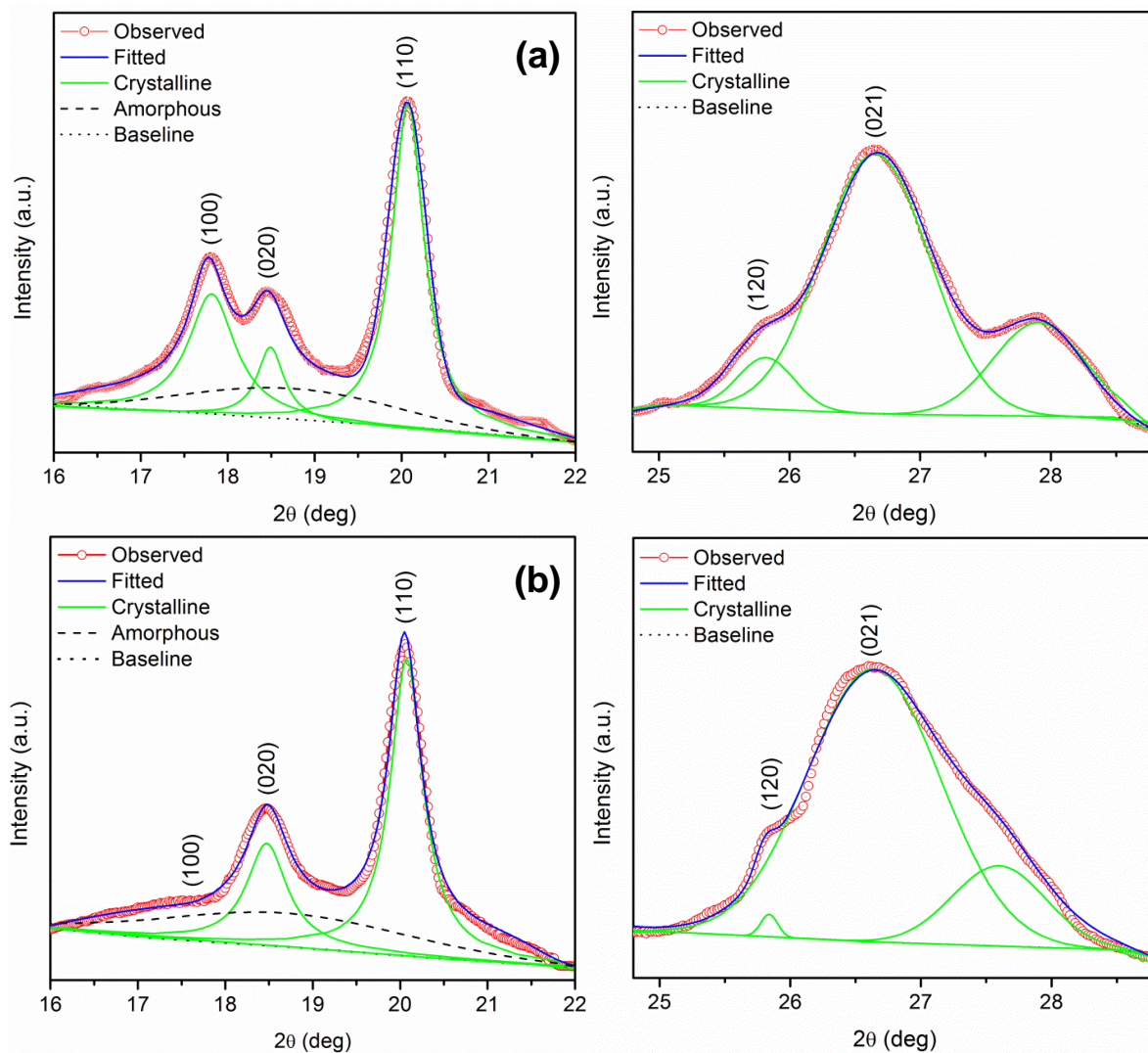


Figure 4.7: Deconvolution of XRD spectra of acetone cast PVDF (a) before and (b) after poling.

PVDF	Bragg angle, 2 $\theta$ degrees	Crystallographic plane	Crystalline form	Area (a.u.) Before poling	Area (a.u.) After poling
Acetone cast	17.7	100	$\alpha$ (Form II)	12.63	0
	18.4	020	$\alpha$ (Form II)	8.80	10.02
	20.1	110	$\alpha$ (Form II)	21.21	22.23
	25.8	120	$\alpha$ (Form II)	1.55	0.08
	26.7	021	$\alpha$ (Form II)	13.33	11.86
MEK cast	17.7	100	$\alpha$ (Form II)	3.94	0
	18.4	020	$\alpha$ (Form II)	8.72	5.05
	20.1	110	$\alpha$ (Form II)	12.11	15.23
	25.8	120	$\alpha$ (Form II)	0.81	0.02
	26.7	021	$\alpha$ (Form II)	6.75	2.79

Table 4.1: Summary of x-ray diffraction results of PVDF (before and after poling).

#### 4.4 Ferroelectric Activity in Form IV PVDF

Figure 4.8 shows the  $D$ - $E$  hysteresis loops for the PVDF thin films annealed at 140 °C and measured at room temperature using a frequency of 100 Hz. The applied electric field is a step wise increased. When the amplitude of  $E$  is lower than 100 MV/m, the  $D$ - $E$  relation is almost linear indicates that the displacement is mainly contributed by the linear dielectric polarization. As amplitude of  $E$  is increased, hysteresis begins to appear rapidly. In contrast to the conventional PVDF-TrFE which always displayed a square loop, a highly rounded hysteresis loop at 500 MV/m is observed. A maximum remanent polarization,  $P_r$  of 70 mC/m<sup>2</sup> and a coercive electric field,  $E_c$  of 240 MV/m was obtained.  $D$ - $E$  hysteresis loops annealed at difference annealing temperature is presented in Figure 4.9. The polarization increases with the annealing temperature from 50 mC/m<sup>2</sup> at 60 °C to 70 mC/m<sup>2</sup> at 140 °C. However, the coercive electric field applied on various annealing temperature are

almost remain unchanged and it is almost independent of annealing. Relatively low remanent polarization for the samples annealed below 100 °C was obtained compared to that of well annealed samples (above 120 °C) due to the enhanced crystallinity. Note that application of high electric fields will result in breakdown of the sample's surface. This is true for the samples annealed below 100 °C.

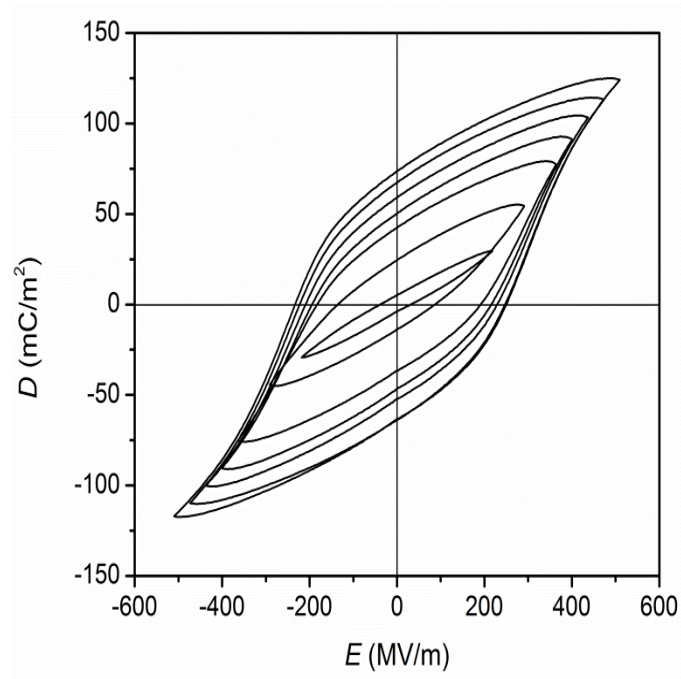


Figure 4.8:  $D$ - $E$  hysteresis loops of acetone cast PVDF annealed at 140 °C in steps of 40 MV/m.

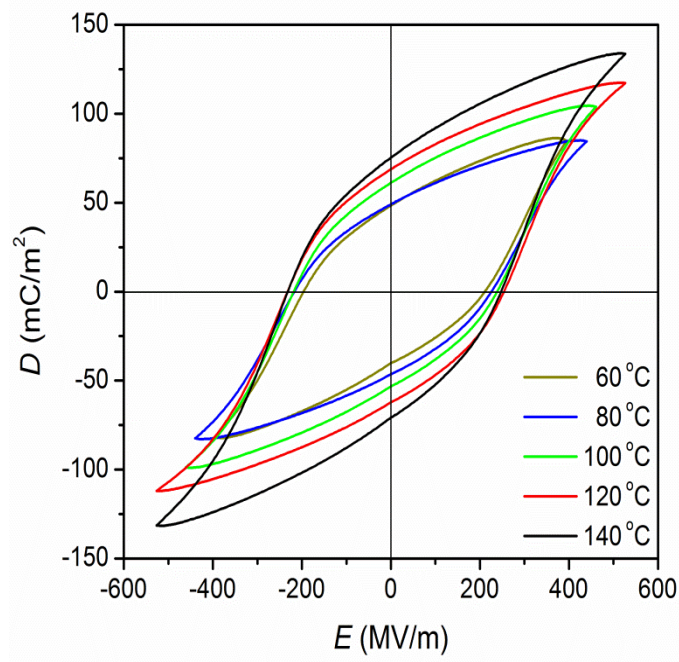


Figure 4.9:  $D$ - $E$  hysteresis loops of acetone cast PVDF annealed at different temperature.

#### 4.5 Pyroelectric Activity in Form IV PVDF

A rectangular waveform of pyroelectric current was obtained when a triangular temperature waveform was applied to a pre-poled acetone cast PVDF annealed at 140 °C, as shown in Figure 4.10 (a). The resultant square pyroelectric current waveform (Figure 4.10 (b)) is due to the change in the spontaneous polarization,  $\Delta P$  of the sample with temperature as shown in Figure 4.10 (c). Figure 4.11 shows plot of the change in spontaneous polarization,  $\Delta P$  with respect to the change of temperature,  $\Delta T$ . The pyroelectric coefficient was then obtained by evaluating the gradient of the graph in Figure 4.11. Figure 4.12 illustrates the dependence of the pyroelectric coefficient,  $p$  on annealing temperatures. The pyroelectric coefficient increases with the increase of annealing temperature. A maximum pyroelectric coefficient, 30  $\mu\text{C}/\text{m}^2\text{K}$  was obtained from the samples annealed at 140 °C.



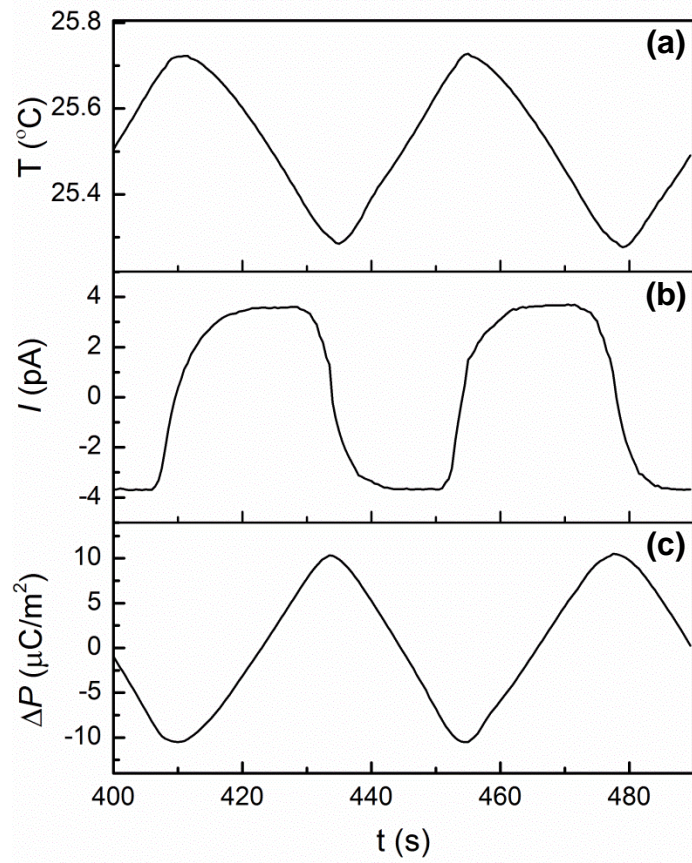


Figure 4.10: Plots of (a) triangular temperature waveform,  $T$ , (b) square pyroelectricity response,  $I$  and (c) change of polarization,  $\Delta P$  as a function of time for pyroelectric measurement.

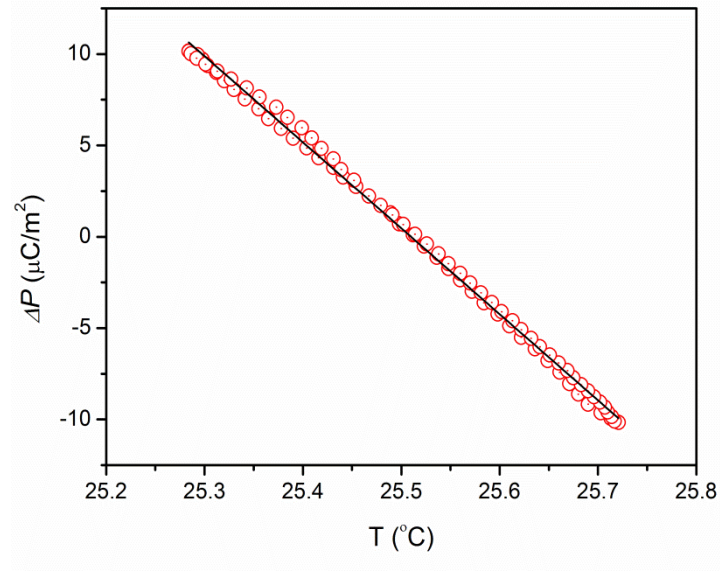


Figure 4.11: Dependence of change of polarization,  $\Delta P$  with respect to the change of temperature,  $\Delta T$ .

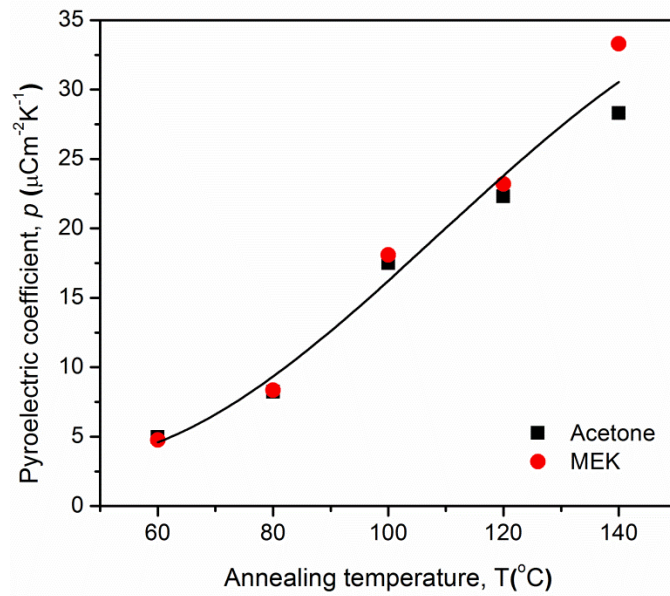


Figure 4.12: Dependence of the pyroelectric coefficient,  $p$  on annealing temperatures.



#### 4.6 Dielectric Relaxation in Form II and Form IV PVDF

The temperature and frequency dependence of  $\epsilon'$  and  $\epsilon''$  for the unpoled and poled PVDF thin films is shown in Figure 4.13. In general, a semicrystalline polymer like PVDF exhibits two relaxation processes near 1 Hz and 1 MHz at room temperature (T. Furukawa, 1989a). It is well established that the low frequency relaxation process of PVDF is attributed to crystalline motions in the  $\alpha$ -relaxation and its high frequency relaxation process is related to the non-crystalline motion,  $\beta$ -relaxation which is associated with the glass transition. The  $\beta$ -phase relaxation is not the main focus in this study as the range of the temperature and frequency is restricted to 25 °C to 140 °C and 10 mHz to 1 MHz respectively. The  $\alpha$ -relaxation is associated with the crystalline motion due to fluctuation of end-to-end dipolar moment in the chain direction. This  $\alpha$ -phase relaxation disappears due to melting (>150 °C). A single  $\epsilon''$  peak as a function of frequency domain which is attributed to the  $\alpha$ -phase relaxation is observed near 10 Hz at room temperature. The intensity of the  $\epsilon''$  peak increases and shifts to a higher frequency with the increasing temperature at every 10 °C from 25 °C to 140 °C. The continuous rise of  $\epsilon''$  is inversely proportional to frequency (< 100 mHz) which exhibits a gradient of -1 are attributed to dc conductivity. This is mainly due to the space charges trapped in between the amorphous and crystalline regions during the poling process.

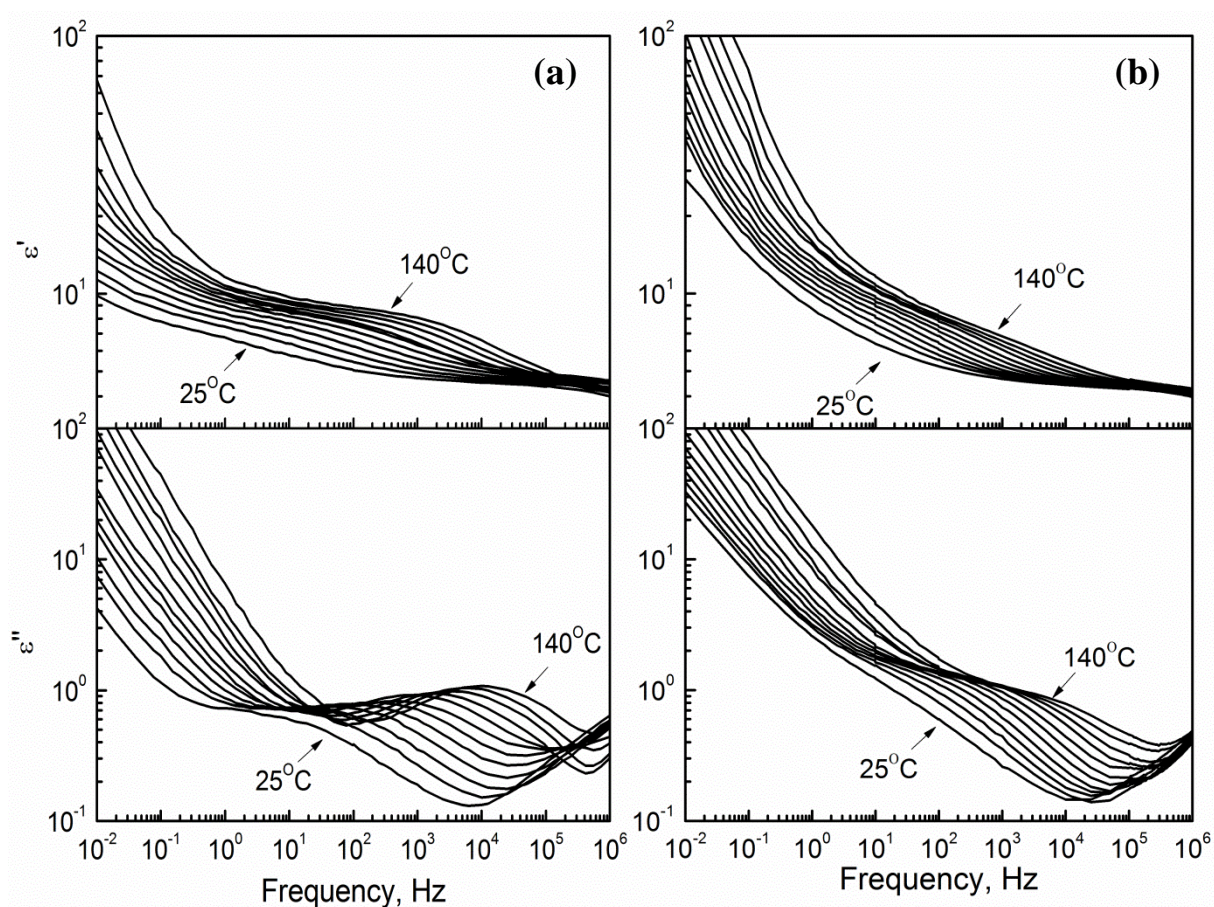


Figure 4.13: Frequency dependence of  $\epsilon'$  and  $\epsilon''$  for (a) unpoled and (b) poled PVDF thin films at a temperature step size of 10 °C.

Figure 4.14 shows the temperature dependence of  $\epsilon'$  and  $\epsilon''$  at 1 kHz for unpoled and poled PVDF. There is no prominent relaxation being observed over the temperature range, which indicates that there is no ferroelectric phase transition taking place as the curie point of PVDF is higher than its melting point. The dielectric constants of the PVDF steadily increased to higher values at the temperature above 100 °C. It is important to note that such behaviours are intimately related to the formation of spherulite and lamellar crystal structure which have been clearly seen from XRD and SEM results.

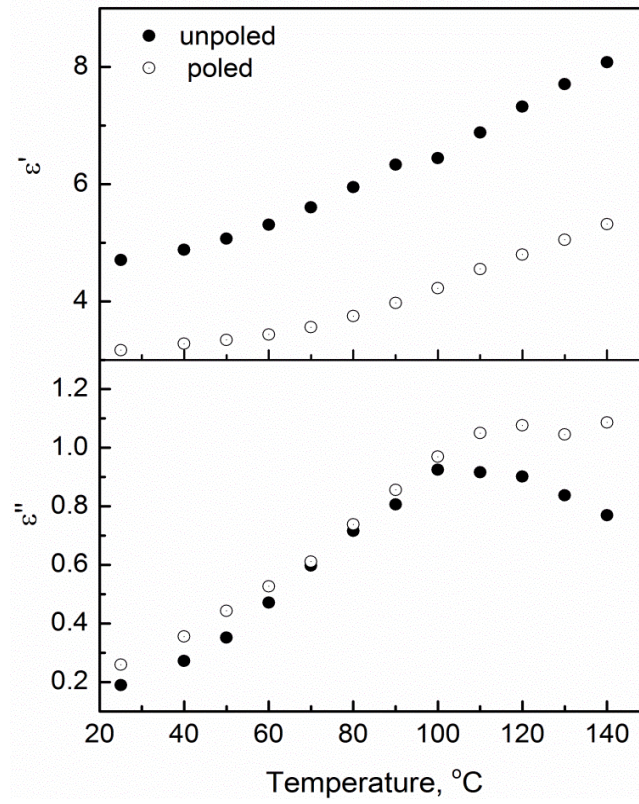


Figure 4.14: Temperature dependence of  $\epsilon'$  and  $\epsilon''$  at 1 kHz for unpoled (filled circles) and poled (open circles) PVDF.

Two significant changes in the dielectric properties are seen in Figure 4.13 and 4.14 as a result of poling process: (1) the dielectric constants,  $\epsilon'$  have been suppressed to the lower values as the frequency increases above 10 kHz.; (2) the crystalline motions  $\alpha$ -relaxation peak of poled PVDF has shifted to the lower frequency over the temperature range.

In order to conduct thorough analysis of the crystalline relaxation process for the frequency dependence of  $\epsilon'$  and  $\epsilon''$ , Havriliak-Negami (HN) function has been employed (T. Furukawa, Yasuda, & Takahashi, 2004).

$$\epsilon = \epsilon_{\infty} + \frac{\Delta\epsilon}{(1 + (i\omega\tau)^{\beta})^{\alpha}} + \frac{\sigma_{dc}}{i\omega} \quad (4.2)$$

where  $\epsilon_{\infty}$  is the instantaneous permittivity,  $\Delta\epsilon$  is the dielectric strength,  $\tau$  is the relaxation time,  $\sigma_{dc}$  is the dc conductivity,  $\alpha$  and  $\beta$  are parameters describing a distribution of

relaxation times. The fitted distribution parameters in this model were closed to value of one. This implies that the shape of the relaxation peaks were almost symmetrical. Figure 4.15 shows the observed (circles) and fitted (solid lines) spectra of  $\epsilon'$  and  $\epsilon''$  for PVDF measured at 140 °C. The fitted result comprised by HN function is evaluated as the best-fit parameters.

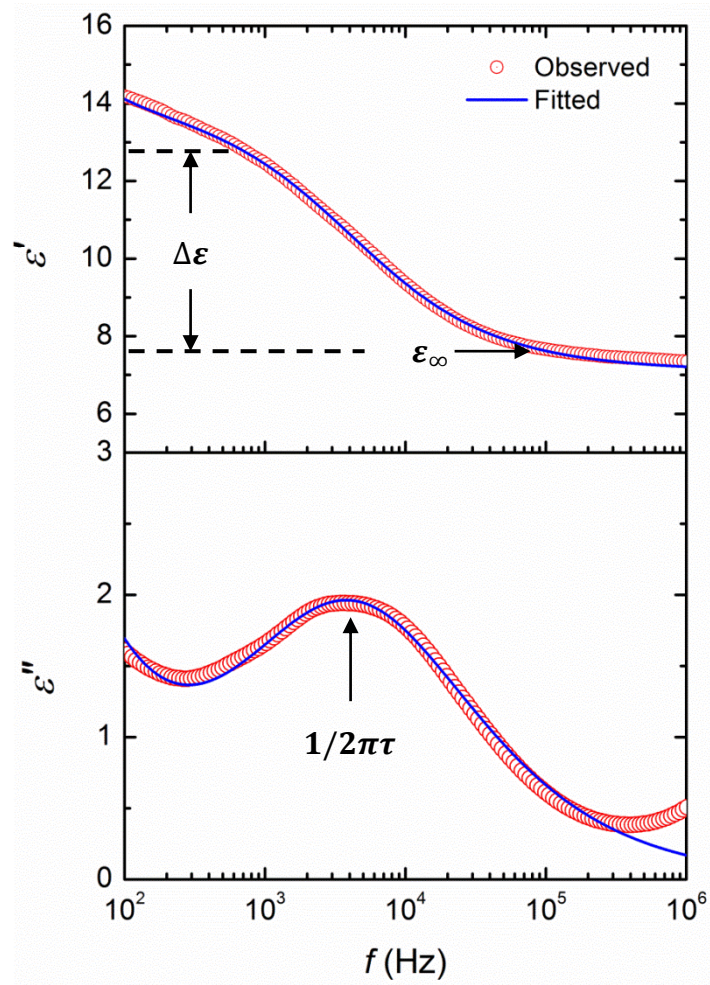


Figure 4.15: Observed and fitted dielectric spectra of PVDF at 140 °C.



## 4.7 Discussion

Combining the X-rays and surface topography analysis by AFM, degree of crystallinity and rms roughness are plotted as a function of annealing temperature in Figure 4.16. It is shown that annealing from 60 °C to 140 °C not only induced the crystallinity of the samples from 30% to 75%, but also helps to smooth the surface roughness from 45 nm to about 10 nm. The smoothed surface is attributed to the reason why high electric field can be applied on the sample annealed at high temperature.

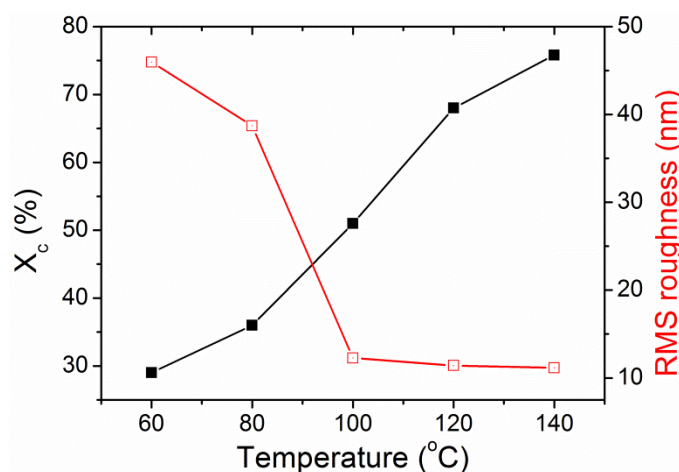


Figure 4.16: Degree of crystallinity and rms roughness plotted as a function of annealing temperature.

Figure 4.17 shows the degree of crystallinity,  $X_c$ ,  $P_r$  and  $p$  are plotted against the annealing temperature. Annealing below 100 °C,  $X_c$  shows a very small value of about 30-40%. It is shown that annealing above 100 °C has induced a significant increase in  $X_c$  and reached a maximum crystallinity of about 75% when annealed at 140 °C. It yields a maximum  $P_r$  and  $p$  of 70 mC/m<sup>2</sup> and 30  $\mu$ C/m<sup>2</sup>K<sup>1</sup>, respectively. Both the  $P_r$  and  $p$  values have shown an identical profile which respect to the annealing. As a result, it can be

suggested that the increase in  $P_r$  and  $p$  due to annealing is primarily attributed to the increase in degree of crystallinity,  $X_c$  in PVDF thin films.

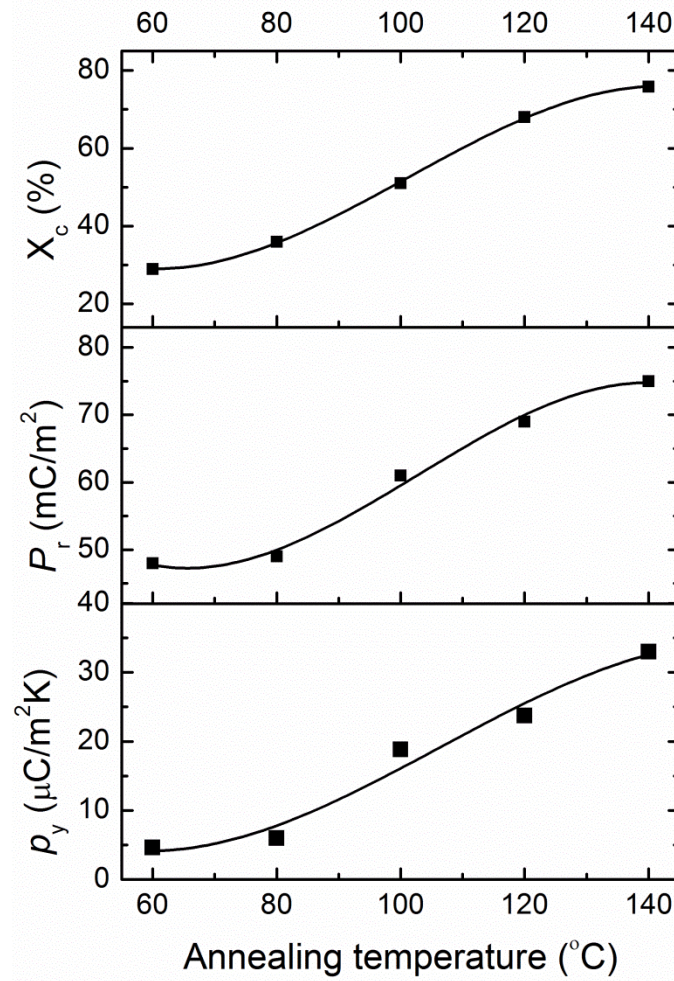


Figure 4.17: Plots of the degree of crystallinity,  $X_c$ , remanent polarization,  $P_r$  and pyroelectric coefficient,  $p$  as a function of annealing temperature.

The observed remanent polarization is comparable to that of typical Form I and melt extruded Form I as shown in Figure 4.18. The  $E_c$  of 240 MV/m in Form IV is very much greater than the widely accepted value of  $E_c$  which is 50-100 MV/m for Form I PVDF (T. Furukawa, Nakajima, & Takahashi, 2006; T. Furukawa, Takahashi, & Nakajima, 2010). This is mainly due to the enriched Form II crystalline in the PVDF thin film as evidenced in

the X-ray results (Takeo Furukawa, 1997). Relatively high coercive field of  $> 200$  MV/m is required in order to transform Form II to Form IV.

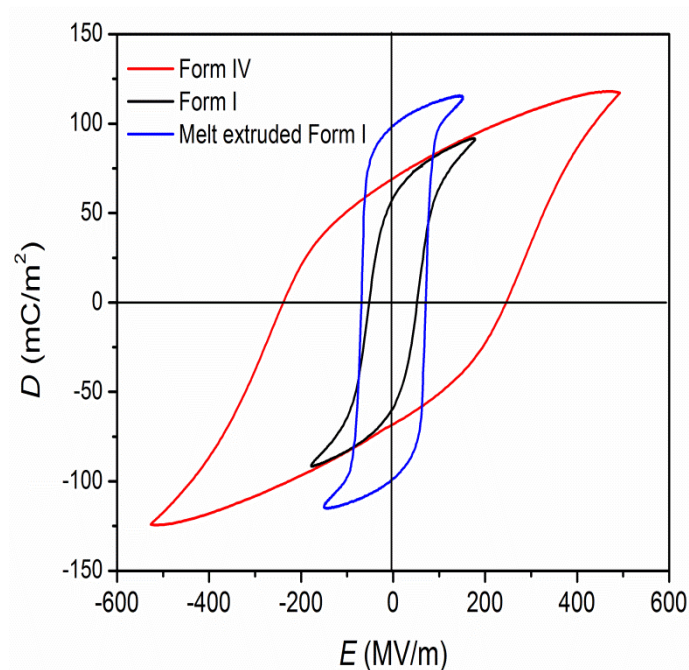


Figure 4.18: Comparison of Form IV and Form I PVDF  $D$ - $E$  hysteresis loops.

The other possible explanation for the observed high  $E_c$  is attributed to the switching mechanism. Switching mechanism in Form I progress through the rotation in the chain molecule instantaneously like a rigid rod in a crystalline lamella and its polarization reversal may progress through successive  $60^\circ$  rotations as shown in Figure 4.19 (T. Furukawa et al., 2006). However, the chain rotation in the  $ab$ -plane of Form IV may progress like a rigid ellipsoid as shown in Figure 4.20. This suggests that the coercive electric field and the required energy of the observed switching process in Form IV are much higher compared to that of Form I. The  $D$  in the observed hysteresis loop contains contributions of various sources such as conducting charges and the dielectric polarization in addition to the ferroelectric polarization. Here, the contribution of conducting charges

can be neglected judging from the linear  $D$ - $E$  relationship in the low-field range. The  $D$  in the hysteresis reflects the degree of dipole orientation and the  $\epsilon$  obtained from the gradient of  $D$ - $E$  loop is a measure of the degree of dipole fluctuation. Therefore, a maximum value of  $\epsilon$  can be obtained at  $D = 0$ . This implies that the fluctuations of dipoles become most active when they lose their orientation direction at 250 MV/m. The shape of the hysteresis loop remains rounded even though very high electric field has been induced. This may be attributed to the effect of depolarization field inherent from the amorphous region.

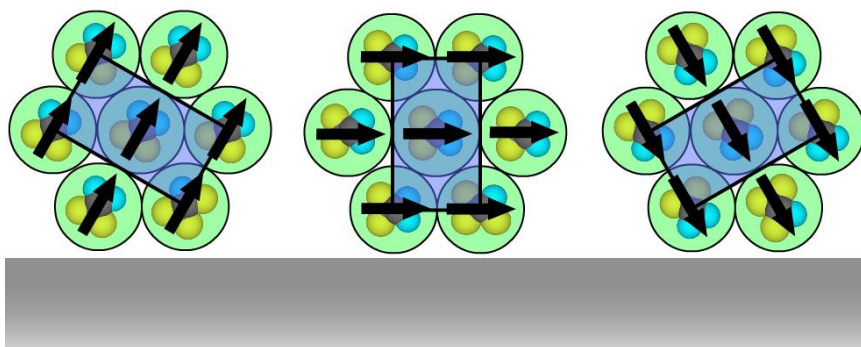


Figure 4.19: Switching process based on 60° rotation model in Form I. Yellow, blue and grey colour indicates the fluorine, hydrogen and carbon atom, respectively. (T. Furukawa et al., 2006).



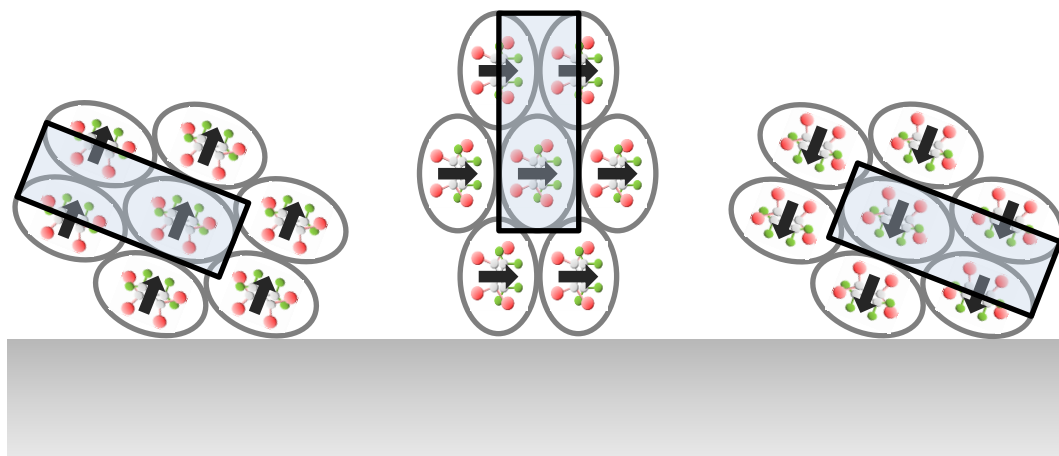


Figure 4.20: Proposed switching process based on 60° rotation model in Form IV.

Red, green and white colour indicates the fluorine, hydrogen and carbon atom, respectively.

From the above findings, we consider the following possible mechanisms which can be attributed to the observed pyroelectric and ferroelectric properties in Form IV PVDF. The factors that governing the  $p$  and  $P_r$  of Form IV PVDF consist of: (1) the spontaneous polarization of crystallites  $P_s$ , (2) the local field effects, (3) the degree of crystallinity and (4) the crystallite orientation.

#### 4.7.1 Spontaneous Polarization of Crystallites, $P_s$ and the Local Field Effects

Figure 4.21 shows the unit cells of Form II and Form IV of PVDF which are projected parallel to the chain axes. The state of the Form IV can be assumed to be thermodynamically similar to the Form II because both of them have identical sized unit cells as well as the chain conformation during the conversion.

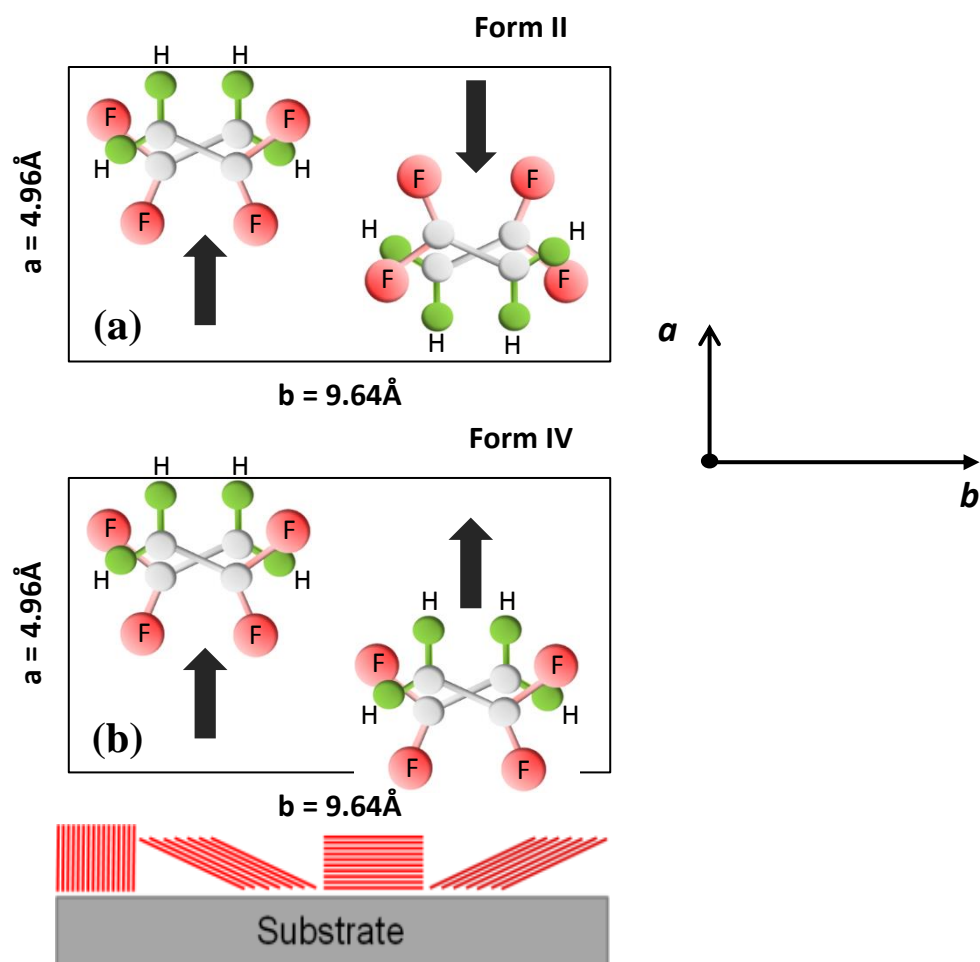


Figure 4.21: Unit cells of (a) the Form II and (b) the Form IV of PVDF shown in projection of  $ab$ -plane. Arrows indicate the dipole direction normal to the molecular axes. Schematic picture at the bottom represent the orientation of the (100), (110), (020) and the mirror image of (110) plane in the spin-coated PVDF thin films.

In Figure 4.21(a), the unit cell of the Form II consists of two chains in  $\text{TGT}\bar{\text{G}}$  conformation, whose dipole components normal to the chain axes are antiparallel. Thus, the dipole moments of the Form II unit cell are internally compensated (Broadhurst & Davis, 1984; Das-Gupta & Doughty, 1977, 1978, 1980; Das-Gupta et al., 1979; Davis et al., 1978; Naegle et al., 1978). In the Form IV unit cell, the atomic coordinates for the first chain remain the same as in the Form II. The significant difference in the Form IV arises

from the  $180^\circ$  rotation of every second chain and the  $c_o/2$  translation along the  $c$ -axis in the unit cell when there is a sufficient electric field applied on the Form II (Davis et al., 1978). In such a way, the transverse dipole components are pointing in the same direction, and thus produce a polar analog as shown in Figure 4.21(b). Dvey-Aharon et al (Dvey-Aharon, Taylor, & Hopfinger, 1980) has also proposed a mechanism of the phase transformation which involve dipole reversal propagation of a twist wave along the chains; whereas, Lovinger (Lovinger, 1981) proposed a simpler mechanism which requires only small intramolecular rearrangements. From the XRD results, Figure 4.6 shows the increase in intensity of the (110) reflection and the significant decrease in the (100), (120) and (021) reflection planes after poling process. It implies that the crystalline transformation from Form II to Form IV induced by a high electric field has taken place. As a result, the pyroelectric constant,  $p$  ( $\sim 30 \mu\text{C}/\text{m}^2\text{K}$ ) and remanent polarization,  $P_r$  ( $\sim 70 \text{ mC}/\text{m}^2$ ) was successfully obtained.

Spontaneous polarization,  $P_s$  is one of the most important criteria in ferroelectric. Various theoretical  $P_s$  values of Form I PVDF have been proposed and listed in Table 4.2. The origin of polarization in Form IV is estimated about one-half that of Form I. It is generally accepted that Form I PVDF consists of a repeat unit ( $-\text{CH}_2\text{CF}_2-$ ) which exhibits a dipole moment  $\mu_v = 7 \times 10^{-30} \text{ Cm}$  associated with positively charged H-atoms and negatively charged F-atoms. Such all-trans conformation with a parallel packing yields a large spontaneous polarization,  $P_s = 130 \text{ mC}/\text{m}^2$  by rigid dipole model. Different values of  $P_s$  with respect to Form I PVDF have been proposed based on the evaluation of the local electric field. The local electric field arises from the point dipoles in an isotropic medium is highly model-dependent. Tashiro et al (Tashiro, Kobayashi, Tadokoro, & Fukada, 1980) has proposed a  $P_s$  of  $140 \text{ mC}/\text{m}^2$  derived from a polymer crystal based on point charge model. Al-Jishi and Taylor (Al-Jishi & Taylor, 1985) have made microscopic calculations

on the basis of field sums due to the surrounding point charges yields a  $P_s$  of 128 mC/m<sup>2</sup>. The predicted  $P_s$  is consistent with a rigid dipole model approximation by neglecting local electric field. Nevertheless, modern computer simulations have suggested large value of  $P_s$  of 180 mC/m<sup>2</sup> in which the monomer dipole moment is increased by 50% as the isolated chains are brought together to form a crystal (Nakhmanson, Nardelli, & Bernholc, 2005). Nakhmanson et al (Nakhmanson et al., 2005) have shown that intrachain interaction yield no increase nor decrease in local electric field. However, interchain interaction generates very strong local field which increase from 130 mC/m<sup>2</sup> to 180 mC/m<sup>2</sup> in Form I PVDF.

Model	Year	$X_c$ (%)	Form I (mC/m <sup>2</sup> )	Form IV (mC/m <sup>2</sup> )	Ref.
Rigid dipoles			130	65 (This work)	
Tashiro et al	1980	100	140	-	[29]
Al-Jishi and Taylor	1985	100	128	-	[30]
Nakhmanson et al	2004	100	180	-	[31]
A. Itoh	2014	100	176	85	[33]
Experiment			100	70 (This work)	

Table 4.2: Spontaneous polarization of PVDF calculated with various theoretical models.

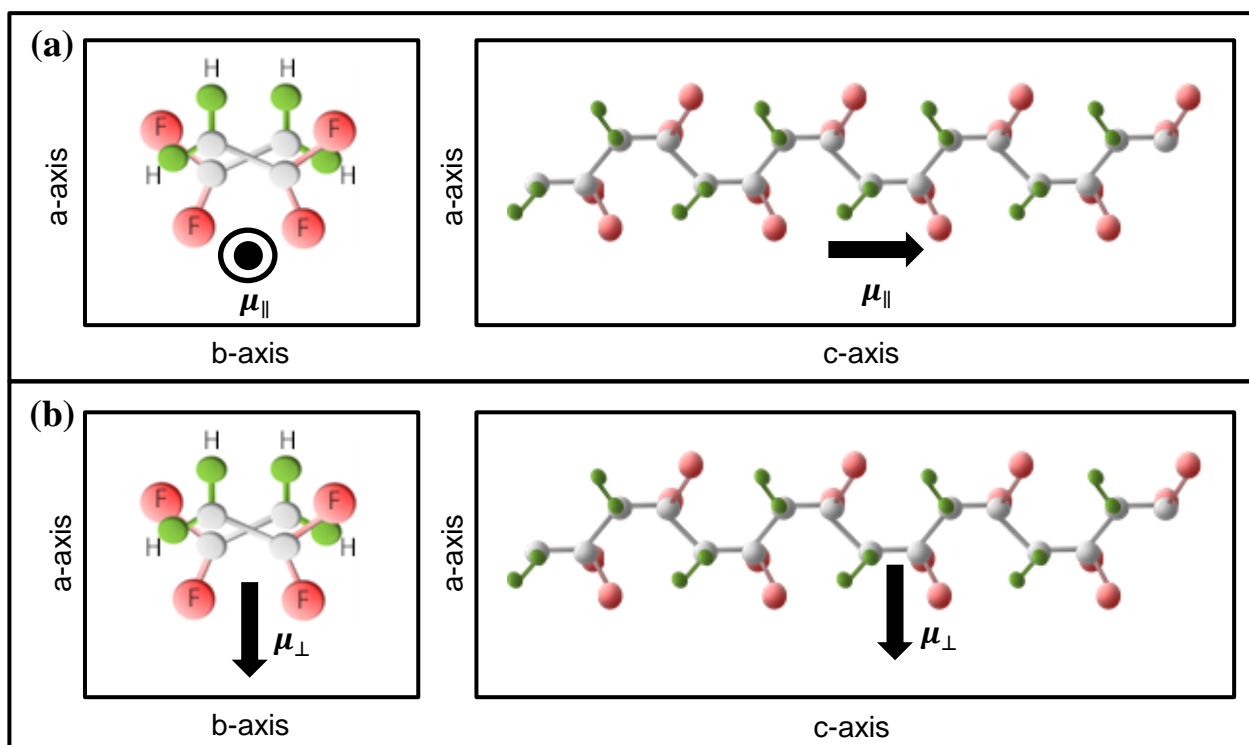


Figure 4.22: Dipole reversal due to molecular motion in the Form II PVDF: (a) vacuum moment is aligned parallel along the molecule chain axis; and (b) vacuum moment is aligned in perpendicular with molecule chain axis.

Unlike Form I PVDF, the theoretical value of  $P_s$  in Form IV PVDF still remains anonymous. To begin the calculation of the Form IV spontaneous polarization, most simply, the rigid dipole model which is similar to that used for Form I is employed. Here, the partial charge values from Tashiro et al (Tashiro et al., 1980) have been utilized to calculate the dipole moment based on the atomic coordinates of Form II PVDF reported by Hasegawa et al (Hasegawa, Takahashi, Chatani, & Tadokoro, 1971). The first assumption to be made is that all chain segments are assumed to contribute homogeneously to relaxation. As a result,  $\mu_{\parallel}$  which is aligned parallel to the molecular axis as shown in Figure 4.22(a) is found to be,  $\mu_{\parallel} = 3.03 \times 10^{-30} Cm$  (0.91 D);  $\mu_{\perp}$  which is aligned

perpendicular with the chain axis (along the *a*-axis) as shown in Figure 4.22(b) is found to be,  $\mu_{\perp} = 3.57 \times 10^{-30} \text{ Cm}$  (1.07 D). Subsequently, the dipole reversals in *ab*-plane as a result of chain rotation about the *c*-axis of Form IV PVDF have yielded a spontaneous polarization:

$$P_s = \frac{4\mu_v}{abc} = 65 \text{ mC/m}^2 \quad (4.3)$$

In view with the hysteresis measurement results, the observed remanent polarization,  $P_r \approx 70 \text{ mC/m}^2$  is found to be larger than the calculated spontaneous polarization,  $P_s \approx 65 \text{ mC/m}^2$ . The proposed  $P_s$  of Form IV PVDF based on the rigid dipole model has neglected the effect of the local field on the polarizable molecule, where the effect of the interchain interaction in a crystal has not taken into consideration. Most recently, the first theoretical prediction of  $P_s$  for Form IV has been revealed by Itoh et al (Itoh, Takahashi, Furukawa, & Yajima, 2014). The calculation with modern quantum chemical approach yields a  $P_s$  of Form IV to be  $85 \text{ mC/m}^2$ , which is nearly one half of that Form I. The chain with gauche conformation and the dipoles incline by  $60^\circ$  from the direction of total polarization was taken into consideration in the calculation. This calculation has provided a fundamental insight on modelling the electronic behaviour of Form IV PVDF. It is shown that the polarization of the crystalline phase is very sensitive to the local field and to the structure of the lattice. The assumption of  $P_s$  by rigid dipole model considers only the value of dipole moment of an isolated chain in a crystal; the effect of the interchain interaction in a crystal has been neglected. Consequently, if we include the local electric field effect as it happened in Form I into Form IV, the calculated  $P_s$  based on the rigid dipole model will be increased by approximately 50% from  $65 \text{ mC/m}^2$  to  $\sim 100 \text{ mC/m}^2$ . Moreover, taking into consideration the crystallinity range of 50-70% in the well annealed thin films, this model therefore predicts a maximum remanent polarization of  $70 \text{ mC/m}^2$ . Furthermore, this

approximation has also offered significant contribution to the pyroelectric coefficient resulting from the changes in the monomer dipole moments, which resulting in changes in the local field as the dimension of the unit cell changes with temperature. Thus, the prediction is consistent with the experimental observed value.

#### 4.7.2 Degree of Crystallinity

The polarization,  $P_r$ , which reverses upon application of an electric field, is highly dependence on the degree of crystallinity in a ferroelectric substance. From the SEM observation, it is found that when the annealing temperature is increased, crystallization occurs and the molecules tended to align in an ordered structure. The structural changes in acetone and MEK cast PVDF thin films induced by annealing are summarized into two parts: (i) Annealing at 60 °C - 100 °C induces a marked decrease in pin-holes and has resulted with effective reduction in the roughness of the samples. (ii) Annealing at 120 °C - 140 °C induces rapid growth of crystallites and formation of spherulites. As shown in Figure 4.5, the molecules begin to acquire sufficient energy to restructure when the annealing temperature was increased to 100 °C. At this stage, the molecules acquired more energy which was supplied by the random thermal motions to overcome the energy barrier of structure rearrangement of the system. As a result, molecules moved in translational motion and filled up the porosity (as depicted in Figure 4.5(a) and (b)) and thus the crystal begins to grow. Hence, the surface roughness of the sample was reduced effectively and the crystallinity also increases. It is important to note that the length of the chain in between folds will led to the crystal grows with a preferred thickness. On the other hand, annealing above 120 °C caused the polymer crystals to grow and rearrange into spherically symmetry polycrystalline structure, spherulites. The spherulites were grown from nucleation of

primary crystal, and followed by radial growth outward from these nuclei in irregular spherical. This is because the spin-coating films have higher free energy per unit volume during annealing compare to that of drawing a solution-cast film (Ohigashi, Omote, & Gomyo, 1995). The growth of molecule chains tends to fold on the lamellar surfaces due to the substrate constraint. The spherulites consist of stack of lamellae crystals that grow outward from a common centre during crystallization as depicted in Figure 4.5 (e). These lamellae are typically 10-20 nm thick, depending on the crystallization condition. The XRD results as depicted in Figure 4.3 have shown that annealing induces growth of the crystalline peaks. This implies that the films which were annealed at 140 °C are highly crystalline and the degree of crystallinity can be achieved to 75%.

#### 4.7.3 Crystallite Orientation

An uniaxially drawn Form I PVDF may exhibits  $P_r$  of 60-70 mC/m<sup>2</sup>, whereas the solid-state coextrusion of a gel film induces a higher  $P_r$  which reached 100 mC/m<sup>2</sup> due to the enhanced crystallinity of the film (Bune et al., 1998; He & Yao, 2006; Kang et al., 2008; Lee, Cooper, Wang, & Liang, 2008; Nakamura et al., 2003; J. Wang et al., 2003; Z. L. Wang, 2007; Zhang, Liu, & Wang, 2011). Besides, the remanent polarization is found not only depended on the degree of crystallinity but also crystalline orientation. To further understand the molecule chain orientation and confirm the proposed mechanism of phase transformation from Form II to Form IV, the crystalline orientation through the XRD results which reflects the correlation of the polarization orientation and the direction of the applied electric field has been examined. It is known that the polarization reversal of Form IV PVDF occurs in the *ab*-plane as a result of chain rotation about the *c*-axis. The *c*-axis is predicted to be oriented to the thin film surface due to the constraint of fiber length as



depicted in Figure 4.4(e) and (f). In such a way, the polarization reversal around the *c*-axis could be induced by the external electric field effectively. The sharp peak of (110) plane as shown in XRD results (Figure 4.6) indicates that the molecules (*c*-axis) have high tendency to align parallel to the film surface because the surface energy per unit area for the (110) plane is much lower than that of the (020) (Ohigashi et al., 1995). The resultant microscopic surface area of the molecules chain which exposed to the air in the hexagonal phase is smaller in (110) plane compare to (020) plane. As a result, the substrate is more favourable to face the most densely packed plane and the preferential orientation is advantageous as the effective electric field acting on the planes is at its optimum.

#### 4.7.4 Dielectric Molecular Dynamics

Apart from structural consideration, a thorough analysis on the dielectric spectra of the Form IV PVDF has been conducted in order to investigate the molecular dynamic motion. Figure 4.23 shows the plots of the logarithm of  $\tau$  against the reciprocal of absolute temperature  $1/T$  (transition map) of unpoled and poled PVDF thin films. It is important to note that relaxation time,  $\tau$  for Form IV PVDF has been prolonged as a result of the poling. Here, we compared our Form II results with the conventional Form II relaxation time cast from cyclohexanone and it is consistent with the typical relaxation time. The relaxation time,  $\tau$  of the unpoled Form II PVDF thin film at room temperature has increased from  $6.3 \times 10^{-2}$  s to  $13.3 \times 10^{-2}$  s after poling process. The poled PVDF after transforming to Form IV has resulted in intermolecular dynamic motions in the unit cell which takes longer time to relax. The molecular origin of the dielectric response obtained has shown fascinating results, it has reflected important consideration of the phase transition in addition to the aforementioned conventional structural analysis. However, activation energies for both Form II and IV remains the same as both gradient of the relaxation time against the

reciprocal temperature are similar. This is due to the state of Form IV is assumed to be thermodynamically similar to Form II because both have identical size of unit cells the chain conformation during the transformation. However, the interatomic distance between the fluorine atoms of the adjacent chains pack in Form IV is closer and thus the dipoles oriented preferentially in the direction of the electric field (Broadhurst & Davis, 1984; Das-Gupta & Doughty, 1978, 1980; Das-Gupta et al., 1979; Davis et al., 1978; Naegle et al., 1978). The molecular structure after poling is now considered to be permanent and stable. The transformation has caused changes in the crystalline relaxation, thus, Form IV exhibits slower dielectric response and undergoes slower motion by almost two fold of the relaxation of that of Form II.

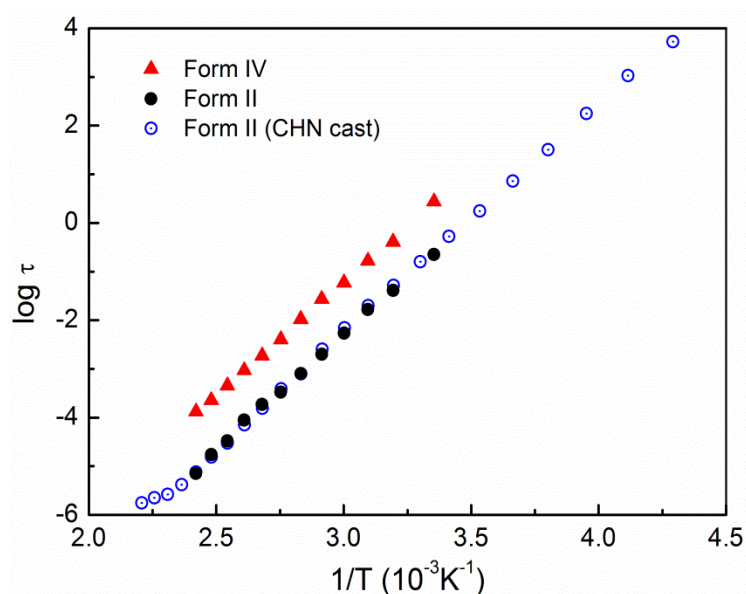


Figure 4.23: Plot of  $\log \tau$  vs  $1/T$  for Form II and Form IV PVDF thin films.

The difference of the crystalline motion relaxation strength is strongly related to the molecular alignment in the films. In view of the quantitative agreement with the experimental results, the mechanism of the  $\alpha$ -relaxation crystalline must be further considered. In fact, the observed  $\alpha$ -relaxation in Form II PVDF is strongly related to the

active dipole fluctuating associated with  $TGT\bar{G}$  and  $T\bar{G}TG$  along the molecular axis due to thermal motion (Miyamoto, Miyaji, & Asai, 1980). The  $\alpha$ -relaxation arose from the dipole fluctuation along the  $c$ -axis contribute a large dielectric strength,  $\Delta\epsilon \approx 30$ . However, a weak  $\alpha$ -relaxation,  $\Delta\epsilon \approx 4$  is observed in this study. For quantitative analysis, a coordinate system to a spin-coated thin film has been assigned. For the ease of calculation, only  $YZ$ -plane is considered where  $Y$ -axis is the orientation direction and  $Z$ -axis is the electric field direction which is orthogonal to  $Y$ -axis. As a result, the angle tilted in between molecular chains and substrate is calculated to be  $18^\circ$ . It can be suggested that the molecule chain orientation of the spin-coated and well annealed Form IV PVDF is preferred to align in-plane with the glass substrate in this study as shown in schematic picture in Figure 4.21. The proposed plausible mechanism is consistent with the XRD results whereby the (100) and (110) planes are preferentially aligned parallel to the substrate surface. In such a way, dipolar alignment occurs by rotation of molecular segments within the crystal phase, about the molecular chain axis. This suggests that the poling process is best done when the molecular segments are normal to the poling direction which is more effective in aligning the dipoles. Even though, the chain orientation is tilted by  $18^\circ$  from the glass substrate, the highly crystalline structure with such chain confirmation is able to yield a  $P_r$  of  $70 \text{ mC/m}^2$ . These insights are strongly supported by the hysteresis measurements and pyroelectric results above. If the molecular chains are aligned in perpendicular to the films surface, they are difficult to be poled and thus, high remanent polarization and pyroelectric coefficient cannot be expected and large  $\Delta\epsilon \approx 30$  will be observed. In general, PVDF phase transformation from Form II to Form I in bulk films under high electric field has to go through the Forms III and IV phase transformation as shown by Das Gupta et al, Davis et al and Naegele et al (Broadhurst & Davis, 1984; Das-Gupta & Doughty, 1977, 1978, 1980; Das-Gupta et al., 1979; Davis et al., 1978; Naegele et al., 1978). However, the transformation from Form II to Form I is rather

difficult in thin films form ( $< 300$  nm). Such a transformation from Form II to Form I may require chain elongation from 0.23 nm to 0.256 nm which is too difficult to occur in thin film due to the in-plane constraint. In this context, chain transformation from TGT $\bar{G}$  to TTT is strictly prohibited, thus, only Form IV is presented even though very high electric field has been applied for ferroelectric switching.

#### 4.7.5 Linear Relationship of Pyroelectric and Ferroelectric Properties

In correspondence to the pyroelectric and ferroelectric results obtained, the relationship of the pyroelectric coefficient,  $p$  as a function of remanent polarization,  $P_r$  is determined as shown in Figure 4.24. The obtained Form IV results were compared to Form I PVDF which is free from the constraint of the substrate (T. Furukawa, 1989c). A linear relationship of the  $p$  and  $P_r$  in Form IV PVDF thin films has been obtained. To begin with, the pyroelectric property have to be validated by evaluating the contribution of secondary effect in the total pyroelectric activity. The pyroelectric coefficient for a mechanically free sample is defined as:

$$P|_{total} = P|_{primary\ effect} + P|_{secondary\ effect} \quad (4.4)$$

and it can be rewritten as (T. Furukawa, 1989b):

$$p_3^x = p_3^x + \sum_{j=1}^3 e_{3j} \alpha_j \quad (4.5)$$

$$e_{3j} = -2P_r \quad (4.6)$$

where  $p_3^x$ ,  $p_3^x$  and  $\sum_{j=1}^3 e_{3j} \alpha_j$  are defined as  $P|_{total}$ ,  $P|_{primary\ effect}$  and  $P|_{secondary\ effect}$  respectively. The first term in Equation 4.4, is the primary pyroelectric effect which express the intrinsic pyroelectricity in a clamped sample. The second term is called secondary pyroelectric effect which takes into consideration the coupling of the piezoelectricity and

the thermal expansion values. The term,  $e_{3j}$  is defined as a piezoelectric constant and  $\alpha_j$  is a thermal expansion coefficient as expressed in Equation 4.5 and 4.6. The pyroelectric dimensional effect can be obtained by the gradient of the slope in Figure 4.24 which is expressed by

$$p_3 = \alpha_3 P_r \quad (4.7)$$

where  $\alpha_3$  is the thermal expansion coefficient along the thickness direction. The obtained result has shown the thermal expansion coefficient of Form I and Form IV to be  $6.3 \times 10^{-4} \text{ K}^{-1}$  and  $4.4 \times 10^{-4} \text{ K}^{-1}$ , respectively.

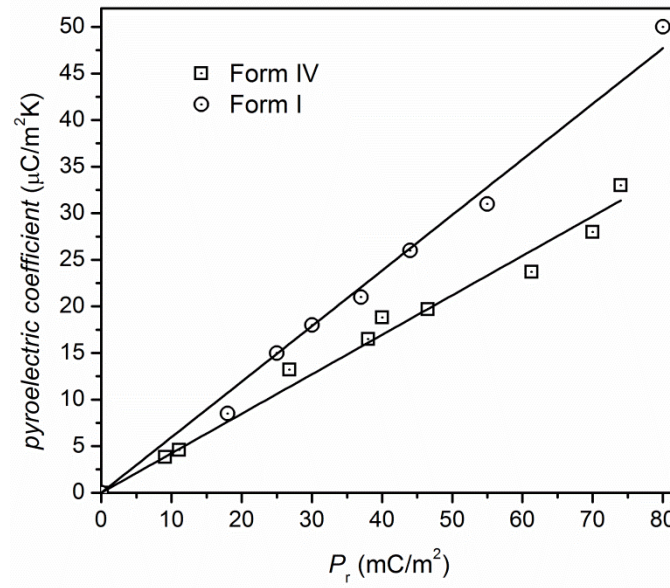


Figure 4.24: Plots of the pyroelectric coefficient,  $p_y$  as a function of remanent polarization,

$P_r$  of PVDF.

The PVDF thin films were prepared by spin-coating technique on glass substrates. As a result, the thin films were only allowed to be thermally expanded in the thickness direction, and not in the in-plane expansion. The obtained thermal expansion coefficient here is comparable to  $\alpha_3 \approx 1 \times 10^{-4} \text{ K}^{-1}$  for PVDF and VDF copolymers as obtained by Koizumi et

al (Koizumi, Haikawa, & Habuka, 1984). Hence, it is clear that the contribution from the dimensional effect to the observed pyroelectric activity is not dominant. The observed thermal expansion value varies in Form IV and Form I PVDF. The difference between the values is attributed to the degree of crystallinity and the molecular motion in both polymorphs. In Form I, the dielectric dipoles associated with the spontaneous polarization are fluctuate in  $b$ -axis are. In contrast, the dielectric dipoles in Form IV are not associated together with the spontaneous polarization as the molecular motion changes only along the molecular axis. As such, it is observed that the coupling effect in Form I allows active thermal expansion coefficient compared to that of Form IV.

#### 4.8 Conclusion

A series of detail experiments has been conducted to understand the electrical properties and structural behaviours of Form IV PVDF prepared by spin-coating technique. It is shown that thermal annealing at  $140^{\circ}\text{C}$  is essential to produce highly crystalline Form II PVDF with smooth surface. An application of a high electric field ( $>200\text{ MV/m}$ ) could induces a crystalline transformation from Form II to Form IV. The transformation is supported by a marked reduction in (100) and (120) X-ray diffraction intensities without further conversion to Form I. The remanent polarization  $P_r$  reached a value of  $70\text{ mC/m}^2$  with a coercive field  $E_c$  of  $200\text{ MV/m}$ . The pyroelectric constant,  $p_y$  determined after the measurement of hysteresis loop was shown to be proportional to the  $P_r$  and it reached  $p_y$  of  $28\text{ }\mu\text{C/m}^2\text{K}$ . Spontaneous polarization in Form IV as obtained by rigid dipole model and modern computational method has suggested that local electric enhancement which arises from the inter-chain interaction in a crystal plays an important role for its exceptional ferroelectricity and pyroelectricity properties observed in this study. Molecular dynamic of

Form IV PVDF has also been investigated by the broadband dielectric spectroscopy. Form IV is found to exhibit inferior dielectric strength and undergoes slower motion where its relaxation time,  $\tau$  of the intermolecular dynamic motion has been slowed down compare to that of Form II.

## References

- Al-Jishi, R., & Taylor, P. L. (1985). Field sums for extended dipoles in ferroelectric polymers. *Journal of Applied Physics*, 57(3), 897-901.
- Broadhurst, M. G., & Davis, G. T. (1984). Physical basis for piezoelectricity in PVDF. *Ferroelectrics*, 60(1), 3-13.
- Bune, A. V., Fridkin, V. M., Ducharme, S., Blinov, L. M., Palto, S. P., Sorokin, A. V., Yudin, S.G. & Zlatkin, A. (1998). Two-dimensional ferroelectric films. *Nature*, 391(6670), 874-877.
- Das-Gupta, D. K., & Doughty, K. (1977). Changes in x-ray diffraction patterns of polyvinylidene fluoride due to corona charging *Applied Physics Letters*, 31, 585-587.
- Das-Gupta, D. K., & Doughty, K. (1978). Piezo- and pyroelectric behaviour of corona-charged polyvinylidene fluoride. *Journal of Physics D: Applied Physics*, 11(17), 2415-2423.
- Das-Gupta, D. K., & Doughty, K. (1980). Piezoelectricity in uniaxially stretched and corona poled polyvinylidene fluoride. *Journal of Physics D: Applied Physics*, 13(1), 95-105.
- Das-Gupta, D. K., Doughty, K., & Shier, D. B. (1979). A study of structural and electrical properties of stretched polyvinylidene fluoride films. *Journal of Electrostatics*, 7(0), 267-282.
- Davis, G. T., McKinney, J. E., Broadhurst, M. G., & Roth, S. C. (1978). Electric-field-induced phase changes in poly(vinylidene fluoride). *Journal of Applied Physics*, 49(10), 4998-5002.

- Dvey-Aharon, H., Taylor, P. L., & Hopfinger, A. J. (1980). Dynamics of the field-induced transition to the polar alpha phase of poly(vinylidene fluoride). *Journal of Applied Physics*, 51(10), 5184-5187.
- Furukawa, T. (1989a). Ferroelectric properties of vinylidene fluoride copolymers. *Phase Transitions*, 18(3-4), 143-211.
- Furukawa, T. (1989b). Piezoelectricity and pyroelectricity in polymers. *IEEE Transactions on Electrical Insulation*, 24(3), 375-394.
- Furukawa, T. (1989c). Piezoelectricity and Pyroelectricity in Polymers. *IEEE Transactions on Dielectrics and Electrical Insulation*, 24(3), 375-394.
- Furukawa, T. (1997). Structure and functional properties of ferroelectric polymers. *Advances in Colloid and Interface Science*, 71-72(0), 183-208.
- Furukawa, T., Nakajima, T., & Takahashi, Y. (2006). Factors governing ferroelectric switching characteristics of thin VDF/TrFE copolymer films. *IEEE Transactions on Dielectrics and Electrical Insulation*, 13(5), 1120-1131.
- Furukawa, T., Takahashi, Y., & Nakajima, T. (2010). Recent advances in ferroelectric polymer thin films for memory applications. *Current Applied Physics*, 10(1, Supplement), e62-e67.
- Furukawa, T., Yasuda, K., & Takahashi, Y. (2004). Dielectric and conductive spectra of the composite of barium titanate and LiClO<sub>4</sub>-doped polyethylene oxide. *IEEE Transactions on Dielectrics and Electrical Insulation*, 11(1), 65-71.
- Gregorio, J. R., & Cestari, M. (1994). Effect of crystallization temperature on the crystalline phase content and morphology of poly(vinylidene fluoride). *Journal of Polymer Science Part B: Polymer Physics*, 32(5), 859-870.
- Gregorio Jr, R., & Borges, D. S. (2008). Effect of crystallization rate on the formation of the polymorphs of solution cast poly(vinylidene fluoride). *Polymer*, 49(18), 4009-4016.
- Gregorio, R. (2006). Determination of the  $\alpha$ ,  $\beta$ , and  $\gamma$  crystalline phases of poly(vinylidene fluoride) films prepared at different conditions. *Journal of Applied Polymer Science*, 100(4), 3272-3279.



- Hasegawa, R., Takahashi, Y., Chatani, Y., & Tadokoro, H. (1971). Crystal Structures of Three Crystalline Forms of Poly(vinylidene fluoride). *Polymer Journal*, 3(5), 600-610.
- He, X., & Yao, K. (2006). Crystallization mechanism and piezoelectric properties of solution-derived ferroelectric poly(vinylidene fluoride) thin films. *Applied Physics Letters*, 89(11), 112909-112903.
- Itoh, A., Takahashi, Y., Furukawa, T., & Yajima, H. (2014). Solid-state calculations of poly(vinylidene fluoride) using the hybrid DFT method: spontaneous polarization of polymorphs. *Polymer Journal* 46, 207-211.
- Kang, S. J., Park, Y. J., Sung, J., Jo, P. S., Park, C., Kim, K. J., & Cho, B. O. (2008). Spin cast ferroelectric beta poly(vinylidene fluoride) thin films via rapid thermal annealing. *Applied Physics Letters*, 92(1), 012921-012923.
- Kobayashi, M., Tashiro, K., & Tadokoro, H. (1975). Molecular Vibrations of Three Crystal Forms of Poly(vinylidene fluoride). *Macromolecules*, 8(2), 158-171.
- Koizumi, N., Haikawa, N., & Habuka, H. (1984). Dielectric behavior and ferroelectric transition of copolymers of vinylidene fluoride and trifluoroethylene. *Ferroelectrics*, 57(1), 99-119.
- Lee, H., Cooper, R., Wang, K., & Liang, H. (2008). Nano-Scale Characterization of a Piezoelectric Polymer (Polyvinylidene Difluoride, PVDF). *Sensors*, 8(11), 7359-7368.
- Li, Y., Shimizu, H., Furumichi, T., Takahashi, Y., & Furukawa, T. (2007). Crystal forms and ferroelectric properties of poly(vinylidene fluoride)/polyamide 11 blends prepared by high-shear processing. *Journal of Polymer Science Part B: Polymer Physics*, 45(19), 2707-2714.
- Lovinger, A. J. (1981). Molecular mechanism for  $\alpha \rightarrow \delta$  transformation in electrically poled poly(vinylidene fluoride). *Macromolecules*, 14(1), 225-227.
- Miyamoto, Y., Miyaji, H., & Asai, K. (1980). Anisotropy of dielectric relaxation in crystal form II of poly(vinylidene fluoride). *Journal of Polymer Science: Polymer Physics Edition*, 18(3), 597-606.

- Naegel, D., Yoon, D. Y., & Broadhurst, M. G. (1978). Formation of a New Crystal Form ( $\alpha\beta$ ) of Poly(vinylidene fluoride) under Electric Field. *Macromolecules*, 11(6), 1297-1298.
- Nakamura, K., Sawai, D., Watanabe, Y., Taguchi, D., Takahashi, Y., Furukawa, T., & Kanamoto, T. (2003). Effect of annealing on the structure and properties of poly(vinylidene fluoride)  $\beta$ -form films. *Journal of Polymer Science Part B: Polymer Physics*, 41(14), 1701-1712.
- Nakhmanson, S. M., Nardelli, M. B., & Bernholc, J. (2005). Collective polarization effects in  $\beta$ -polyvinylidene fluoride and its copolymers with tri- and tetrafluoroethylene. *Physical Review B*, 72(11), 115210.
- Ohigashi, H., Omote, K., & Gomyo, T. (1995). Formation of "single crystalline films" of ferroelectric copolymers of vinylidene fluoride and trifluoroethylene. *Applied Physics Letters*, 66(24), 3281-3283.
- Osaki, S., & Kotaka, T. (1981). Electrical properties of form III poly(vinylidene fluoride). *Ferroelectrics*, 32(1), 1-11.
- Southgate, P. D. (1976). Room-temperature poling and morphology changes in pyroelectric polyvinylidene fluoride. *Applied Physics Letters*, 28(5), 250-252.
- Tashiro, K., Itoh, Y., Kobayashi, M., & Tadokoro, H. (1985). Polarized Raman spectra and LO-TO splitting of poly(vinylidene fluoride) crystal form I. *Macromolecules*, 18(12), 2600-2606.
- Tashiro, K., Kobayashi, M., Tadokoro, H., & Fukada, E. (1980). Calculation of Elastic and Piezoelectric Constants of Polymer Crystals by a Point Charge Model: Application to Poly(vinylidene fluoride) Form I. *Macromolecules*, 13(3), 691-698.
- Wang, J., Li, H., Liu, J., Duan, Y., Jiang, S., & Yan, S. (2003). On the  $\alpha \rightarrow \beta$  Transition of Carbon-Coated Highly Oriented PVDF Ultrathin Film Induced by Melt Recrystallization. *Journal of the American Chemical Society*, 125(6), 1496-1497.
- Wang, Z. L. (2007). Nanopiezotronics. *Advanced Materials*, 19(6), 889-892.
- Zhang, Y., Liu, Y., & Wang, Z. L. (2011). Fundamental Theory of Piezotronics. *Advanced Materials*, 23(27), 3004-3013.

## CHAPTER 5: Pyroelectric Activity Enhancement in PVDF/TiO<sub>2</sub> Composite Thin Films

### 5.1 Introduction

In order to improve the functional properties of the ferroelectric polymer, ferroelectric ceramic inclusions such as BaTiO<sub>3</sub> (Fang, Yang, Zhang, & Wang, 2009), PbTiO<sub>3</sub> (Ploss, Ploss, Shin, Chan, & Choy, 1998; Ploss, Ploss, Shin, Chan, & Choy, 2000; Ploss, Ploss, Shin, Chan, & Choy, 2000) and PbZrTiO<sub>3</sub> (Furukawa & Fukada, 1977; Furukawa, Ishida, & Fukada, 1979; Ploss, Ng, Chan, Ploss, & Choy, 2001) were embedded in a polymer matrix as a filler to form 0-3 type composites to enhance the desired functional properties. These ceramic inclusions are conventional ferroelectric materials which exhibit high dielectric permittivity as well as large spontaneous polarization. Furthermore, the remarkable piezoelectric, pyroelectric and ferroelectric properties of these ceramic fillers, together with the high degree of flexibility of the polymers component have offered a promising potential for functional electronic application. Furukawa *et al.* and Ploss *et al.* (Furukawa & Fukada, 1977; Furukawa *et al.*, 1979; Ploss *et al.*, 2001; Ploss *et al.*, 1998, 2000; Ploss *et al.*, 2000) have shown that ferroelectric ceramic inclusions such as lead titanate (PT) and PZT embedded in the ferroelectric polymer matrix of PVDF and its copolymer (PVDF-TrFE), could enhance the pyroelectric and piezoelectric properties of the composite.

The Form II PVDF thin films were prepared. A non-ferroelectric inclusion, titanium dioxide (TiO<sub>2</sub>), was then dispersed in the Form II PVDF, to form a polymer-matrix composite. TiO<sub>2</sub> was chosen as the non-ferroelectric inclusion due to its high chemical stability, mechanical resistance and high optical transmittance in the visible to infrared

spectral range. Ideally, it seemed that a non-ferroelectric inclusion like TiO<sub>2</sub> might not contribute to the functional properties in ferroelectric polymer composites because it is impossible to polarize a non-ferroelectric inclusion and the net dipole moment of the inclusion is almost zero (B. Ploss et al., 2000). However, a new approach in the use of non-ferroelectric inclusion involving a two phase system which can enhance the pyroelectric activity after poling process has been demonstrated. An interfacial relaxation phenomenon (Maxwell-Wagner effect) which is attributed to the heterogeneity structure of the constituents in the polymer matrix is taken into consideration to explain the enhanced efficiency of the poling process. As a result, the pyroelectric coefficient of the polymer composite can be enhanced at a much lower poling electric field than that of the pure PVDF.

## **5.2 Structural Analysis**

### **5.2.1 Fourier Transform Infrared Spectroscopy**

Figure 5.1(a) illustrates the transmission mode infrared (IR) spectra of the PVDF thin films annealed at different temperatures from 60 °C to 140 °C. Here, the pure PVDF films was labelled as P1 and the PVDF/TiO<sub>2</sub> composite thin films with doping concentrations of 10 wt%, 20 wt% and 30 wt% were labelled as PT1, PT2 and PT3, respectively. The presence of both Form I and II in the infrared spectra denotes the most important characteristics that are responsible for the piezo- and pyroelectric activities in PVDF. The characteristic vibration spectra of the Form II are well-defined at 531, 612, 765, 796, 855 and 976 cm<sup>-1</sup> whereas the absorption band at 510 cm<sup>-1</sup> and 840 cm<sup>-1</sup> are the characteristic of the Form I in PVDF (Gregorio Jr & Borges, 2008). It is shown that the absorption peak for Form I is relatively small even though the films are treated with different annealing temperature up to 140 °C.

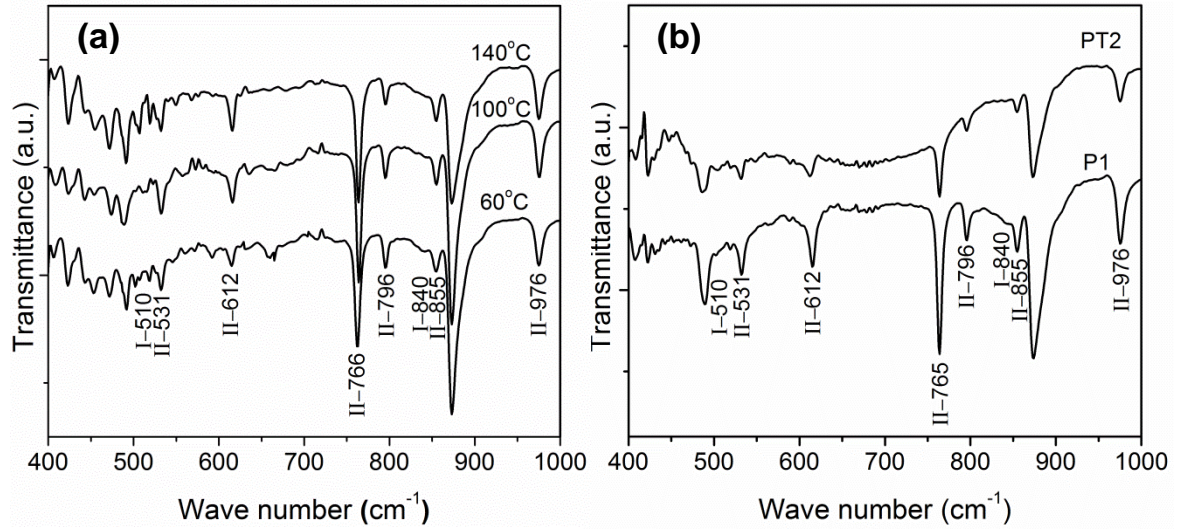


Figure 5.1: FTIR spectra of (a) the PVDF films annealed at 60 °C, 100 °C and 140 °C, (b) samples P1 and PT2 annealed at 140 °C.

The fraction of Form II in the samples which contain both Form I and Form II is further confirmed by Lambert-Beer law (J. R. Gregorio & Cestari, 1994; Li, Shimizu, Furumichi, Takahashi, & Furukawa, 2007):

$$F(II) = \frac{A_{II}}{A_{II} + 0.769A_I} \quad (5.1)$$

where  $A_I$  and  $A_{II}$  are the intensities at 840 cm<sup>-1</sup> (representing Form I) and 766 cm<sup>-1</sup> (representing Form II), respectively. The calculated results indicate that the content of Form II of the PVDF thin films cast is relatively high (> 90%) which proved that the PVDF thin films prepared is Form II dominant. Figure 5.1(b) shows IR spectra of the PVDF thin films and the PVDF/TiO<sub>2</sub> composite thin films incorporated with 10-30 wt% of TiO<sub>2</sub> after annealing at 140 °C. It is anticipated that no phase transition will take place with the presence of TiO<sub>2</sub> in PVDF films. No significant changes are observed among the IR spectra of the PVDF/TiO<sub>2</sub> composite thin films incorporated with difference weight percentages.

### 5.2.2 X-ray Diffraction

The FTIR results are further confirmed by XRD results as shown in Figure 5.2. The prominent peaks at  $2\theta = 17.6^\circ$  (100),  $18.6^\circ$  (020) and  $19.9^\circ$  (110) as shown in are assigned to Form II mainly observed in the PVDF thin films that were annealed at  $140^\circ\text{C}$ , which indicates the domination of the Form II in the PVDF thin films. The effect of annealing on the PVDF thin films is difficult to observe and analyze from the IR spectra. Moreover, it is important to note that annealing is essential in the process of enhancing the crystallinity of the PVDF films. No prominent peak was observed for PVDF sample that was treated with an annealing temperature below  $100^\circ\text{C}$ . The sample annealed at temperature above  $100^\circ\text{C}$  displayed strong crystalline peaks.

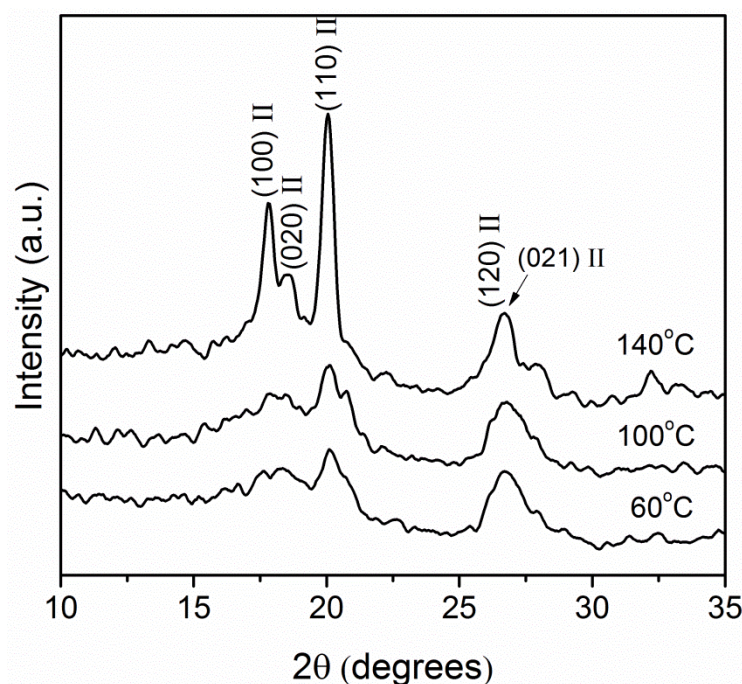


Figure 5.2: XRD spectra of PVDF annealed at  $60^\circ\text{C}$ ,  $100^\circ\text{C}$  and  $140^\circ\text{C}$ .

Figure 5.3 indicates the XRD pattern of the PVDF and PVDF/TiO<sub>2</sub> composite annealed at  $140^\circ\text{C}$ . The peaks at  $27.4^\circ$  and  $36.2^\circ$  correspond to the (110) and (101) planes,

respectively, of the tetragonal rutile phase TiO<sub>2</sub> particles in the PVDF/TiO<sub>2</sub> composite thin films (Kim, Ko, Park, Ryu, & Chang, 2003). The Form II was found to be retained in the PVDF/TiO<sub>2</sub> composite thin films prior to poling process. The XRD patterns were that of the PVDF and PVDF/TiO<sub>2</sub> composite annealed at 140 °C prior to poling.

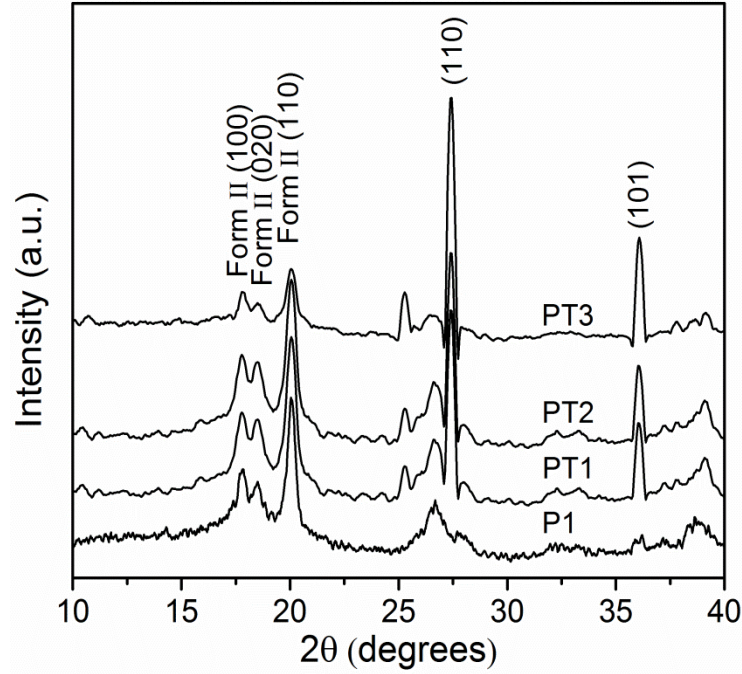


Figure 5.3: XRD spectra of PVDF and PVDF/TiO<sub>2</sub> films annealed at 140 °C.

### 5.2.2.1 Effect of Poling Process

Figure 5.4(a) shows the XRD spectra of PVDF before and after poling at an electric field of 260 MV/m. Major changes to be noted are the increase in intensity of the (110) reflection and the significant decrease in the (100) reflection after poling. When a very high electric field (> 120 MV/m) is applied to the PVDF thin films, a phase transition from Form II to the highly polar Form IV is expected. The results are further confirmed by the XRD results as shown in Figure 5.4(b).



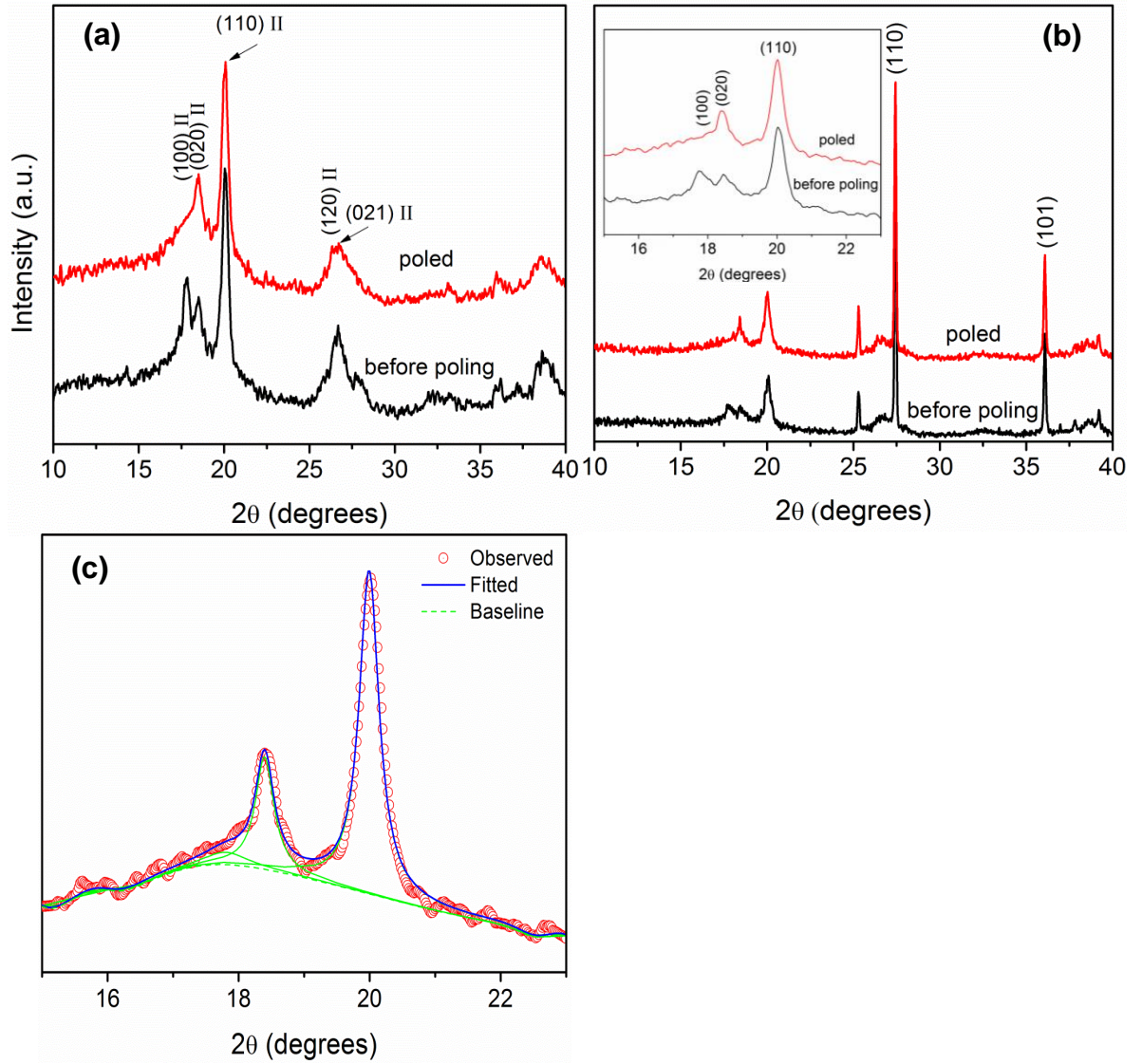


Figure 5.4: XRD spectra for unpoled and poled (a) PVDF and (b) PT2 thin film; (c) deconvolution of XRD spectrum for poled PT2 thin film.

It shows the XRD patterns of the PVDF/TiO<sub>2</sub> composite thin films (annealed at 140 °C) prior to and after poling process for sample PT2. After the poling process, the intensity of the (100) reflection at 17.6 ° is found to decrease significantly with respect to the (020) reflection at 18.6. The intensity of the (110) reflection at 19.9 ° is found to increase slightly as can be seen clearly in the figure inserted in Figure 5.4(b). In order to conduct thorough



quantitative analysis, deconvolution of the XRD patterns based on Figure 5.4(b) has been performed and shown in Figure 5.4(c). It is found that there are large reductions of around 60 % and 75 % for PVDF and PT2, respectively in the areas under (100) reflection plane after poling process. The reflection planes of Form II and polar Form IV are quite similar, except for the two particular reflection planes of (100) and (120) present at  $2\theta = 17.6^\circ$  and  $25.8^\circ$ . However, the position of (120) and (110) reflection planes which are attributed to PVDF and TiO<sub>2</sub> are intimately close at  $2\theta = 25.8^\circ$  and  $27.4^\circ$ . Thus, thorough deconvolution on the particular peaks has not been conducted. Furthermore, no Form I crystalline peak at  $2\theta = 20.9^\circ$  is being observed after the poling process as similarly found by Das Gupta et al (Das-Gupta, Doughty, & Shier, 1979). These can be attributed to a phase transition from Form II to the highly polar Form IV in PVDF has taken place during poling process (Das-Gupta & Doughty, 1977, 1978, 1980; Das-Gupta et al., 1979; Davis, McKinney, Broadhurst, & Roth, 1978; Naegele, Yoon, & Broadhurst, 1978).

### **5.2.3 Scanning Electron Microscopy**

The amorphous and crystalline regions in semicrystalline polymers like PVDF are intimately interconnected, and it is hard to separate them into distinct regions (R. Gregorio, Jr. & Ueno, 1999). The samples crystallized at a lower annealing temperature in this work have displayed molecular order which is consistent with the amorphous region (disorder). When the annealing temperature of the PVDF thin films was increased, the molecules tended to align in an ordered structure as shown in the SEM images in Figure 5.5.

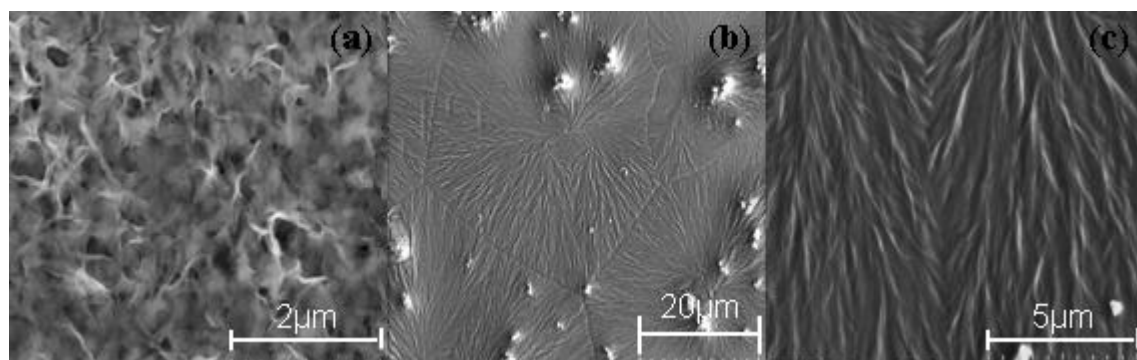


Figure 5.5: SEM images of (a) sample P1 annealed at 60 °C, (b) sample PT2 annealed at 140 °C and (c) an amplified picture of (b).

Figure 5.5(a) shows a SEM image of P1 sample annealed at 60 °C. The sample exhibits a sponge-like structure with a high percentage of volume porosity. The porosity observed in the SEM image is due to the low mechanical strength of the film, which is a useful feature in polymer membrane applications. However, the appearance of such porosity is undesirable for the poling process. The so-called pin-hole effect due to the existence of porosity will cause the samples to break down easily at a relatively low poling electric field. Thus, it is essential to anneal the samples to eliminate the pin-hole effect. Only after annealing, a sufficiently high electric field can be applied to the samples. Application of such a high electric field is required to reorient the electric dipoles such that a strong pyroelectric activity can be observed. As the annealing temperature was increased up to 140 °C, the sponge-like porosity of the film was totally eliminated as shown in Figure 5.5(b). Irregular shaped boundaries of spherulite crystals can be easily seen in the samples. The particles that were distributed on the surface of the spherulite structure are identified as TiO<sub>2</sub>. Figure 5.5(c) shows an amplified detail of the morphology presented in Figure 5.5(b). Clearer pictures of the lamellar structure on the spherulite surface can be easily seen.

These lamellae are normally observed in polycrystalline organic materials. The increase in annealing temperature from 60 °C to 140 °C has improved the crystallinity of the films, as indicated by the formation of the spherulite structure and the diffusion of the pin-holes. The change in the crystallinity of the PVDF polymer may explain the improvement in the pyroelectric activity of the samples, which will be discussed in Section 5.3.

### 5.3 Pyroelectric Activity and Poling Effect

A square waveform of pyroelectric current was obtained when a triangular temperature waveform was applied to a pre-poled PVDF thin film dispersed with 20 wt% of TiO<sub>2</sub>, as shown in the insert of Figure 5.6. The resultant square pyroelectric current waveform is due to the change in the spontaneous polarization of the sample with temperature. The accumulated surface charge density that is allowed to flow in the circuit can be defined as:

$$I_p = pA \frac{\Delta T}{\Delta t} \quad (5.2)$$

where  $I_p$  is the pyroelectric current,  $p$  is the pyroelectric coefficient,  $A$  is the electrode area and  $\Delta T/\Delta t$  is the heating rate.

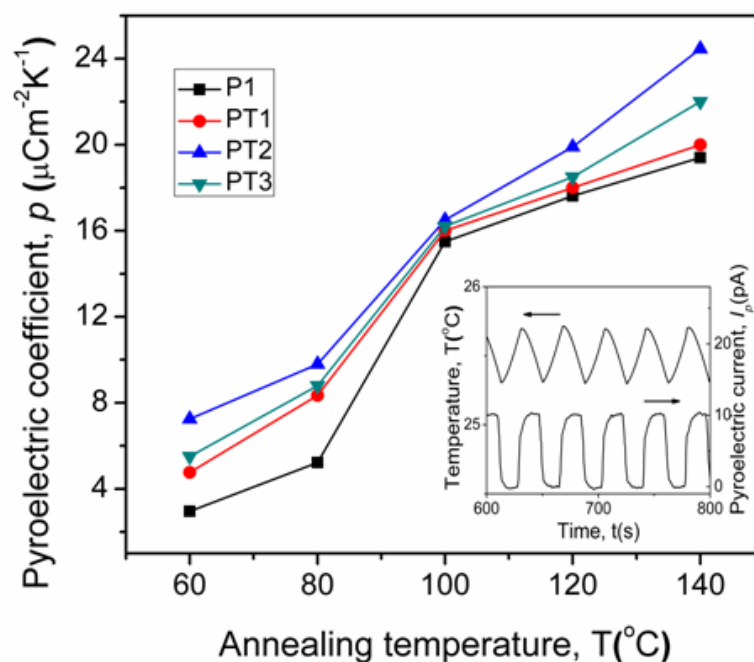


Figure 5.6: The dependence of the pyroelectric coefficient  $p$  with respect to the weight percentage of TiO<sub>2</sub> and the annealing temperature.

Figure 5.6 shows a comparison of the pyroelectric coefficients between the pure PVDF which were poled at 260 MV/m and the PVDF/TiO<sub>2</sub> composite thin films which were poled at 120 MV/m. The dependence of the pyroelectric coefficient  $p$  on different annealing temperatures was investigated. It was found that 140 °C is the optimum annealing temperature. The Form II dominant PVDF exhibited the highest value of pyroelectric coefficient: 19.4  $\mu\text{C}/\text{m}^2\text{K}$  at 140 °C. The poor pyroelectric performance of the samples annealed at temperatures below 100 °C is due to the pin-hole effect, which reduces the effective poling electric field. The improvement in the crystallinity of the PVDF composite thin films' structure after being treated with the annealing process was confirmed by the XRD patterns and SEM pictures, as shown in Figure 5.2 and 5.5, respectively. This improvement is the key factor that contributes to the enhancement of the pyroelectric

activity in both PVDF and PVDF/TiO<sub>2</sub> composite thin films. The optimum poling electric field to be applied to the PVDF/TiO<sub>2</sub> composite thin films is 120 MV/m. The value is reduced by a factor of two than that applied to the pure PVDF thin film, which is 260 MV/m. It is believed that the presence of the TiO<sub>2</sub> particles in the ferroelectric polymer matrix (PVDF) has formed space charge layers at the interface between the inclusions and the polymer matrix in the composite. The space charge layers at the interface result in an increase of the bound charges on the electrodes in phase with the applied electric field  $E$ , which give rise to an increase of the dielectric constant in the composite (this mechanism is called the Maxwell-Wagner effect) (Furukawa & Fukada, 1977). Consequently, the space charges in the PVDF/TiO<sub>2</sub> composite can drift and accumulate at the inclusion-particle/matrix interfaces at a faster rate. In addition, higher local fields in the inclusion phase allowed a more effective poling field in a shorter time. Thus, the applied poling electric field required for the PVDF/TiO<sub>2</sub> composites is much lower than that for the pure PVDF thin films. Moreover, a low electric field is recommended during the poling process to preserve the insulating nature of the composite thin films. Any further increase in the poling electric field on these composite thin films will lead to dielectric breakdown of the samples. A remarkable increase in the pyroelectric coefficient is observed as 20 wt% of TiO<sub>2</sub> is dispersed into the Form II dominant PVDF thin films. The pyroelectric coefficient of sample PT2 was successfully increased by 26% to 24.5  $\mu\text{C}/\text{m}^2\text{K}$ . However, as the weight percentage of TiO<sub>2</sub> was increased to 30 wt% the pyroelectric coefficient was reduced to a lower value of 22.0  $\mu\text{C}/\text{m}^2\text{K}$ . A detailed discussion of the TiO<sub>2</sub> contribution on the pyroelectric activity of the composite thin films is discussed in Section 5.4.

#### 5.4 Dielectric Properties and the Effect of Poling

Figure 5.7 shows the complex permittivity for samples (a) P1 and (b) PT2, which have been annealed at 140 °C. The applied frequency ranged from 1 Hz to 1 MHz, and the permittivity was measured at room temperature. The effective dielectric constant of the PVDF/TiO<sub>2</sub> composites increased as expected with an increase in the TiO<sub>2</sub> weight percentage.

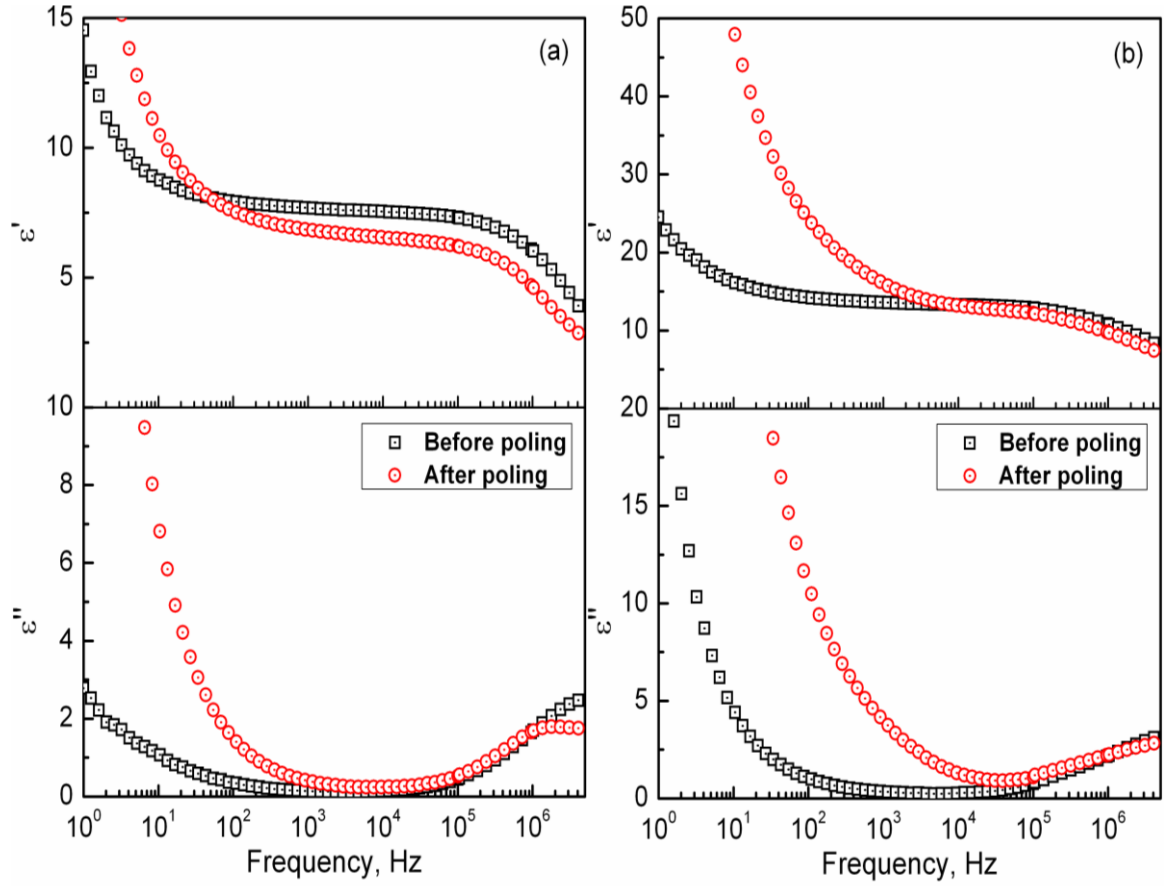


Figure 5.7: Dielectric spectra of (a) PVDF and (b) PT2 composite after annealed at 140 °C respectively.

In addition, an increment of the annealing temperature applied to the samples led to an increase in the dielectric constant as shown in Figure 5.8. The enhancement of the crystallinity of the samples caused by an increase of the annealing temperature has resulted in the molecules to align in a much ordered conformation with high molecular chain packing, which in turn increased the dipole density in the system and led to an increase in the dielectric constant. The high dielectric constant resulting from the increased annealing temperatures indicates that the enhancement in the pyroelectric activity is predominantly due to an increase in the crystallinity of the films. The abrupt increase of  $\varepsilon'$  and  $\varepsilon''$  for the PVDF/TiO<sub>2</sub> composite thin films in the low frequency range are due to the contributions of space charges trapped in between the interfaces after poling process. This can be understood by the following equation, which is adapted from complex dielectric permittivity,  $\varepsilon^* = \varepsilon' - i\varepsilon''$  and complex conductivity,  $\sigma = \sigma' + i\sigma''$ :

$$\sigma^* = i\omega\varepsilon^* \quad (5.3)$$

$$\varepsilon' = \frac{\sigma''}{\omega}, \varepsilon'' = \frac{\sigma'}{\omega} \quad (5.8)$$

where  $\omega$  is the angular frequency. Thus, the contribution of ceramic inclusions such as TiO<sub>2</sub>, which have higher conductivity, will definitely cause  $\varepsilon''$  to rise rapidly at low frequency.

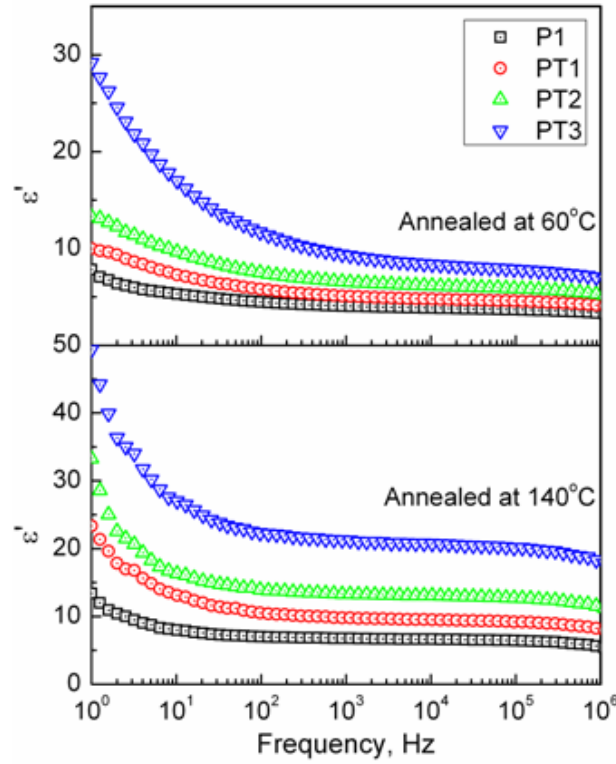


Figure 5.8: Dielectric spectra of various samples annealed at 60°C and 140°C.

The interfacial polarization exists in heterogeneous dielectrics is induced by the mobile charge carriers. The charges trapped at the interfaces cause large-scale field distortions in contrast to other types of polarization (atomic, electronic or dipolar), which are produced by the displacement, or orientation, of bound charge carriers. Theoretical approaches like Debye-type relaxation processes have been employed to understand the phenomenon (Tsangaris, Kouloumbi, & Kyvelidis, 1996):

$$\varepsilon^* = \varepsilon'_\infty + \frac{\varepsilon'_s - \varepsilon'_\infty}{1 + j\omega\tau} - j\frac{\sigma}{\omega} \quad (5.5)$$

where  $\varepsilon'_s$  and  $\varepsilon'_\infty$  are the values of  $\varepsilon'$  when  $\omega \rightarrow 0$  and  $\omega \rightarrow \infty$  respectively. The values of  $\varepsilon'_s$ ,  $\varepsilon'_\infty$  and  $\sigma$  depend on the conductivities of the constituents and their weight fraction



in the composites. In addition, it has been observed that the dielectric constants of both the PVDF and PVDF/TiO<sub>2</sub> composite thin films after poling process have been suppressed after 10 kHz. The imaginary dielectric constants of the both samples are found to experience phase transition from the Form II to the highly polar Form IV due to the poling effect at around 1 MHz. The following factor can be considered for the observed suppression of dielectric constant above 10 kHz. The state of Form IV can be assumed to be thermodynamically similar to Form II because both phases have identical size of unit cells and chain conformation during the transformation. However, the interatomic distance between the fluorine atoms of the adjacent chains pack in Form IV is closer and thus the dipoles oriented preferentially in the direction of the electric field (Das-Gupta & Doughty, 1977, 1978, 1980; Das-Gupta et al., 1979; Davis et al., 1978; Naegle et al., 1978). The phase transformation due to the poling process has caused significant changes in the crystalline relaxation. Thus, Form IV exhibits lower dielectric response and undergo slower motion by almost two fold of the relaxation of that of Form II.

The composite samples in this work can be modeled by a two-phase dispersion system consisting of a polymer matrix (phase 1: PVDF) and spherical inclusions (phase 2: TiO<sub>2</sub>) as shown in Figure 5.9. The effective dielectric constant of a polymer composite might strongly influence by the size, shape and weight fraction of the inclusions. Thus, a few models have been employed to understand the effective dielectric response of the composite thin films. Figure 5.10 shows the observed room temperature dielectric constant of PVDF composite with 20 wt% of TiO<sub>2</sub> after annealed at 140 °C.

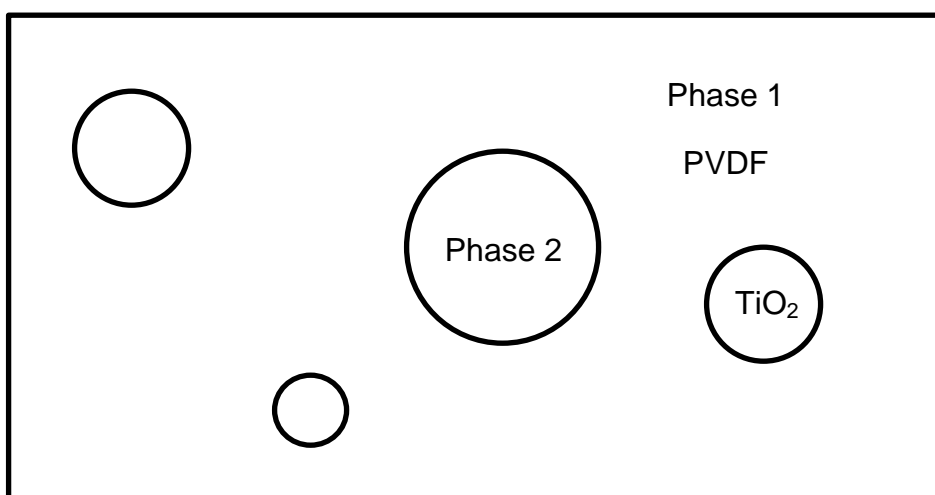


Figure 5.9: A two phase system composed of a polymer matrix (phase 1) and spherical inclusions (phase 2).

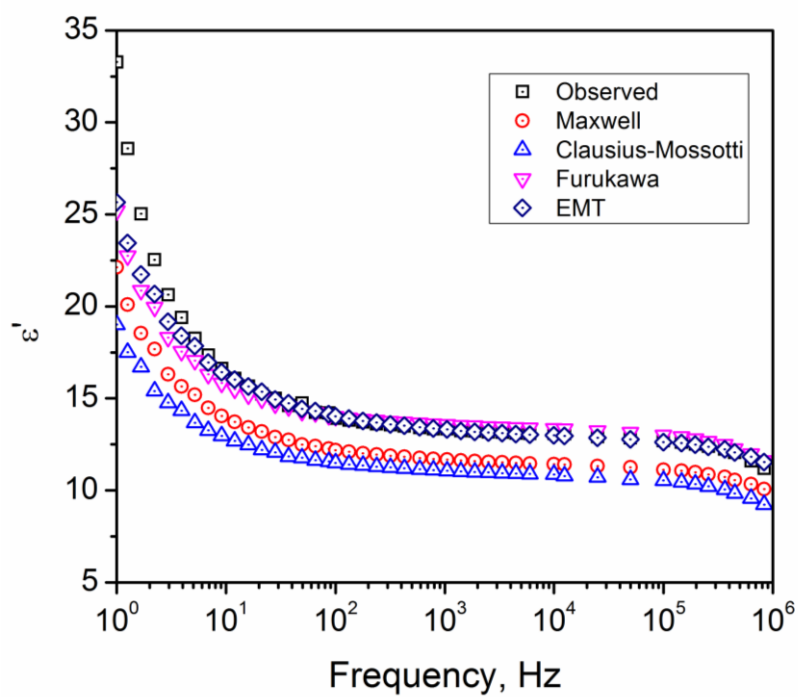


Figure 5.10: Various models of the effective dielectric constant of PT2 annealed at 140°C.

The calculated dielectric constants derived from various models are included in the same figure. The first theoretical model used in this study was derived by Maxwell. This model considered the dielectric property of a diphasic dielectric mixture comprising spherical inclusions with a high dielectric constant dispersed in a low dielectric constant polymer matrix which can be described by the following equation (Thomas, Varughese, Dwarakanath, & Varma, 2010):

$$\varepsilon = \frac{\varepsilon_1(1-\phi)(2/3 + \varepsilon_2/3\varepsilon_1) + \phi\varepsilon_2}{(1-\phi)(2/3 + \varepsilon_2/3\varepsilon_1) + \phi} \quad (5.6)$$

where  $\varepsilon_1$ ,  $\varepsilon_2$  and  $\phi$  refer to the dielectric constants of the polymer matrix and inclusions and the weight fraction of the inclusions, respectively. However, the predicted effective dielectric constant from this model deviates from the experimental value. Another convenient theoretical model used in this study was derived by Furukawa years ago, through the following equation (Furukawa, Fujino, & Fukada, 1976; Furukawa, Yasuda, & Takahashi, 2004):

$$\varepsilon = \frac{1+2\phi}{1-\phi} \varepsilon_1 \quad (5.7)$$

This model considers a simple two phase system with 0-3 connectivity. The inclusions are assumed to be spherical and there is no interface effect takes place in the composite. The value of  $\varepsilon_2$  is assumed to be  $\gg \varepsilon_1$ , and  $\phi \ll 1$ . The predicted effective dielectric constants from this model are found to be very close to the experimental data. The deviation between the theoretical prediction and the experiment data is  $\sim 3\%$ . Another simple explicit formula for binary 0-3 composites which is developed by Clausius-Mossotti (Thomas et al., 2010) was employed to predict the effective dielectric constant using the following equation:

$$\varepsilon = \varepsilon_1 \left[ 1 + 3\phi \frac{\varepsilon_2 - \varepsilon_1}{\varepsilon_2 + 2\varepsilon_1} \right] \quad (5.8)$$

However, the predicted values from this model seem to deviate by large magnitudes from the observed experimental data for weight fractions of the inclusions more than 20 wt% for the entire frequency range.

The effective medium theory (EMT) model has been established taking into consideration the morphology of the inclusions. The effective dielectric response of the EMT model is given by (Yang, Qu, Marinis, & Wong, 2000):

$$\varepsilon = \left( 1 + \frac{\phi(\varepsilon_2 - \varepsilon_1)}{\varepsilon_1 + n(1 - \phi)(\varepsilon_2 - \varepsilon_1)} \right) \varepsilon_1 \quad (5.9)$$

where  $n$  is the ceramic inclusion's morphology fitting factor. The small value of  $n$  indicates the filler particles to be in near-spherical shape, while a high value of  $n$  indicates largely non-spherically shaped particles. The experimental values were found to be well fitted by this model with the shape parameter  $n = 0.187$ . The difference between the experiment data and the predicted value is less than 1%. However, the predicted values below 5 Hz are found to be slightly deviated from the experimental data. This is due to the conducting behavior of TiO<sub>2</sub> as an inclusion for this composite. The high conducting response of the TiO<sub>2</sub> has caused a strong interfacial phenomenon at low frequency regime which attributed to famous Maxwell-Wagner effect. From the theoretical models employed above, it is clearly seen that Furukawa and EMT model with a small fitting parameter,  $n$ , gave the best fit among the rest. As a result, the particles size of the TiO<sub>2</sub> inclusion could be assumed to be spherical and this is consistent with our SEM observation.

So, why is the pyroelectric coefficient of the PVDF/TiO<sub>2</sub> composite thin films is larger than that of pure PVDF as it is known that the TiO<sub>2</sub> is not a ferroelectric inclusion? First, a two-phase dispersion system consisting of a polymer matrix (phase 1: PVDF) and spherical inclusions (phase 2: TiO<sub>2</sub>) as shown in Figure 5.9 is considered. The average electric field,  $E$  and displacement,  $D$  in the composite can be written as follows (Furukawa et al., 1976; Lam, Wong, Tai, Poon, & Shin, 2004; B. Ploss et al., 2000):

$$D = D_0 + \varepsilon E \quad (5.10)$$

$$D_1 = D_{01} + \varepsilon_1 E_1 \quad (5.11)$$

$$D_2 = D_{02} + \varepsilon_2 E_2 \quad (5.12)$$

where  $D_0$  is the average dielectric displacement at  $E = 0$ , subscripts 1 and 2 denote to polymer phase and ceramic inclusion respectively. By considering the weight fraction,  $\phi$  of the inclusions, the total average electric field,  $E$  and displacement are:

$$D = (1 - \phi)D_1 + \phi D_2 \quad (5.13)$$

$$E = (1 - \phi)E_1 + \phi E_2 \quad (5.14)$$

If an electric field,  $E$  is applied to the composite system, the condition of  $D_0$  becomes  $D_0 = D_1 = D_2 = 0$ . Introducing the eqs. (5.10) - (5.12) into eq. (5.13), the electric displacement can be written as

$$\varepsilon E = (1 - \phi)\varepsilon_1 E_1 + \phi \varepsilon_2 E_2 \quad (5.15)$$

In order to obtain the local field coefficient,  $L_E$  of the polymer phase and inclusion,  $E_1$  and  $E_2$  can be eliminated from the equations. (5.14) and (5.15). Here, we obtained:

$$L_{E1} = \frac{E_1}{E} = \frac{1}{1-\phi} \frac{\varepsilon_2 - \varepsilon}{\varepsilon_2 - \varepsilon_1} \quad (5.16)$$

$$L_{E2} = \frac{E_2}{E} = \frac{1}{\phi} \frac{\varepsilon_1 - \varepsilon}{\varepsilon_1 - \varepsilon_2} \quad (5.17)$$

where  $L_{E1}$  and  $L_{E2}$  is defined as the ratio of the local field  $E_1$  in the inner sphere to the average field over a composite and the ratio of the local field  $E_2$  in the inner sphere to the average field over a composite. In a composite system, the value of  $\varepsilon_2$  is always found to be  $\varepsilon_2 \gg \varepsilon_1$ , thus, the local electric field applied on phase 1 (polymer matrix) is much higher than local electric field on phase 2 (inclusion),  $L_{E1} \gg L_{E2}$ . As a result, polymer matrix such as PVDF in this work can be poled effectively. This effect also led to an increase in the effective applied field between the interfaces and, consequently, reduced the required poling electric field on the thin film during poling process. This may explain why the pyroelectric response of a composite in this work is higher than that of pure PVDF. Since the TiO<sub>2</sub> used in this work is a non-ferroelectric inclusion, it is impossible to pole the inclusion of the composite. The pyroelectric response of the composite is still mainly originated by PVDF. However, it is important to note that higher conductivities and higher losses are expected as the weight fraction of the inclusion increases. The conductivity of the matrix should be limited to a certain level; otherwise, it may induce dissipation and degradation of the properties of the materials. Higher weight fraction of TiO<sub>2</sub> in a composite will contribute to higher d.c. conduction in a composite. The high d.c. conduction in the composite will forms space charge layers in between the electrode and the composite, this may decrease the effective electric field applied in the composite during poling process. As a result, the effect of the conductivity in the inclusion became prominent. Consequently, the conductivities of both inclusion and polymer must both be addressed.

This in turn results in the poor performance of the pyroelectric activity as demonstrated by sample PT3. Thus, it suggests that the optimum weight percentage of TiO<sub>2</sub> dispersed in the polymer composite thin films should not be more than 20 wt%.

## 5.5 Conclusion

It has been shown that a remarkable increase in the pyroelectric activity can be achieved by the inclusion of TiO<sub>2</sub> into Form II dominant PVDF. The annealing temperature was found to be an essential parameter that can be used to enhance the crystallinity of the films. The increase in the dielectric constant of the composite with decreasing frequency is due to the Maxwell-Wagner effect. Several classical models have been evaluated to predict the effective dielectric constant of these composites over the entire frequency range from 10<sup>0</sup> to 10<sup>6</sup> Hz. It was found that Furukawa and EMT models give the best fit among the others. The incorporation of the non-ferroelectric inclusion in the polymer matrix composite has successfully increased the local electric field on the polymer matrix during the poling process. Thus, the required poling electric field has been reduced by a factor of two from 260 MV/m to 120 MV/m. These findings imply that an increase in the conductivity of the polymer matrix has significantly led to a more efficient poling process and as a result, it has improved the pyroelectric activity of the composites. However, the conductivity of a polymer composite matrix must be limited to a certain level. Above that level, an increased in the conductivity only deteriorates the pyroelectric activity of the polymer composite matrix, due to the increased in leakage current which can be observed in the composites containing more than 30 wt% of TiO<sub>2</sub>.

## References

- Das-Gupta, D. K., & Doughty, K. (1977). Changes in x-ray diffraction patterns of polyvinylidene fluoride due to corona charging *Applied Physics Letters*, 31, 585-587.
- Das-Gupta, D. K., & Doughty, K. (1978). Piezo- and pyroelectric behaviour of corona-charged polyvinylidene fluoride. *Journal of Physics D: Applied Physics*, 11(17), 2415-2423.
- Das-Gupta, D. K., & Doughty, K. (1980). Piezoelectricity in uniaxially stretched and corona poled polyvinylidene fluoride. *Journal of Physics D: Applied Physics*, 13(1), 95-105.
- Das-Gupta, D. K., Doughty, K., & Shier, D. B. (1979). A study of structural and electrical properties of stretched polyvinylidene fluoride films. *Journal of Electrostatics*, 7(0), 267-282.
- Davis, G. T., McKinney, J. E., Broadhurst, M. G., & Roth, S. C. (1978). Electric-field-induced phase changes in poly(vinylidene fluoride). *Journal of Applied Physics*, 49(10), 4998-5002.
- Fang, F., Yang, W., Zhang, M. Z., & Wang, Z. (2009). Mechanical response of barium-titanate/polymer 0–3 ferroelectric nano-composite film under uniaxial tension. *Composites Science and Technology*, 69(5), 602-605.
- Furukawa, T., Fujino, K., & Fukada, E. (1976). Electromechanical Properties in the Composites of Epoxy Resin and PZT Ceramics. *Japanese Journal of Applied Physics*, 15, 2119-2129.
- Furukawa, T., & Fukada, E. (1977). Piezoelectric Relaxation in Composite Epoxy-PZT System due to Tonic Conduction. *Japanese Journal of Applied Physics*, 16(3), 453-458.
- Furukawa, T., Ishida, K., & Fukada, E. (1979). Piezoelectric properties in the composite systems of polymers and PZT ceramics. *Journal of Applied Physics*, 50(7), 4904-4912.
- Furukawa, T., Yasuda, K., & Takahashi, Y. (2004). Dielectric and conductive spectra of the composite of barium titanate and LiClO<sub>4</sub>-doped polyethylene oxide. *IEEE Transactions on Dielectrics and Electrical Insulation*, 11(1), 65-71.



- Gregorio, J. R., & Cestari, M. (1994). Effect of crystallization temperature on the crystalline phase content and morphology of poly(vinylidene fluoride). *Journal of Polymer Science Part B: Polymer Physics*, 32(5), 859-870.
- Gregorio Jr, R., & Borges, D. S. (2008). Effect of crystallization rate on the formation of the polymorphs of solution cast poly(vinylidene fluoride). *Polymer*, 49(18), 4009-4016.
- Gregorio, R., Jr., & Ueno, E. M. (1999). Effect of crystalline phase, orientation and temperature on the dielectric properties of poly (vinylidene fluoride) (PVDF). *Journal of Materials Science*, 34(18), 4489-4500.
- Kim, K. M., Ko, J. M., Park, N.-G., Ryu, K. S., & Chang, S. H. (2003). Characterization of poly(vinylidene fluoride-co-hexafluoropropylene)-based polymer electrolyte filled with rutile TiO<sub>2</sub> nanoparticles. *Solid State Ionics*, 161(1-2), 121-131.
- Lam, K. S., Wong, Y. W., Tai, L. S., Poon, Y. M., & Shin, F. G. (2004). Dielectric and pyroelectric properties of lead zirconate titanate/polyurethane composites. *Journal of Applied Physics*, 96(7), 3896-3899.
- Li, Y., Shimizu, H., Furumichi, T., Takahashi, Y., & Furukawa, T. (2007). Crystal forms and ferroelectric properties of poly(vinylidene fluoride)/polyamide 11 blends prepared by high-shear processing. *Journal of Polymer Science Part B: Polymer Physics*, 45(19), 2707-2714.
- Naegle, D., Yoon, D. Y., & Broadhurst, M. G. (1978). Formation of a New Crystal Form ( $\alpha$ p) of Poly(vinylidene fluoride) under Electric Field. *Macromolecules*, 11(6), 1297-1298.
- Ploss, B., Ng, W.-Y., Chan, H. L.-W., Ploss, B., & Choy, C.-L. (2001). Poling study of PZT/P(VDF-TrFE) composites. *Composites Science and Technology*, 61(7), 957-962.
- Ploss, B., Ploss, B., Shin, F. G., Chan, H. L. W., & Choy, C. L. (1998). *Separate poling of inclusions and matrix in PT/P(VDF-TrFE) 0-3 composites*. Paper presented at the Applications of Ferroelectrics, 1998. ISAF 98. Proceedings of the Eleventh IEEE International Symposium on Applications of Ferroelectrics.
- Ploss, B., Ploss, B., Shin, F. G., Chan, H. L. W., & Choy, C. L. (2000). Pyroelectric activity of ferroelectric PT/PVDF-TRFE. *IEEE Transactions on Dielectrics and Electrical Insulation*, 7(4), 517-522.

- Ploss, B., Ploss, B., Shin, F. G., Chan, H. L. W., & Choy, C. L. (2000). Pyroelectric or piezoelectric compensated ferroelectric composites. *Applied Physics Letters*, 76(19), 2776-2778.
- Thomas, P., Varughese, K. T., Dwarakanath, K., & Varma, K. B. R. (2010). Dielectric properties of Poly(vinylidene fluoride)/CaCu<sub>3</sub>Ti<sub>4</sub>O<sub>12</sub> composites. *Composites Science and Technology*, 70(3), 539-545.
- Tsangaris, G. M., Kouloumbi, N., & Kyvelidis, S. (1996). Interfacial relaxation phenomena in particulate composites of epoxy resin with copper or iron particles. *Materials Chemistry and Physics*, 44(3), 245-250.
- Yang, R., Qu, J., Marinis, T., & Wong, C. P. (2000). A precise numerical prediction of effective dielectric constant for polymer-ceramic composite based on effective-medium theory. *IEEE Transactions on Components and Packaging Technologies*, 23(4), 680-683.

## **CHAPTER 6: Pyroelectric and Ferroelectric Activities Enhancement in PVDF/La<sub>2</sub>O<sub>3</sub> Composite Thin Films**

### **6.1 Introduction**

In chapter 5, we have introduced an alternative method to improve the functional properties of polymer matrix compare to the conventional studies by using a ferroelectric inclusion in the composite films with high volume fraction (Chau, Wong, & Shin, 2007; Furukawa & Fukada, 1977; Furukawa, Ishida, & Fukada, 1979; Ploss, Ploss, Shin, Chan, & Choy, 2000; Ploss, Ploss, Shin, Chan, & Choy, 2000). In this chapter, a non-ferroelectric inclusion, La<sub>2</sub>O<sub>3</sub> was introduced into a polymer matrix, Form II PVDF to form a two-phase composite system. The obtained results suggest that contribution of the electrical conductivity of the inclusion would enhance the pyroelectric and ferroelectric properties of the polymer matrix. A simple Maxwell-Wagner model which is attributed to the heterogeneity structure of the constituents in the polymer matrix is taken into consideration to explain the enhanced efficiency of poling process. This work provides a fundamental insight to enhance pyroelectric and ferroelectric properties of the polymer by introducing the low conductivity non-ferroelectric inclusion in a composite system.

### **6.2 Dielectric Properties**

The relative permittivities and conductive spectra of pure PVDF and PVDF/La<sub>2</sub>O<sub>3</sub> composites with La<sub>2</sub>O<sub>3</sub> weight fraction,  $\phi$  of 0.01, 0.03 and 0.05 are shown in Figure 6.1. The applied frequency was ranged from 40 Hz to 1 MHz, and measured at room temperature. The samples exhibit an increase in both relative permittivity and conductivity with the increase in La<sub>2</sub>O<sub>3</sub> weight fraction.

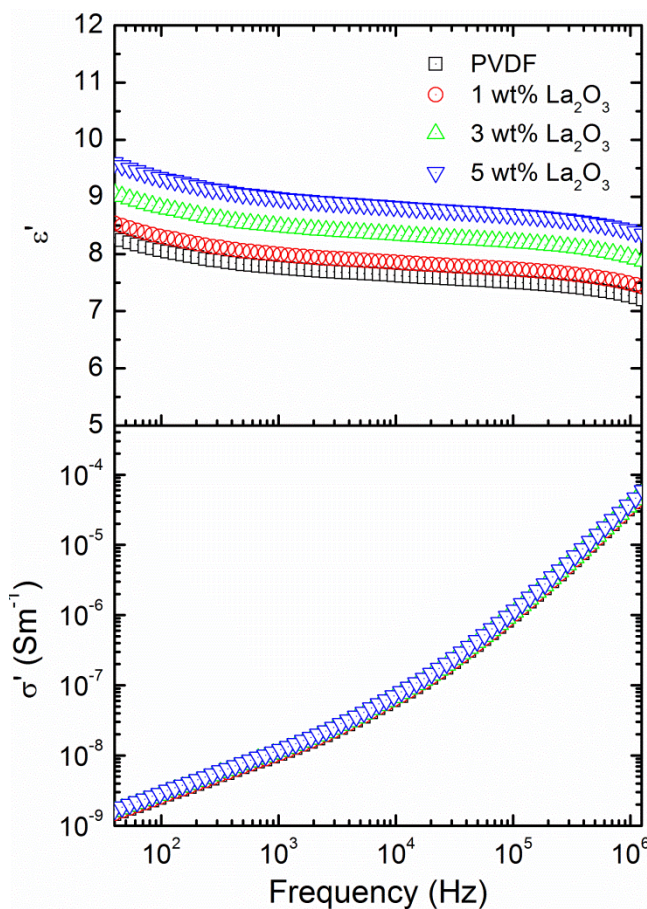


Figure 6.1: Dielectric and conductive spectra for PVDF and PVDF/La<sub>2</sub>O<sub>3</sub> composites at room temperature.

The composite samples in this work can be modeled by a two-phase dispersion system consisting of a polymer matrix (phase 1: PVDF) and spherical inclusions (phase 2: La<sub>2</sub>O<sub>3</sub>) as shown in Figure 6.2. The effective dielectric constant of a polymer composite is strongly influenced by the size, shape and weight fraction of the inclusions. Thus, a few models have been employed to understand the effective dielectric response of the composite thin films. Figure 6.3 shows the observed room temperature dielectric constant of PVDF

composite with 3 wt% of La<sub>2</sub>O<sub>3</sub> after annealed at 140 °C. The calculated dielectric constants derived from various models are included in the same figure.

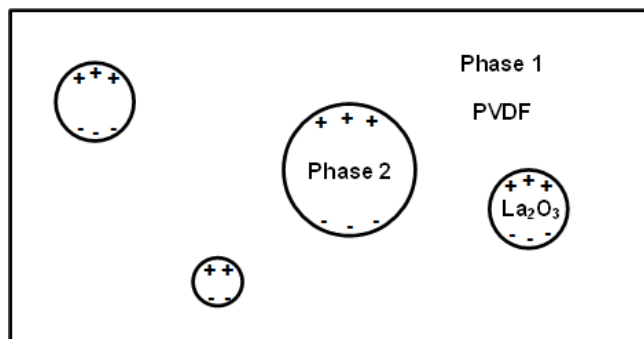


Figure 6.2: A two-phase system composed of a polymer matrix (phase 1) and spherical inclusions (phase 2).

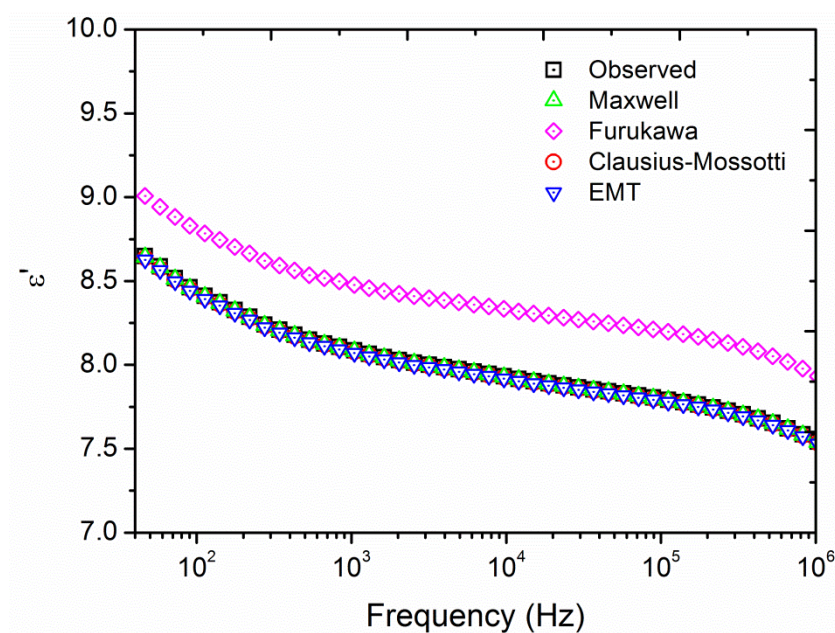


Figure 6.3: Various models of the effective dielectric constant of PVDF/La<sub>2</sub>O<sub>3</sub> with 3 wt% of La<sub>2</sub>O<sub>3</sub> annealed at 140 °C.

The first theoretical model used in this study was derived by Maxwell. This model considered the dielectric property of a diphasic dielectric mixture comprising spherical inclusions with a high dielectric constant dispersed in a low dielectric constant polymer matrix which can be described by the following equation (Thomas, Varughese, Dwarakanath, & Varma, 2010):

$$\varepsilon = \frac{\varepsilon_1(1 - \phi)(2/3 + \varepsilon_2/3\varepsilon_1) + \phi\varepsilon_2}{(1 - \phi)(2/3 + \varepsilon_2/3\varepsilon_1) + \phi} \quad (5.6)$$

where  $\varepsilon_1$ ,  $\varepsilon_2$  and  $\phi$  refer to the dielectric constants of the polymer matrix and inclusions and the weight fraction of the inclusions, respectively. The predicted effective dielectric constants from this model are found to be very close to the experimental data. The deviation between the theoretical prediction and the experiment data is ~3%.

Another convenient theoretical model used in this study was derived by Furukawa years ago, through the following equation (Furukawa, Fujino, & Fukada, 1976; Furukawa, Yasuda, & Takahashi, 2004):

$$\varepsilon = \frac{1 + 2\phi}{1 - \phi} \varepsilon_1 \quad (5.7)$$

This model considers a simple two-phase system with 0-3 connectivity. The inclusions are assumed to be spherical and there is no interface effect takes place in the composite. The value of  $\varepsilon_2$  is assumed to be  $\gg \varepsilon_1$ , and  $\phi \ll 1$ . However, the predicted values from this model seem to deviate by large magnitudes from the observed experimental data for the entire frequency range as the condition of  $\varepsilon_2 \gg \varepsilon_1$  was not fulfilled in this experiment. Another simple explicit formula for binary 0-3 composites is developed by Clausius-Mossotti (Thomas et al., 2010) was employed to predict the effective dielectric constant using the following equation:

$$\varepsilon = \varepsilon_1 \left[ 1 + 3\phi \frac{\varepsilon_2 - \varepsilon_1}{\varepsilon_2 + 2\varepsilon_1} \right] \quad (5.8)$$

The experimental values were found to be well fitted by this model. The difference between the experiment data and the predicted value is less than 2 %. The effective medium theory (EMT) model has been established taking into consideration the morphology of the inclusions. The effective dielectric response of the EMT model is given by (Yang, Qu, Marinis, & Wong, 2000):

$$\varepsilon = \left( 1 + \frac{\phi(\varepsilon_2 - \varepsilon_1)}{\varepsilon_1 + n(1 - \phi)(\varepsilon_2 - \varepsilon_1)} \right) \varepsilon_1 \quad (5.9)$$

where  $n$  is the ceramic inclusion's morphology fitting factor. The small value of  $n$  indicates the filler particles to be in near-spherical shape, while a high value of  $n$  indicates largely non-spherically shaped particles. The experimental values were found to be well fitted by this model with the shape parameter  $n = 0.35$ . The difference between the experiment data and the predicted value is less than 3 %. From the theoretical models employed above, it is clearly seen that Maxwell, Clausius-Mossotti and EMT model with a reasonable fitting parameter,  $n$ , gave the best fit. The good agreement between the theoretical and experimental results implies that the composites have a good 0-3 connectivity and homogeneity.

### 6.3 Pyroelectric Properties

The pyroelectric coefficients of the composite thin films with various La<sub>2</sub>O<sub>3</sub> weight fractions are plotted and shown in Figure 6.4. It is found that the pyroelectric coefficients of the composite thin films increase proportionately with the increase of La<sub>2</sub>O<sub>3</sub> weight fraction. However, the pyroelectric coefficients for the composite thin film which consists of La<sub>2</sub>O<sub>3</sub> exceeding 3 wt% are found to deteriorate. The highest pyroelectric coefficient was obtained from the 3 wt% composite thin film, which has been annealed at 140 °C. It

reaches about  $38 \mu\text{C}/\text{m}^2\text{K}$ , which is 40% higher than that of pure PVDF. As mentioned in previous report, the increase in annealing temperature from  $60^\circ\text{C}$  to  $140^\circ\text{C}$  has improved the crystallinity of the films, as indicated by the formation of the spherulite structure and the diffusion of the pin-holes (Gan & Majid, 2014). The poor pyroelectric performance for annealing temperatures below  $100^\circ\text{C}$  is due to the pin-hole effect, which reduces the effective poling electric field. The improvement in the crystallinity of the PVDF composite thin films structure and smoother sample surface after annealing process allowed higher electric field to be applied to the samples. The change in the crystalline structure of the PVDF polymer may explain the improvement in the pyroelectric activity of the samples.

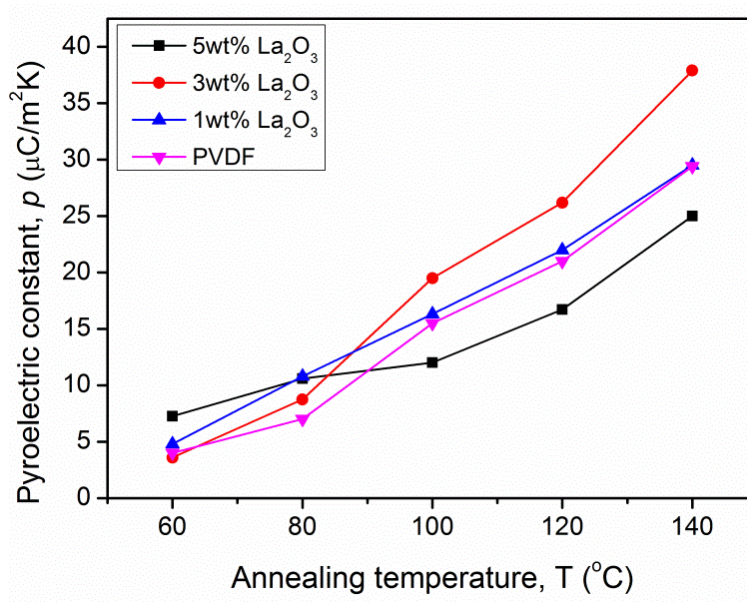


Figure 6.4: Pyroelectric coefficients as a function of annealing temperature.



There are a few models which has been established to calculate the effective pyroelectric coefficient,  $p$  of 0-3 polymer based composites. The widely accepted one is described by the following equation (B. Ploss et al., 2000):

$$p = \frac{\varepsilon - \varepsilon_1}{\varepsilon_2 - \varepsilon_1} p_2 + \frac{\varepsilon_2 - \varepsilon}{\varepsilon_2 - \varepsilon_1} p_1 \quad (6.1)$$

where  $p_1$  and  $\varepsilon_1$  are the pyroelectric coefficient and the dielectric permittivity of the polymer, respectively;  $p_2$  and  $\varepsilon_2$  are the pyroelectric coefficient and the dielectric permittivity of the inclusion, respectively. Since the La<sub>2</sub>O<sub>3</sub> is a non-ferroelectric inclusion, no contribution for the pyroelectric enhancement from the inclusion site is expected. It is obvious that the calculated results from this model are smaller than the observed experiment results.

The following causes have been considered for being responsible for the observed enhancement in the pyroelectric current of the composite thin films. They include the generation of additional conductivity of the system, the phase structure of PVDF as well as the promotion of heterogeneous domain at the lowered activation field in the presence of inclusions. The presence of the La<sub>2</sub>O<sub>3</sub> inclusion has introduced extra free charges required to compensate the dipoles switching domain. Since the amount of La<sub>2</sub>O<sub>3</sub> used is at a very small concentration of 3 wt%, it seems to be unlikely to contribute to sufficient conductivity to enhance the switching process. However, by using Maxwell-Wagner's model as employed by Furukawa et al (Furukawa & Fukada, 1977; Furukawa et al., 1979), the local electric field acting on the inclusions and polymer matrix can be shown to facilitate the poling mechanism of the thin-film composite.

In general, the dispersion of an inclusion in a two phase system has a combination of parallel and series models. The enhanced pyroelectric and ferroelectric properties in the PVDF is assisted and controlled by the conductivity in the series model. Consider a two-

phase dispersion system which consists of a polymer matrix (phase 1: PVDF) and spherical inclusions (phase 2: La<sub>2</sub>O<sub>3</sub>) as shown in Figure 6.2. The average electric field,  $E$  and displacement,  $D$  in the composite can be written as follows (Furukawa et al., 1976; Furukawa & Fukada, 1977; Furukawa et al., 1979; Furukawa, Suzuki, & Date, 1986; Lam, Wong, Tai, Poon, & Shin, 2004; B. Ploss et al., 2000):

$$D = D_0 + \varepsilon E \quad (6.2)$$

$$D_1 = \varepsilon_1 E_1 + P_1 \quad (6.3)$$

$$D_2 = \varepsilon_2 E_2 \quad (6.4)$$

where  $D_0$  is the average dielectric displacement at  $E=0$ . Since La<sub>2</sub>O<sub>3</sub> is a non-ferroelectric inclusion, thus  $P_2 = 0$  is expected. By considering the weight fraction,  $\phi$  of the inclusions, the total average electric field,  $E$  and displacement are:

$$E = (1 - \phi)E_1 + \phi E_2 \quad (6.5)$$

In the present study, the inclusions with a higher conductivity were introduced into a polymer system with the purpose of increase the conductivity of the composite system. As a result, free charge flows easily due to inclusions in the composite system and the continuity condition with respect to  $D$  could be replaced by current,  $I$ .

$$I = \frac{\partial D_1}{\partial t} + \sigma_1 E_1 = \frac{\partial D_2}{\partial t} + \sigma_2 E_2 \quad (6.6)$$

Here,  $\sigma$  is conductivity. Assume that  $\varepsilon_2 > \varepsilon_1$  and  $\sigma_2 > \sigma_1$ , and putting the Equations (6.3) – (6.5) into Equation (6.6), it yields,

$$\varepsilon_1 \frac{\partial E_1}{\partial t} + \frac{\partial P_1}{\partial t} = \varepsilon_2 \frac{\partial E_2}{\partial t} + \sigma_2 E_2 \quad (6.7)$$

$$\varepsilon_1 \frac{\partial E_1}{\partial t} + \frac{\partial P_1}{\partial t} = \varepsilon_2 \left[ \frac{1}{\phi} \frac{\partial E}{\partial t} + \left( \frac{\phi - 1}{\phi} \right) \frac{\partial E_1}{\partial t} \right] + \frac{\sigma_2}{\phi} E + \left( \frac{\phi - 1}{\phi} \right) \sigma_2 E_1 \quad (6.8)$$

$$\frac{\partial P_1}{\partial t} = \varepsilon_2 \left[ \frac{1}{\phi} \frac{\partial E}{\partial t} + \left( \frac{\phi - 1}{\phi} \right) \frac{\partial E_1}{\partial t} \right] + \frac{\sigma_2}{\phi} E + \left( \frac{\phi - 1}{\phi} \right) \sigma_2 E_2 - \varepsilon_1 \frac{\partial E_1}{\partial t} \quad (6.9)$$

When the electric field,  $E$  was applied during the poling process, the presence of the La<sub>2</sub>O<sub>3</sub> particles in the ferroelectric polymer matrix (PVDF) has formed space charge layers at the interface between the inclusions and the polymer matrix in the composite. The space-charge layers at the interface result in an increase of the bound charges on the electrodes in phase with the applied electric field  $E$ , which give rise to an increase in the dielectric constant in the composite (this mechanism is called the Maxwell-Wagner effect) (Furukawa & Fukada, 1977). Consequently, the space charges in the PVDF/ La<sub>2</sub>O<sub>3</sub> composite can drift and accumulate at the inclusion-particle/matrix interfaces at a faster rate. Under such circumstance, it can be assumed that  $\frac{\partial E_1}{\partial t} = 0$ ,  $E_1 = E_c$ . When the applied electric field,  $E_1$  reaches  $E_c$ , the spontaneous polarization of the polymer matrix begins to arise while  $E_1$  remains constant. The rate of change in  $P_1$  is limited by  $\sigma_2$  so that  $P_1$  is equal to the density of charges accumulated near the surface of the inclusion. Finally, it yields,

$$P_1 = \left( \frac{\varepsilon_2 E}{\phi} \right) + \frac{\sigma_2}{\phi} (E + \phi E_1 - E_1) \times t \quad (6.10)$$

In the present study, the electrical conductivity of the inclusion,  $\sigma_2 = 2 \times 10^{-7} \text{Sm}^{-1}$  was limited to tenfold larger than that of the polymer matrix,  $\sigma_1 = 1 \times 10^{-8} \text{Sm}^{-1}$ . In such a way, enhanced pyroelectric coefficient was obtained in the PVDF/La<sub>2</sub>O<sub>3</sub> composite system and it implies that by introducing a considerably amount of electrical conductivity in the composite system could further increase the overall pyroelectric coefficient.

In particular, ferroelectric inclusions such as lead titanate (PT) (B. Ploss et al., 2000) and lead zirconate titanate (PZT) (Furukawa & Fukada, 1977; Furukawa et al., 1979; Lam et al., 2004) have always been the preferable materials to be dispersed in composite thin

films in order to achieve high pyroelectric activity from the thin film. However, dielectric constant of the polymer matrix,  $\epsilon_1$  is much smaller compare to that of the above-mentioned inclusion,  $\epsilon_2$  (typically  $> 100$  times). As a result, the local electric field on the inclusions' site is comparatively small, and the dipoles in the inclusion phase cannot be aligned with that of the polymer matrix. In this work, a non-ferroelectric inclusion, La<sub>2</sub>O<sub>3</sub> was selected due to its extremely low dissipation factor, and permittivity ( $\epsilon = 27$ ). The non-ferroelectric inclusion, La<sub>2</sub>O<sub>3</sub> also has a reasonable conductivity behavior compares to that of ZnO nanoparticles, gold nanoparticles and CNT, which have a fairly large conductivity. During the poling process, space charges in the polymer phase will drift and accumulate at the boundary of the inclusions and the polymer matrix in order to compensate the discontinuity of the electric displacement at the locations (Kwok, Lau, Wong, & Shin, 2007). Without the accumulated space charges at the boundary which are sometimes known as interfacial charges, the dipoles may relax back to a random orientation due to the presence of depolarizing fields. However, with the presence of the interfacial polarization, the local electric field has increased significantly in the inclusion phase. Hence, the required poling field of the thin-film composite decreased and thus, the poling efficiency of the system has been considerably enhanced.

#### 6.4 Ferroelectric Properties

The ferroelectric behavior of PVDF and PVDF-La<sub>2</sub>O<sub>3</sub> thin film composite was studied by the *D-E* hysteresis measurement. The results are depicted in Figure 6.5. It is clearly seen that the remnant polarization of PVDF dispersed with 3 wt% of La<sub>2</sub>O<sub>3</sub> reaches 83 mC/m<sup>2</sup>. The remnant polarization has been increased by 20% compare to that of pure PVDF. Adding more La<sub>2</sub>O<sub>3</sub> to the composite has increased the dielectric permittivity and

loss of the thin film. The leakage current becomes excessively high when the La<sub>2</sub>O<sub>3</sub> inclusions are surpassing the 5 wt%. Enhancing ferroelectricity by adding inclusion of high conductivity strongly reduces the ferroelectric polarization. This is because some of the polarization dipoles have been neutralized by the additional space charges. As the excessive leakage current prevents the  $D$ - $E$  measurement, the content of La<sub>2</sub>O<sub>3</sub> has been limited to 5 wt%.

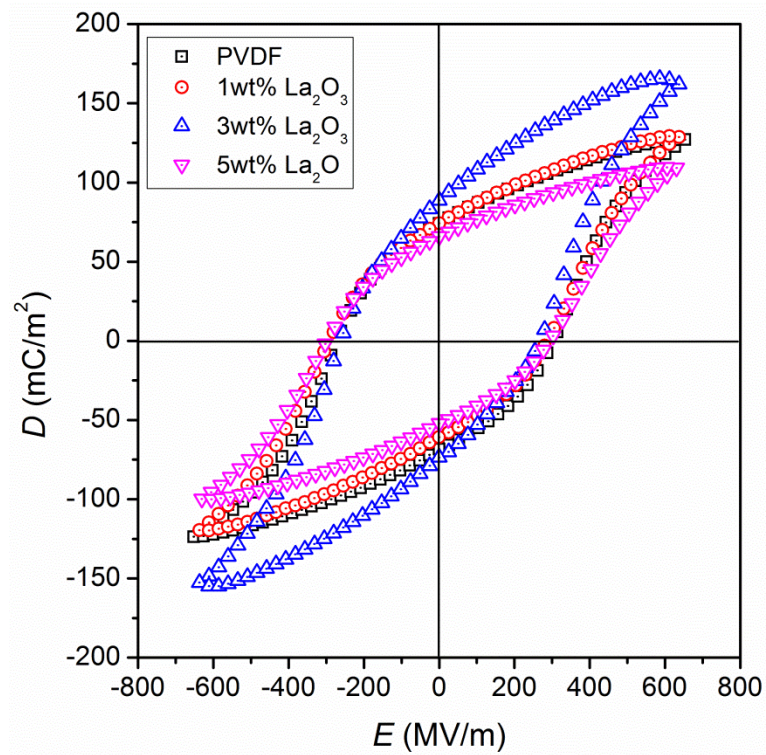


Figure 6.5:  $D$ - $E$  hysteresis loops of PVDF and PVDF/La<sub>2</sub>O<sub>3</sub> annealed at 140 °C.

As mentioned in the previous section, the two-phase system has a combination of parallel and series models. The enhanced pyroelectric and ferroelectric properties in the PVDF are governed by the conductivity in the series model. In the context of the dispersion 0-3 composite system, increase of the weight fraction of phase 2 will eventually lead to aggregation along the direction of thickness to form a structure similar to parallel model.

On the other hand, the internal fields and the electric displacements are additive in the parallel model yields,

$$E = E_1 = E_2 \quad (6.11)$$

$$D = (1 - \phi)D_1 + \phi D_2 \quad (6.12)$$

This has explained why when the inclusion of La<sub>2</sub>O<sub>3</sub> was increased to 5 wt%, the pyroelectricity and ferroelectricity in the polymer phase were obscured by the dc conduction in the parallel model. The pyroelectric and ferroelectric in the polymer phase is independent of the La<sub>2</sub>O<sub>3</sub>. The flow of current from one side of the inclusion La<sub>2</sub>O<sub>3</sub> to the other side has resulted in a continuous rise of  $D$  with time. Thus, the poling process in the polymer phase has been obscured by the dc conduction in the phase 2.

## 6.5 Phase Transformation from Form II to IV PVDF

XRD analysis as shown in Figure 6.6 was performed in order to investigate the crystalline and phase structure of PVDF composite in the presence of La<sub>2</sub>O<sub>3</sub>. It is discovered that the phase structure of PVDF in the (100) plane does not change upon the addition of La<sub>2</sub>O<sub>3</sub> particles. Major changes to be noted in Figure 6.6(a) is the increase in intensity of the (110) reflection and the significant decrease in the (100) reflection plane after poling process, as can be observed clearly in the inset of the figure. These are attributed to phase transition in PVDF that takes place during poling process (Broadhurst & Davis, 1984; Das-Gupta & Doughty, 1977, 1978, 1980; Das-Gupta, Doughty, & Shier, 1979; Davis, McKinney, Broadhurst, & Roth, 1978; Naegel, Yoon, & Broadhurst, 1978). Quantitative analysis on the XRD results has been performed by deconvolution of the XRD

patterns as shown in Figure 6.6(b). It is found that there are large reductions in the areas of (100) reflection plane after poling process. When a very high electric field ( $> 120$  MV/m) is applied to PVDF composite thin films, a phase transition from Form II to the highly polar Form IV is expected. The reflection planes of Form II and IV are quite similar, except for two particular reflection planes of (100) and (120) located at  $2\theta = 17.6^\circ$  and  $25.8^\circ$ . Here, the peak intensity of (120) reflection plane is too small to be observed and thus it is not examined in details.

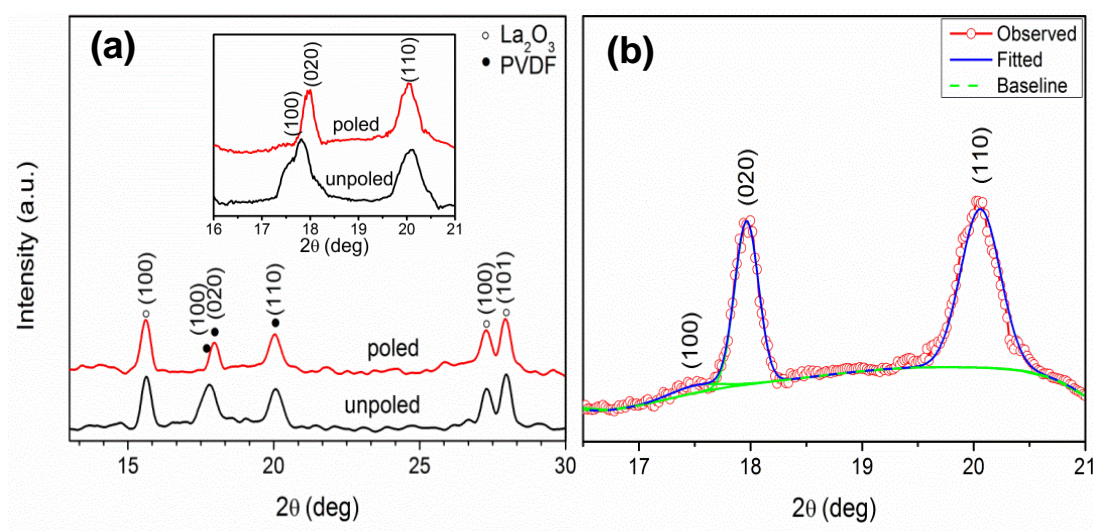


Figure 6.6: X-ray diffractograms of PVDF-La<sub>2</sub>O<sub>3</sub> (3 wt%) thin films: (a) effect of poling and (b) XRD deconvolution of Form IV PVDF after poling.

In order to elucidate the finding further, the crystalline orientation of the molecule was examined from the XRD results. The information obtained on the orientation of the molecule can be used to correlate the polarization orientation and the direction of the applied electric field. The proposed mechanism of phase transformation from Form II to Form IV can then be confirmed and is illustrated in Figure 4.20. It is known that the

polarization reversal of Form IV PVDF occurs in the *ab*-plane as a result of chain rotation about the *c*-axis as explained in Chapter 4, Section 4.7.1. The sharp peak of (110) plane as shown in the XRD results indicates that the molecules (*c*-axis) have high tendency to align parallel to the film surface because the surface energy per unit area for the (110) plane is much lower than that of the (020) (Ohigashi, Omote, & Gomyo, 1995). In such a way, the polarization reversal around the *c*-axis could be induced by the external electric field effectively. In addition, the resultant microscopic surface area of the molecules' chain which exposed to the air in the hexagonal phase is smaller in (110) plane compare to (020) plane. As a result, the substrate is more favorable to face the most densely packed plane. The preferential orientation is advantageous as the effective electric field acting on the planes will be at its optimum.

XRD, ferroelectric hysteresis measurement and pyroelectric results indicate that the spontaneous polarization of Form IV PVDF is subjected to a very large local electric field. The findings also suggest that the space charge in the PVDF/LaO composite thin film can drift and accumulate at the particle-matrix interface and cause the local electric field in the inclusion phase to increase. This implies that more charges can accumulate at the interfaces. As a result, the dipoles in the matrix surrounding the inclusions could be easily aligned. The presence of La<sub>2</sub>O<sub>3</sub> has introduced additional free charges required to compensate and stabilize the polarization domain. The additional free charges have enhanced the heterogeneous domain. The heterogeneous domain has been considered to play an important part in the enhancement of local electric field in addition to the apparent enhanced alignment of the (110) plane during poling. These factors are responsible for the enhanced pyroelectric and ferroelectric properties observed.



## 6.6 Comparison in Between the TiO<sub>2</sub> and La<sub>2</sub>O<sub>3</sub> as a Non-ferroelectric Inclusion

It has been shown that incorporation of non-ferroelectric into PVDF polymer matrix could enhanced the pyroelectric and ferroelectric properties as a 0-3 composite thin films. The factors governed the enhanced functionality of a ferroelectric polymer can be attributed to:

1. Enhanced local electric field on the polymer matrix.
2. An increase in conductivity of the polymer matrix led to poling efficiency and reduced the required electric field.

Table 6.1 shows the local electric field acting on the polymer phase and inclusion, respectively. The local field coefficients were obtained using equations as shown in Chapter 5:

$$L_{E1} = \frac{E_1}{E} = \frac{1}{1-\phi} \frac{\varepsilon_2 - \varepsilon}{\varepsilon_2 - \varepsilon_1} \quad (5.16)$$

$$L_{E2} = \frac{E_2}{E} = \frac{1}{\phi} \frac{\varepsilon_1 - \varepsilon}{\varepsilon_1 - \varepsilon_2} \quad (5.17)$$

Here,  $L_{E1}$  and  $L_{E2}$  is defined as the ratio of the local field  $E_1$  in the inner sphere to the average field over a composite and the ratio of the local field  $E_2$  in the inner sphere to the average field over a composite. The local electric coefficient,  $L_{E1}$  acting on the polymer phase increases with the increase of inclusion wt%. In generally, the value of  $\varepsilon_2$  is always found to be  $\varepsilon_2 \gg \varepsilon_1$  (100 times greater) in a composite system. Consequently, the local electric field applied on phase 1 (polymer matrix) is much higher than local electric field on phase 2 (inclusion),  $L_{E1} \gg L_{E2}$ . However, similar value of  $L_{E1}$  could be achieved by employed relatively small wt% of La<sub>2</sub>O<sub>3</sub> due to its low dielectric constant ( $\varepsilon = 27$ ) if compared to that of TiO<sub>2</sub> ( $\varepsilon = 90$ ). The magnitude of dielectric constant of La<sub>2</sub>O<sub>3</sub> and TiO<sub>2</sub>

are 3 and 10 times larger than PVDF, respectively. As a result, the incorporation of non-ferroelectric inclusions in the polymer matrix has successfully directed the local electric field on the polymer matrix during the poling process.

In addition, the electrical conductivity of the inclusions plays an important role to accelerate the poling process. The conductivity of the PVDF, La<sub>2</sub>O<sub>3</sub> and TiO<sub>2</sub> inclusions, are  $\sigma_2 = 1 \times 10^{-8} Sm^{-1}$ ,  $2 \times 10^{-7} Sm^{-1}$  and  $3 \times 10^{-6} Sm^{-1}$ , respectively. The magnitude of conductivity of inclusion was limited to tenfold larger than that of the polymer matrix, by using La<sub>2</sub>O<sub>3</sub>. These finding implies that increase in considerable amount of conductivity in a 0-3 composite system has significantly led to a more efficient poling process by reducing the required electric field. As a result, the pyroelectric and ferroelectric properties of the PVDF matrix have been further enhanced. However, TiO<sub>2</sub> is found to be less advantage compared to that of La<sub>2</sub>O<sub>3</sub> due to its excessive high conductivity (100 times higher than PVDF). Hence, La<sub>2</sub>O<sub>3</sub> is recommended to be better candidate as a non-ferroelectric inclusion to increase the efficiency of the poling process.

<b>TiO<sub>2</sub></b>	<b><math>L_{E1}</math></b>	<b><math>L_{E2}</math></b>	<b>La<sub>2</sub>O<sub>3</sub></b>	<b><math>L_{E1}</math></b>	<b><math>L_{E2}</math></b>
10 wt%	1.056	0.5	1 wt%	1.004	0.565
20 wt%	1.125	0.5	3 wt%	1.014	0.554
30 wt%	1.161	0.625	5 wt%	1.024	0.551

Table 6.1: Local field coefficient as a function of inclusion wt% (subscripts 1 and 2 denote the polymer phase and inclusion, respectively).

## 6.7 Conclusion

A significant improvement in pyroelectric and ferroelectric properties in PVDF composite thin films have been demonstrated when 3 wt% of La<sub>2</sub>O<sub>3</sub> is dispersed in the composite thin film. The incorporation of the non-ferroelectric inclusion with negligible conductivity in the polymer matrix composite has successfully improved the poling efficiency by increased the local electric field on the polymer matrix. These results are confirmed by the simple Maxwell-Wagner's model which considers the conductivities of the constituents of the composite thin film. It implies that an increase in the conductivity of the polymer matrix has significantly led to a more efficient poling process and as a result, it has improved the pyroelectric and ferroelectric properties of the composites. However, the conductivity of a polymer composite matrix must be limited to a certain level. The leakage current becomes excessively high when the La<sub>2</sub>O<sub>3</sub> inclusions are surpassing the 5 wt% and deteriorates the pyroelectric and ferroelectric properties of the polymer composite matrix.

## References

- Broadhurst, M. G., & Davis, G. T. (1984). Physical basis for piezoelectricity in PVDF. *Ferroelectrics*, 60(1), 3-13.
- Chau, K. H., Wong, Y. W., & Shin, F. G. (2007). Enhancement of piezoelectric and pyroelectric properties of composite films using polymer electrolyte matrix. *Applied Physics Letters*, 91(25), 252910.
- Das-Gupta, D. K., & Doughty, K. (1977). Changes in x-ray diffraction patterns of polyvinylidene fluoride due to corona charging *Applied Physics Letters*, 31, 585-587.
- Das-Gupta, D. K., & Doughty, K. (1978). Piezo- and pyroelectric behaviour of corona-charged polyvinylidene fluoride. *Journal of Physics D: Applied Physics*, 11(17), 2415-2423.
- Das-Gupta, D. K., & Doughty, K. (1980). Piezoelectricity in uniaxially stretched and corona poled polyvinylidene fluoride. *Journal of Physics D: Applied Physics*, 13(1), 95-105.
- Das-Gupta, D. K., Doughty, K., & Shier, D. B. (1979). A study of structural and electrical properties of stretched polyvinylidene fluoride films. *Journal of Electrostatics*, 7(0), 267-282.
- Davis, G. T., McKinney, J. E., Broadhurst, M. G., & Roth, S. C. (1978). Electric-field-induced phase changes in poly(vinylidene fluoride). *Journal of Applied Physics*, 49(10), 4998-5002.
- Furukawa, T., Fujino, K., & Fukada, E. (1976). Electromechanical Properties in the Composites of Epoxy Resin and PZT Ceramics. *Japanese Journal of Applied Physics*, 15, 2119-2129.
- Furukawa, T., & Fukada, E. (1977). Piezoelectric Relaxation in Composite Epoxy-PZT System due to Tonic Conduction. *Japanese Journal of Applied Physics*, 16(3), 453-458.
- Furukawa, T., Ishida, K., & Fukada, E. (1979). Piezoelectric properties in the composite systems of polymers and PZT ceramics. *Journal of Applied Physics*, 50(7), 4904-4912.

- Furukawa, T., Suzuki, K., & Date, M. (1986). Switching process in composite systems of PZT ceramics and polymers. *Ferroelectrics*, 68(1), 33-44.
- Furukawa, T., Yasuda, K., & Takahashi, Y. (2004). Dielectric and conductive spectra of the composite of barium titanate and LiClO<sub>4</sub>-doped polyethylene oxide. *IEEE Transactions on Dielectrics and Electrical Insulation*, 11(1), 65-71.
- Gan, W. C., & Majid, W. H. A. (2014). Effect of TiO<sub>2</sub> on enhanced pyroelectric activity of PVDF composite. *Smart Materials and Structures*, 23(4), 045026.
- Kwok, K. W., Lau, S. T., Wong, C. K., & Shin, F. G. (2007). Effects of electrical conductivity on poling of ferroelectric composites *Journal of Physics D: Applied Physics*, 40(21), 6.
- Lam, K. S., Wong, Y. W., Tai, L. S., Poon, Y. M., & Shin, F. G. (2004). Dielectric and pyroelectric properties of lead zirconate titanate/polyurethane composites. *Journal of Applied Physics*, 96(7), 3896-3899.
- Naegle, D., Yoon, D. Y., & Broadhurst, M. G. (1978). Formation of a New Crystal Form ( $\alpha$ ) of Poly(vinylidene fluoride) under Electric Field. *Macromolecules*, 11(6), 1297-1298.
- Ohigashi, H., Omote, K., & Gomyo, T. (1995). Formation of "single crystalline films" of ferroelectric copolymers of vinylidene fluoride and trifluoroethylene. *Applied Physics Letters*, 66(24), 3281-3283.
- Ploss, B., Ploss, B., Shin, F. G., Chan, H. L. W., & Choy, C. L. (2000). Pyroelectric activity of ferroelectric PT/PVDF-TRFE. *IEEE Transactions on Dielectrics and Electrical Insulation*, 7(4), 517-522.
- Ploss, B., Ploss, B., Shin, F. G., Chan, H. L. W., & Choy, C. L. (2000). Pyroelectric or piezoelectric compensated ferroelectric composites. *Applied Physics Letters*, 76(19), 2776-2778.
- Thomas, P., Varughese, K. T., Dwarakanath, K., & Varma, K. B. R. (2010). Dielectric properties of Poly(vinylidene fluoride)/CaCu<sub>3</sub>Ti<sub>4</sub>O<sub>12</sub> composites. *Composites Science and Technology*, 70(3), 539-545.
- Yang, R., Qu, J., Marinis, T., & Wong, C. P. (2000). A precise numerical prediction of effective dielectric constant for polymer-ceramic composite based on effective-

medium theory. *IEEE Transactions on Components and Packaging Technologies*, 23(4), 680-683.

## CHAPTER 7: CONCLUSION

### 7.1 Conclusion

This study is mainly divided into two aspects. The first aspect is focus on electric field induced Form IV from Form II PVDF. Details analysis and discussion were carried out on the fundamental insight of the dielectric molecular dynamics of Form IV PVDF and its functional behaviors like pyroelectric and ferroelectric properties. In the second part, attempts were made to correlate the effect of non-ferroelectric inclusions in a functional polymer matrix and its poling mechanism in the 0-3 polymer matrix composites by using non-ferroelectric inclusions.

In the present work, the structures, pyroelectric and ferroelectric properties of solvent-cast PVDF with special emphasis on the observation of polarization switching in Form IV PVDF have been revealed. The primary objective in this thesis is to re-examine the underlying ferroelectric switching characteristics and pyroelectric properties of Form IV PVDF since the properties of this polymorph has been abandoned for many decades. In particular, the Form IV PVDF thin films were prepared by spin-coating technique. It is shown that thermal annealing at 140°C is essential to produce highly crystalline Form II PVDF and smooth surface roughness. An application of a high electric field (>200 MV/m) could induced a phase transformation from Form II to Form IV which was supported by a marked reduction of (100) (120) X-ray diffraction intensities without further conversion to Form I. The remanent polarization  $P_r$  of 70 mC/m<sup>2</sup> with a coercive field  $E_c$  of 200 MV/m has been exhibited. The pyroelectric constant  $p_y$  determined after hysteresis loop measurement was shown to be proportional to the  $P_r$  and reached a value of 28  $\mu\text{C}/\text{m}^2\text{K}$ . These values are comparable to those of Form I PVDF and of the copolymer P(VDF-TrFE). Spontaneous polarization in Form IV obtained by rigid dipole model and modern

computational method has suggested that local electric enhancement which arises from the inter-chain interaction in a crystal play an important role for its exceptional ferroelectricity and pyroelectricity which has been observed in this study. Molecular dynamics of Form IV PVDF has also been investigated by the broadband dielectric spectroscopy. For the very first time, Form IV is found to exhibit inferior dielectric strength and undergoes slower motion where its relaxation time,  $\tau$  of the intermolecular dynamics motion has been slowed down compare to that of Form II. These observations have shed new light on the ferroelectric and molecular dynamic in Form IV PVDF ever, and such discoveries are critical to further extend the possibility for realizing its application in organic electronics.

In the second aspect, it is found that a remarkable increase in the pyroelectric activity can be achieved by the inclusion of  $\text{TiO}_2$  into Form II dominant PVDF. The incorporation of the non-ferroelectric inclusion in the polymer matrix composite has successfully increased the local electric field on the polymer matrix during the poling process. Thus, the required poling electric field has been reduced by a factor of two from 260 MV/m to 120 MV/m. These findings imply that an increase in the conductivity of the polymer matrix has significantly led to a more efficient poling process and as a result, it has improved the pyroelectric activity of the composites. However, the conductivity of a polymer composite matrix must be limited to a certain level. Above that level, an increased in the conductivity only deteriorates the pyroelectric activity of the polymer composite matrix, due to the increased in leakage current which can be observed in the composites containing more than 30 wt% of  $\text{TiO}_2$ .

The conductivity of the  $\text{TiO}_2$  is found to be too conducting in a polymer matrix to enhance its functionality of the composites system. Here, an alternative candidate,  $\text{La}_2\text{O}_3$  has been proposed to be introduced into a polymer matrix, Form II PVDF to form a two-phase composite system. A significant improvement in pyroelectric and ferroelectric



properties in PVDF composite thin films have been demonstrated when 3 wt% of  $\text{La}_2\text{O}_3$  is dispersed in the composite thin film. The incorporation of the non-ferroelectric inclusion with negligible conductivity in the polymer matrix composite has successfully improved the poling efficiency by increased the local electric field on the polymer matrix. These results are confirmed by the simple Maxwell-Wagner's model which considers the conductivities of the constituents of the composite thin film. It implies that an increase in the conductivity of the polymer matrix has significantly led to a more efficient poling process and as a result, it has improved the pyroelectric and ferroelectric properties of the composites. However, the conductivity of a polymer composite matrix must be limited to a certain level. The leakage current becomes excessively high when the  $\text{La}_2\text{O}_3$  inclusions are surpassing the 5 wt% and deteriorates the pyroelectric and ferroelectric properties of the polymer composite matrix.

In this work, the pyroelectric coefficient of Form IV PVDF has been further enhanced by 26 % and 40 % with the incorporation of non-ferroelectric,  $\text{TiO}_2$  and  $\text{La}_2\text{O}_3$ , respectively. A remarkable increase of 20 % in  $P_r$  has also been observed with the incorporation of  $\text{La}_2\text{O}_3$ . These findings imply that an increase in the conductivity of the polymer matrix has significantly led to a more efficient poling process by reducing the required electric field. Hence, the investigation of pyroelectric and ferroelectric properties of the Form IV PVDF and its composite thin films are worthwhile. They could be an ideal candidate for functional organic ferroelectric in data storage applications, field effect transistor and microelectromechanical systems (MEMs).

## 7.2 Future Works

To date, this thesis has provided fundamental understanding on the extraordinary electrical responses of Form IV PVDF induced by electric field. However, there are yet a number of different aspects of PVDF which required further investigation both in terms of fundamentals and applications. The obtained Form IV results prepared by spin-coating technique are actually restricted from substrate constraint. During the pyroelectric measurement, the thin films were only allowed to be thermally expanded in thickness direction, and not in the in-plane expansion. In particular,  $e_{3j}$  and  $\alpha_j$  which are defined as piezoelectric constant and thermal expansion coefficient could not be determined accurately. In addition, a Form IV sample which is free from any substrate constraint should be prepared in order to measure its true piezoelectric constants using piezoelectric resonance method. Since piezoelectric has a wide range of application potentials in sensors, actuators and energy harvesting, it is foremost important to explore functional properties of Form IV before it could be actually realized for application purpose.

## Appendix

### Calculation of dipole moment and spontaneous polarization, $P_s$ of PVDF

Partial charge in elementary charge unit  $q_0=1.6 \times 10^{-19}$  C

Atom	Partial charge value
$q_{C_H}$	-0.134
$q_{H_1}, q_{H_2}$	0.067, 0.067
$q_{C_F}$	0.438
$q_{F_1}, q_{F_2}$	-0.219, -0.219

Table A1: Partial charge value after (Tashiro, Kobayashi, Tadokoro, & Fukada, 1980).

### Atomic coordinates of Form I PVDF: $a=0.858$ nm, $b=0.491$ nm, $c=0.256$ nm

Atom	$x/a$	$y/b$	$z/c$
$C_H$	0.0	0.0	0.0
$H_1$	0.105	-0.124	0.0
$H_2$	-0.105	-0.124	0.0
$C_F$	0.0	0.174	0.500
$F_1$	0.126	0.355	0.500
$F_2$	-0.126	0.355	0.500

Table A2: Atomic coordinates of Form I PVDF after (Hasegawa, Takahashi, Chatani, & Tadokoro, 1971)

**Dipole moment and  $P_s$  of Form I PVDF along  $b$ -axis:**

$$\frac{\mu_b}{bq_0} = (q_{F_1} \times F_1) + (q_{F_2} \times F_2) + (q_{C_F} \times C_F) + (q_{H_1} \times H_1) + (q_{H_2} \times H_2) + (q_{C_H} \times C_H)$$

$$\begin{aligned} \mu_b / bq_0 &= -0.219 \times (0.355 + 0.355) + 0.438 \times (0.174) + 0.067 \times (-0.124 - 0.124) - 0.134 \times (0) \\ &= -0.156 + 0.077 - 0.017 - 0 = -0.096 \end{aligned}$$

$$\begin{aligned} \mu_b &= -0.096 \times bq_0 = -0.096 \times 0.491 \times 10^{-9} \times 1.6 \times 10^{-19} = -7.51 \times 10^{-30} \text{ Cm} \\ &= -2.3 \text{ Debye} \end{aligned}$$

$$\begin{aligned} P_s &= \frac{2 \times \mu_b}{abc} = \frac{2 \times 7.51 \times 10^{-30}}{0.858 \times 0.491 \times 0.256 \times 10^{-27}} = \frac{2 \times 7.51 \times 10^{-30}}{107.8 \times 10^{-30}} \\ &= 0.139 \text{ C/m}^2 = 139 \text{ mC/m}^2 \end{aligned}$$

**Atomic coordinate of Form IV PVDF:  $a=0.496$  nm,  $b=0.964$  nm,  $c=0.462$  nm**

Atom	$x/a$	$y/b$	$z/c$
$C_H$	0.238	0.183	-0.175
$H_1$	0.366	0.096	-0.240
$H_2$	0.021	0.166	-0.194
$C_F$	0.308	0.186	0.150
$F_1$	0.218	0.070	0.276
$F_2$	0.576	0.178	0.185

Table A3: Atomic coordinates of Form II (or Form IV) PVDF after (Hasegawa, Takahashi, Chatani, & Tadokoro, 1971)

**Dipole moment and  $P_s$  of Form IV PVDF along  $a$ -axis:**

$$\begin{aligned}\mu_a / aq_0 &= -0.219 \times (0.218 + 0.576) + 0.438 \times (0.308) + 0.067 \times (0.366 + 0.021) - 0.134 \times (0.238) \\ &= -0.173 + 0.135 + 0.025 - 0.032 = -0.0449\end{aligned}$$

$$\mu_a = -0.0449 \times aq_0 = -0.0449 \times 0.496 \times 10^{-9} \times 1.6 \times 10^{-19} = -3.56 \times 10^{-30} \text{ Cm}$$

$$= -1.1 \text{ Debye}$$

$$\begin{aligned}P_s &= \frac{4 \times \mu_a}{abc} = \frac{4 \times 3.56 \times 10^{-30}}{0.496 \times 0.964 \times 0.462 \times 10^{-27}} = \frac{4 \times 3.56 \times 10^{-30}}{220.9 \times 10^{-30}} \\ &= 0.064 \text{ C/m}^2 = 64 \text{ mC/m}^2\end{aligned}$$

**Dipole moment and  $P_s$  of Form IV PVDF along  $c$ -axis:**

$$\begin{aligned}\mu_c / cq_0 &= -0.219 \times (0.276 + 0.185) + 0.438 \times (0.150) + 0.067 \times (-0.240 - 0.194) - 0.134 \times (-0.175) \\ &= -0.1001 + 0.0657 - 0.029 + 0.02345 = -0.039\end{aligned}$$

$$\mu_c = -0.039 \times cq_0 = -0.039 \times 0.462 \times 10^{-9} \times 1.6 \times 10^{-19} = -2.95 \times 10^{-30} \text{ Cm}$$

$$= -0.9 \text{ Debye}$$

$$\begin{aligned}P_s &= \frac{4 \times \mu_c}{abc} = \frac{4 \times 2.95 \times 10^{-30}}{0.496 \times 0.964 \times 0.462 \times 10^{-27}} = \frac{4 \times 2.95 \times 10^{-30}}{220.9 \times 10^{-30}} \\ &= 0.053 \text{ C/m}^2 = 53 \text{ mC/m}^2\end{aligned}$$

**References:**

- Hasegawa, R., Takahashi, Y., Chatani, Y., & Tadokoro, H. (1971). Crystal Structures of Three Crystalline Forms of Poly(vinylidene fluoride). *Polymer Journal*, 3(5), 600-610.
- Tashiro, K., Kobayashi, M., Tadokoro, H., & Fukada, E. (1980). Calculation of Elastic and Piezoelectric Constants of Polymer Crystals by a Point Charge Model: Application to Poly(vinylidene fluoride) Form I. *Macromolecules*, 13(3), 691-698.